JOURNAL OF THE AERONAUTICAL SCIENCES

VOLUME 21 MARCH, 1954 NUMBER 3

Extension of Power Spectral Methods of Generalized Harmonic Analysis to Determine Non-Gaussian Probability Functions of Random Input Disturbances and Output Responses of Linear Systems*

BERNARD MAZELSKY†

Lockheed Aircraft Corporation

ABSTRACT

The power spectral methods of generalized harmonic analysis are extended to determine the higher order moments above the second of the probability frequency functions for either the input forcing function or the output response of a linear system. Several techniques are then indicated for determining the corresponding probability distributions from the calculated moments. The conditions under which a non-Gaussian forcing function and a Gaussian output response can exist are indicated and discussed. The most significant requirement is that the bandwidth of the input power spectrum is large compared with the bandwidth of the system transfer function.

INTRODUCTION

THE DETERMINATION OF THE RESPONSE of a dynamic system due to random disturbances, such as an airplane subjected to atmospheric turbulence, buffeting, landing impacts, taxiing over rough surfaces, etc., has recently received consideration with the point of view of applying the concepts and knowledge of stochastic processes for describing the statistical character of the problem in a more concise mathematical form. In references 1, 2, 3, and 4 investigations are presented of the application of power-spectral methods of generalized harmonic analysis to several of these airplane response problems. Although all of the studies realize the necessity of describing the disturbance function statistically, its description is usually restricted to knowledge of only the correlation function or its Fourier transform, the power-spectral density function. If the probability distribution of the disturbance function is Gaussian, then for linear systems the power-spectral density approach is sufficient for describing not only the probability distribution of the disturbance function but also the output response function.[1] For the case of non-Gaussian disturbance functions, this information by itself does not, in general, adequately describe the statistical properties of either the input or the output functions.

The purpose of the present paper is to present an extension of the power-spectral density concepts to the case of non-Gaussian distributions of the disturbance or response functions. In addition, it will be shown that, for the case of a lightly damped dynamic system and a flat input power spectrum (relative to the transfer function of the dynamic system), the input function may be non-Gaussian but the response function would be, in general, Gaussian. Limited experimental evaluation of an airplane's acceleration probability distribution while penetrating atmospheric turbulence[1] indicated that, while the measured cumulative frequency functions were approximately Gaussian, the deviations from the Gaussian were largest for the largest accelerations; consequently, proper designation of the critical loads experienced by the airplane

Received October 16, 1953.

* The author gratefully acknowledges the discussions on this subject with Dr. Bernard Gold, of the Hughes Aircraft Company.

† Dynamics Engineer.

based on the Gaussian distribution appears questionable. In addition, the degree of proximity of the probability distribution to Gaussian appeared to be a function of the dynamic stability of the airplane, thus indicating that, in general, the atmospheric turbulence is probably non-Gaussian and that the usefulness of the Gaussian distribution to approximate the response probability distribution would depend upon the transfer function of the airplane. Thus, for the general case it would appear desirable to assume non-Gaussian frequency distributions for both the input and the output but to realize the usefulness of the Gaussian distribution as a good first approximation in some instances.

Symbols

t	= time, sec.
t_1, t_2	= dummy variables of integration
τ_1, τ_2	= arbitrary displacements in time, sec.
T	= arbitrary value of t, sec.
$x(t)$	= random input forcing function
$y(t)$	= random output response function
$h(t)$	= response of linear system to a unit impulse forcing function
f	= frequency, cycles per sec.
$H(f)$	= transfer function or frequency response of linear system, $H(f) = \int_0^\infty h(t)e^{-j2\pi ft}\,dt$
$G_x(f_1, f_2, \ldots f_n)$	= power spectrum of input generalized to multiple frequencies
$G_y(f_1, f_2, \ldots f_n)$	= power spectrum of output generalized to multiple frequencies
$\varphi(x)$	= Gaussian probability frequency function
$\Phi(x)$	= Gaussian probability distribution function, $\Phi(x) = \int_{-\infty}^{x} \varphi(x)\,dx$
$f(x)$	= non-Gaussian probability frequency function
$F(x)$	= non-Gaussian probability distribution function, $F(x) = \int_{-\infty}^{x} f(x)\,dx$
μ_n	= nth central moment of probability frequency function
m	= mean of probability frequency function
σ	= standard deviation of probability frequency function
$E(\ )$	= mean value of a function of a random variable
j	= $\sqrt{-1}$
$\overline{y(t)}$	= average value of $y(t)$, $\overline{y(t)} = \lim_{T\to\infty} \frac{1}{2T}\int_{-T}^{T} y(t)\,dt$
η^3	= third absolute moment about the mean of probability frequency function
$R(\tau_1, \tau_2, \ldots \tau_n)$	= correlation function generalized to multiple arbitrary displacements
a	= arbitrary constant
C_T	= defined by Eq. (A-3)
Λ_T	= defined by Eq. (A-7) or (A-8)

Analysis

Relations Between the Input-Output Moments of the Probability Distributions for a Known Transfer Function

Consider the problem of determining the moments of the probability distributions for either the random input, $x(t)$, or output, $y(t)$, given one or the other and the transfer function of the system, $H(f)$. If the random input is stationary over sufficiently large time intervals and the system is linear, the ergodic hypothesis becomes valid, implying that time averages are equivalent to ensemble averages for both the input and output. This feature of the random process can simplify the calculation of the moments of the probability distribution through the use of the correlation function. This function, together with its Fourier transform, the power-spectral density function, provides a technique of calculating the second moment of either the input or output given the transfer function of the system and the power-spectral density of either the output or input functions. Denoting, respectively, $G_x(f)$ and $G_y(f)$ as the power-spectral density functions of the input and output, a useful relation for determining the desired second moments is

$$G_y(f) = G_x(f)\,|H(f)|^2 \tag{1}$$

where the bars indicate the modulus of the function. A derivation of Eq. (1) is given in reference 5. The input or output spectrum can be obtained algebraically from Eq. (1) relatively simply; the corresponding second central moments or standard deviations, σ_x and σ_y, are determined readily from the integral of the power spectrum.

$$\left.\begin{aligned} \mu_{2x} &= \sigma_x^2 = \frac{1}{2}\int_{-\infty}^{\infty} G_x(f)\,df \\ \mu_{2y} &= \sigma_y^2 = \frac{1}{2}\int_{-\infty}^{\infty} G_y(f)\,df \end{aligned}\right\} \tag{2}$$

but since $G_x(f)$ and $G_y(f)$ are even functions, Eqs. (2) simplify to

$$\left.\begin{aligned} \mu_{2x} &= \sigma_x^2 = \int_0^{\infty} G_x(f)\,df \\ \mu_{2y} &= \sigma_y^2 = \int_0^{\infty} G_y(f)\,df \end{aligned}\right\} \tag{3}$$

If the input and output probability functions are Gaussian—that is, in a form given by Eq. (4),

$$\varphi(x) = (1/\sigma_x\sqrt{2\pi})\,e^{-(x^2/2\sigma_x^2)} \tag{4}$$

then all that is required for determining the probability frequency function, $\varphi(x)$, is the standard deviation, σ_x.

Examination of Eq. (1) indicates that the effects of phasing in the transfer function are obviously not required in determining the probability distributions for the Gaussian case. For the general case—that is,

the non-Gaussian case—it is known that the higher order moments (third, fourth, fifth, etc.) become significant in determining the probability distributions, thus implying a need for the effects of the transfer function phasing. It would be desirable then to determine the equivalent relation given by Eq. (1) which will allow for the calculation of the higher order moments, as well as properly accounting for the effects of transfer function phasing. A development of these relationships is shown as follows:

Consider the following convolution integral relating the input and output responses in the time plane:

$$y(t) = \int_0^\infty x(t - t_1)h(t_1)\, dt_1 \tag{5}$$

where $h(t)$ is the response to a unit impulse and $h(t) = 0$ for $t \leq 0$. The output response for an arbitrary displacement, τ_1, of the input response is

$$y(t + \tau_1) = \int_0^\infty x(t + \tau_1 - t_2)h(t_2)\, dt_2 \tag{6}$$

Similarly, for a second arbitrary displacement, τ_2, in the input response, the output response becomes

$$y(t + \tau_2) = \int_0^\infty x(t + \tau_2 - t_3)h(t_3)\, dt_3 \tag{7}$$

Since the ergodic hypothesis is assumed valid, a three-dimensional correlation function can be formed for the input function and output response from Eqs. (5), (6), and (7). For the output, this correlation function is

$$R_y(\tau_1, \tau_2) = \overline{y(t)\, y(t + \tau_1)y(t + \tau_2)} \tag{8}$$

where the bar denotes an averaging process, as follows:

$$\overline{y(t)y(t + \tau_1)y(t + \tau_2)} = \lim_{T \to \infty} \frac{1}{2T} \int_{-T}^{T} y(t)y(t + \tau_1)y(t + \tau_2)\, dt$$

or substituting Eqs. (5), (6), and (7) into Eqs. (8) gives

$$R_y(\tau_1, \tau_2) = \int_0^\infty \int_0^\infty \int_0^\infty \overline{x(t - t_1)x(t + \tau_1 - t_2)x(t + \tau_2 - t_3)}\, h(t_1)h(t_2)h(t_3)\, dt_1\, dt_2\, dt_3 \tag{9}$$

where the input correlation function is

$$R_x(\tau_1 - t_2 + t_1, \tau_2 - t_3 + t_1) = \overline{x(t - t_1)x(t + \tau_1 - t_2)x(t + \tau_2 - t_3)} \tag{10}$$

Substitution of Eq. (10) into Eq. (9) gives the important relationship for $R_y(\tau_1, \tau_2)$,

$$R_y(\tau_1, \tau_2) = \int_0^\infty \int_0^\infty \int_0^\infty R_x(\tau_1 - t_2 + t_1, \tau_2 - t_3 + t_1)h(t_1)h(t_2)h(t_3)dt_1dt_2dt_3 \tag{11}$$

As is shown in the literature for the two-dimensional case,[5] a Fourier transform pair also exists for the power-spectral density and correlation functions for the three-dimensional case. These relations are

$$G(f_1, f_2) = 2 \int_{-\infty}^\infty \int_{-\infty}^\infty R(\tau_1, \tau_2)e^{-j2\pi(f_1\tau_1 + f_2\tau_2)}\, d\tau_1\, d\tau_2 \tag{12}$$

$$R(\tau_1, \tau_2) = \frac{1}{2} \int_{-\infty}^\infty \int_{-\infty}^\infty G(f_1, f_2)e^{j2\pi(f_1\tau_1 + f_2\tau_2)}\, df_1\, df_2 \tag{13}$$

A derivation of Eqs. (12) and (13) is given in Appendix (A). Substitution of Eq. (11) into Eq. (12) for the case of the output response results in the following expression:

$$G_y(f_1, f_2) = 2 \int_{-\infty}^\infty \int_{-\infty}^\infty \int_0^\infty \int_0^\infty \int^\infty R_x(\tau_1 - t_2 + t_1, \tau_2 - t_3 + t_1)e^{-j2\pi(f_1\tau_1 + f_2\tau_2)}\, h(t_1)h(t_2)h(t_3)dt_1dt_2dt_3d\tau_1d\tau_2 \tag{14}$$

Substitution of the following variables in Eq. (14)

$$p_1 = \tau_1 - t_2 + t_1, \qquad p_2 = \tau_2 - t_3 + t_1 \tag{15}$$

gives the result for $G_y(f_1, f_2)$

$$G_y(f_1, f_2) = 2 \int_{-\infty}^{\infty}\int_{-\infty}^{\infty}\int_{0}^{\infty}\int_{0}^{\infty} R_x(p_1, p_2)e^{-j2\pi[f_1(p_1+t_2-t_1)+f_2(p_2+t_3-t_1)]}\, h(t_1)h(t_2)h(t_3)dt_1dt_2dt_3dp_1dp_2 \tag{16}$$

or

$$G_y(f_1, f_2) = 2 \int_{-\infty}^{\infty}\int_{-\infty}^{\infty} R_x(p_1, p_2)e^{-j2\pi(f_1p_1+f_2p_2)}\, dp_1dp_2 \cdot \left.\begin{aligned} &\int_{0}^{\infty} e^{j2\pi t_1(f_1+f_2)}\, h(t_1)\, dt_1 \cdot \\ &\int_{0}^{\infty} e^{-j2\pi f_1t_2}\, h(t_2)\, dt_2 \cdot \int_{0}^{\infty} e^{-j2\pi f_2t_3}\, h(t_3)\, dt_3 \end{aligned}\right\} \tag{17}$$

but

$$G_x(f_1, f_2) = 2 \int_{-\infty}^{\infty}\int_{-\infty}^{\infty} R_x(p_1, p_2)\, e^{-j2\pi(f_1p_1+f_2p_2)}\, dp_1dp_2 \tag{18}$$

$$H^*(f_1 + f_2) = \int_{0}^{\infty} e^{j2\pi t_1(f_1+f_2)}\, h(t_1)\, dt_1 \tag{19}$$

$$H(f_1) = \int_{0}^{\infty} e^{-j2\pi f_1t_2}\, h(t_2)\, dt_2 \tag{20}$$

$$H(f_2) = \int_{0}^{\infty} e^{-j2\pi f_2t_3}\, h(t_3)\, dt_3 \tag{21}$$

where the asterisk denotes the complex conjugate.

Substitution of Eqs. (18), (19), (20), and (21) into Eq. (17) gives the important relationship,

$$G_y(f_1, f_2) = G_x(f_1, f_2)H^*(f_1 + f_2)H(f_1)\, H(f_2) \tag{22}$$

from which the third central moments for either the input or output can be determined [see Eq. (13) when $\tau_1 = \tau_2 = 0$]

$$\mu_{3x} = R_x(0, 0) = \frac{1}{2}\int_{-\infty}^{\infty}\int_{-\infty}^{\infty} G_x(f_1, f_2)\, df_1\, df_2 \tag{23a}$$

$$\mu_{3y} = R_y(0, 0) = \frac{1}{2}\int_{-\infty}^{\infty}\int_{-\infty}^{\infty} G_y(f_1, f_2)\, df_1df_2 \tag{23b}$$

Note that Eq. (22), which is analogous to Eq. (1) for determining the second moment, introduces the effects of phasing of the transfer function.

The analysis shown for the third moment can be extended to the case of the fourth moment. Since the technique involved is essentially the same, only the significant results are given. The correlation functions for the input and output are defined by the following relations:

$$\left.\begin{aligned} R_x(\tau_1, \tau_2, \tau_3) &= \overline{x(t)\, x(t+\tau_1)\, x(t+\tau_2)x(t+\tau_3)} \\ R_y(\tau_1, \tau_2, \tau_3) &= \overline{y(t)y(t+\tau_1)y(t+\tau_2)y(t+\tau_3)} \end{aligned}\right\} \tag{24}$$

The Fourier transform pair relating the correlation function and the power spectrum for either the input or output is

$$G(f_1, f_2, f_3) = 2\int_{-\infty}^{\infty}\int_{-\infty}^{\infty}\int_{-\infty}^{\infty} R(\tau_1, \tau_2, \tau_3)e^{-j2\pi(f_1t_1+f_2\tau_2+f_3\tau_3)}d\tau_1d\tau_2d\tau_3 \tag{25}$$

$$R(\tau_1, \tau_2, \tau_3) = \frac{1}{2}\int_{-\infty}^{\infty}\int_{-\infty}^{\infty}\int_{-\infty}^{\infty} G(f_1, f_2, f_3)e^{j2\pi(f_1\tau_1+f_2\tau_2+f_3\tau_3)}df_1df_2df_3 \tag{26}$$

The input-output power-spectrum relation, which corresponds to Eqs. (1) and (22), for determining the fourth moment is

$$G_y(f_1, f_2, f_3) = G_x(f_1, f_2, f_3)H^*(f_1 + f_2 + f_3)H(f_1)H(f_2)H(f_3) \tag{27}$$

The fourth central moments for the input and output are

$$\mu_{4x} = R_x(0, 0, 0) = \frac{1}{2}\int_{-\infty}^{\infty}\int_{-\infty}^{\infty}\int_{-\infty}^{\infty} G_x(f_1, f_2, f_3)\, df_1df_2df_3 \tag{28}$$

$$\mu_{4y} = R_y(0, 0, 0) = \frac{1}{2}\int_{-\infty}^{\infty}\int_{-\infty}^{\infty}\int_{-\infty}^{\infty} G_y(f_1, f_2, f_3)\, df_1df_2df_3 \tag{29}$$

From an inspection of the results for the third and fourth central moments, extension of the results to higher order moments becomes obvious; the respective generalized equations for Eqs. (24), (25), (26), (27), (28), and (29) are

$$R_x(\tau_1, \tau_2, \ldots \tau_n) = \overline{x(t)x(t+\tau_1)x(t+\tau_2)\ldots x(t+\tau_n)} \tag{30}$$

$$R_y(\tau_1, \tau_2, \ldots \tau_n) = \overline{y(t)y(t+\tau_1)y(t+\tau_2)\ldots y(t+\tau_n)} \tag{31}$$

$$G(f_1, f_2, \ldots f_n) = 2\int_{-\infty}^{\infty}\int_{-\infty}^{\infty}\cdots\int_{-\infty}^{\infty} R(\tau_1, \tau_2, \ldots \tau_n)e^{-j2\pi(f_1\tau_1+f_2\tau_2+\ldots f_n\tau_n)}\, d\tau_1\, d\tau_2 \ldots d\tau_n \tag{32}$$

$$R(\tau_1, \tau_2, \ldots \tau_n) = \frac{1}{2}\int_{-\infty}^{\infty}\int_{-\infty}^{\infty}\cdots\int_{-\infty}^{\infty} G(f_1, f_2, \ldots f_n)e^{j2\pi(f_1\tau_1+f_2\tau_2+\ldots f_n\tau_n)}df_1df_2 \ldots df_n \tag{33}$$

$$G_y(f_1, f_2 \ldots f_n) = G_x(f_1, f_2, \ldots f_n)H^*(f_1 + f_2 + \ldots f_n)H(f_1)H(f_2), \ldots H(f_n) \tag{34}$$

$$\mu_{n+1x} = R_x(0, 0, \ldots 0_n) = \frac{1}{2}\int_{-\infty}^{\infty}\int_{-\infty}^{\infty}\cdots\int_{-\infty}^{\infty} G_x(f_1, f_2, \ldots f_n)\, df_1\, df_2 \ldots df_n \tag{35}$$

$$\mu_{n+1y} = R_y(0, 0, \ldots 0_n) = \frac{1}{2}\int_{-\infty}^{\infty}\int_{-\infty}^{\infty}\cdots\int_{-\infty}^{\infty} G_y(f_1, f_2, \ldots f_n)\, df_1df_2, \ldots df_n \tag{36}$$

Inspection of Eqs. (30) through (36) indicates that the calculations necessary for determining moments higher than the fourth become extremely laborious. Consequently, a method for determining the probability distribution that requires a minimum number of moments is desirable.

Representation of Non-Gaussian Probability Distributions in Terms of Moments

One of the well-known techniques of estimating a probability distribution is in terms of its moments. This method, introduced by Pearson[6-8] consists in determining a number of moments that are functions of unknown parameters describing the probability functions. For an equal number of known moments and parameters to be estimated, a set of simultaneous equations may be formulated. Solution of the equations with respect to the unknown parameters provides a means of expressing an approximation of the probability frequency function in terms of the measured moments. More refined methods for developing expressions for the probability functions in terms of moments, as well as the implications involved, are available. An excellent dissertation of these techniques, as well as a detailed list of references, is covered by Shohat and Tamarkin.[9]

One special technique of describing the probability distribution and frequency functions in terms of the moments is the Edgeworth series. This technique may be the most practical method for the gust problem, since probability functions of measured load responses appear to be approximately Gaussian. A series representation of the actual distribution in terms of a Gaussian having the same second moment would be advantageous, since only a minimum of terms in the series would be required. Essentially, the Edgeworth series consists of an expansion in terms of the Gaussian distribution, its derivatives, and certain constants. These constants are evaluated with the aid of an orthogonal expansion of Hermite polynomials in terms of known central moments, μ_n, and the standard deviation, σ. If we define $\varphi(x)$ and $\Phi(x)$, the Gaussian frequency and distribution functions, respectively, and $f(x)$ and $F(x)$, the observed frequency and distributions functions, respectively, then the Edgeworth series can be written as

$$f(x) = \varphi(x) - \frac{1}{\underline{|3}}\frac{\mu_3}{\sigma^3}\frac{d^3\varphi(x)}{dx^3} + \frac{1}{\underline{|4}}\left(\frac{\mu_4}{\sigma^4} - 3\right)\frac{d^4\varphi(x)}{dx^4} + \frac{10}{\underline{|6}}\left(\frac{\mu_3}{\sigma^3}\right)^2\frac{d^6\varphi(x)}{dx^6} + \frac{1}{\underline{|5}}\left(\frac{\mu_5}{\sigma^5} - 10\,\frac{\mu_3}{\sigma^3}\right)\frac{d^5\varphi(x)}{dx^5} - \frac{35}{\underline{|7}}\frac{\mu_3}{\sigma^3}\left(\frac{\mu_4}{\sigma^4} - 3\right)\frac{d^7\varphi(x)}{dx^7} - \frac{280}{\underline{|9}}\left(\frac{\mu_3}{\sigma^3}\right)^3\frac{d^9\varphi(x)}{dx^9} \tag{37}$$

where the terms on any one line are of the same order of magnitude. The corresponding expansion for $F(x)$ in terms of $\Phi(x)$ can be obtained from Eq. (37) by replacing $\varphi(x)$ by $\Phi(x)$. For a more detailed discussion of the Edgeworth series, the reader is referred to the excellent dissertation given by Cramér.[10] Examination of Eq. (37) indicates that, if the second, third, and fourth moments are known, a three-term approximation is obtained and appears sufficient for representing either the frequency or distribution functions for approximately Gaussian functions.

Determination of either $f(x)$ or $F(x)$ by Eq. (37), together with the technique developed in the previous section for determining either the input or output mo-

ments, allows for an accurate description of the statistical character of many dynamic problems in a concise mathematical form. As an example, consider the problem of establishing, as well as applying, a rational design criterion for the load factor experienced by an airplane encountering atmospheric turbulence. Old designs that are critical for gust loads and have logged long satisfactory gust experiences can be used to determine the statistical characteristics of turbulence, as well as to establish a "reference" or "level" for new designs—that is, to establish the design probability of exceeding the design gust load related to past safe experience. Analyses of a large number of response time histories of accelerations or stresses measured on these airplanes while penetrating turbulence can be made in the manner suggested herein. The moments and their associated power spectrums, as well as the probability functions, $f(x)$ and $F(x)$, can be obtained for a variety of atmospheric conditions—that is, turbulence over flat land, sea, mountains, etc., as well as turbulence at various altitude levels.

The level of probability of exceeding the design gust load factor must be selected from previous designs that were critical for gust loads. This procedure consists of calculating the probability function, $F(y)$, from records of a large number of airplane responses due to flight in turbulence from the techniques presented herein. For each design, the desired level of probability—that is, the value of $F(y)$ corresponding to y_{design} or $F(y_{\text{design}})$ can be determined. If desired, an average value of $F(y_{\text{design}})$ obtained from several airplanes may be chosen as a rational level of probability. Once $F(y_{\text{design}})$ is known, as well as the statistical properties of turbulence, the value of y_{design} for a new airplane can be determined from its probability function, $F(y)$. The technique of determining $F(y)$ is essentially identical to the inverse problem of determining the $F(x)$ function for atmospheric turbulence from measured airplane responses.

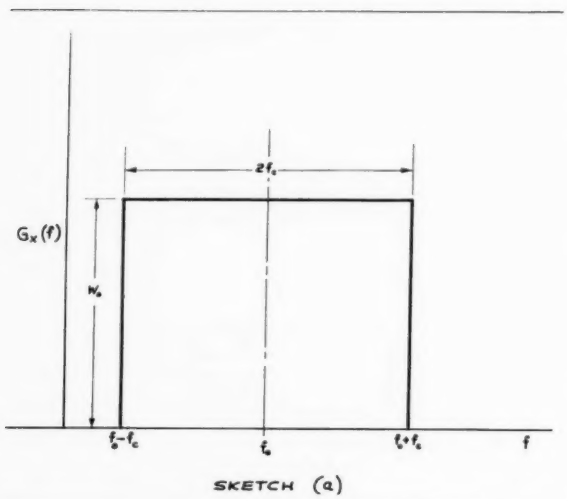

SKETCH (a)

The Special Case of a Non-Gaussian Input and a Gaussian Output

If the bandwidth of the random input, $x(t)$, is much wider than the bandwidth of the system transfer function, then the output, $y(t)$, is *often* Gaussian. Proof of this result is possible with the aid of a theorem due to Liapounoff given in Cramér (reference 10, page 215). Essentially, this theorem states that, if the output is a result of a sum of independent variables,

$$y(t) = y_1(t) + y_2(t) \ldots y_n(t)$$

with mean m_{y_ν}, and standard deviation, σ_{y_ν}, and the third absolute moment of $y_\nu(t)$, about its mean,

$$\eta_{y_\nu}{}^3 = E(|y_\nu - m_{y_\nu}|^3)$$

is finite for every $\nu = 1, 2, 3 \ldots n$, where

$$\eta_y{}^3 = \eta_{y_1}{}^3 + \eta_{y_2}{}^3 + \eta_{y_3}{}^3 + \ldots \eta_{y_n}{}^3$$

then the sum $y(t) = y_1(t) + y_2(t) + \ldots y_n(t)$ is asymptotically Gaussian if

$$\lim_{n \to \infty} \eta_y / \sigma_y \to 0 \tag{38}$$

Assume the following conditions:

(1) Mean of the input, $\bar{x}$, equal to zero (no loss of generality results from choosing zero mean).

(2) The input power spectrum (two-dimensional), $G_x(f)$, is constant with respect to the system transfer function, $H(f)$. [See Sketch (a)].

Let f_0 be the natural frequency of $H(f)$ and let f_c approach infinity or in the time plane $\Delta\tau = 1/2f_c$ approach zero. For this specified input power spectrum, $G_x(f)$, it can be shown[5] that the standard deviation of the input is

$$\sigma_x{}^2 = w_0/2\Delta\tau \tag{39}$$

The standard deviation of the output can be expressed in terms of σ_x and the system response to an impulse, $h(t)$, with the aid of the convolution integral. Writing this integral in finite form, the output standard deviation becomes

$$\sigma_y{}^2 = \sum_0^\infty \sigma_x{}^2 h^2(t - \tau)\ (\Delta\tau)^2 \tag{40}$$

Substitution of Eq. (39) into Eq. (40) gives

$$\sigma_y{}^2 = \frac{w_0}{2} \sum_0^\infty h^2(\tau)\Delta\tau \tag{41}$$

For the third absolute moment the convolution integral can again be used to give the relation

$$\eta_y{}^3 = \sum_0^\infty \eta_x{}^3 h^3(t - \tau)\ (\Delta\tau)^3 \tag{42}$$

If the condition given by Eq. (38) is to be satisfied as

f_c approaches infinity (or Δt approaches zero), then η_y must approach zero, since σ_y must always be greater than zero [$H(f)$ is not an impulse]. In order that η_y approach zero, it is seen from Eq. (42) that $\eta_x{}^3$ must approach $1/(\Delta t)^2$ as $\Delta\tau$ approaches zero for finite $h(t)$. For the output, $y(t)$, to be Gaussian, η_y/σ_y approaches zero if $\eta_x{}^3$ approaches infinity slower than $1/(\Delta\tau)^2$ approaches infinity. But since $\sigma_x{}^2$ is proportional to $1/\Delta\tau$ [Eq. (2)], then $\eta_x{}^{3/2}$ must approach infinity slower than $\sigma_x{}^2$ approaches infinity. Thus if the input is non-Gaussian but its spectrum is wide compared with the spectrum of the system transfer function, then the output is Gaussian if the input second moment and third absolute moment are such that

$$0(\sigma_x{}^{4/3}) > 0(\eta_x) \tag{43}$$

where the order 0 means the rate as σ_x or η_x converges to infinity.

Consideration of the significance of Eq. (43) indicates that, unless the input probability function contains an abnormally large amount of skewness, the output distribution is Gaussian. Although in many instances little or no information may be available on the second and third absolute input moments, calculations for these quantities for satisfying the requirement given by Eq. (43) can be made from measured output responses employing the techniques developed in the present paper.

For turbulence problems, it is doubtful that its probability frequency function contains sufficient skewness to violate the requirement given by Eq. (43). In order to obtain some physical insight as to the meaning of Eq. (43), an example is shown which will indicate the relative order of skewness and standard deviation for a well-known unsymmetrical probability function, the Rayleigh, defined as follows:

$$\left.\begin{aligned} f(x) &= 0 \quad (\text{for } x \leq 0) \\ f(x) &= (x/a^2)e^{-x^2/2a^2} \quad (\text{for } x \geq 0) \end{aligned}\right\} \tag{44}$$

A plot of Eq. (44) for a typical value of a is given in Sketch b.

The standard deviation of $f(x)$ defined by Eq. (44) is

$$\sigma_x = a\sqrt{2 - (\pi/2)} \tag{45}$$

while its mean is

$$m_x = a\sqrt{\pi/2} \tag{46}$$

Substitution of the change in variable

$$u = x - m_x$$

in Eq. (44) gives the following result:

$$f(u) = \frac{u + m_x}{a^2}\, e^{-(u+m_x)^2/2a^2} \quad (\text{for } u \geq -m_x) \tag{47}$$

The third absolute moment cubed of $f(u)$ is

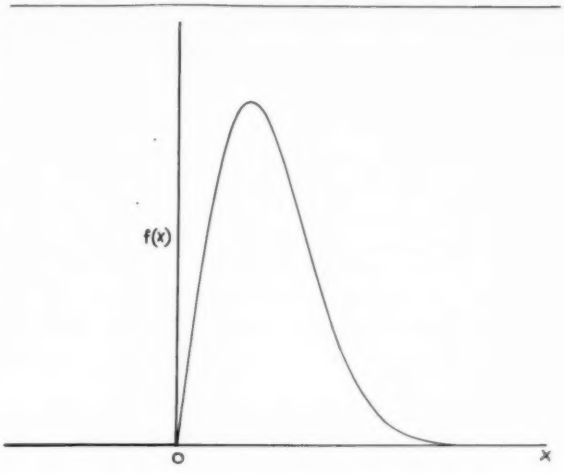

SKETCH (b)

$$\eta_u{}^3 = \int_{-m_x}^{\infty} |u|^3 \left(\frac{u + m_x}{a^2}\right) e^{-(u+m_x)^2/2a^2}\, du \tag{48}$$

Let $v = u/a$ and substitute Eq. (46) into Eq. (48); the resulting equation becomes

$$\eta_v{}^3 = a^3 \int_{-\sqrt{\pi/2}}^{\infty} |v|^3 \left(v + \sqrt{\frac{\pi}{2}}\right) e^{-(v+\sqrt{\pi/2})^2/2}\, dv \tag{49}$$

Since the value of the integral in Eq. (49) is not a function of a, then $\eta_v{}^3$ is proportional to a^3 or $\eta_x{}^3$ is proportional to a^3. This result, together with the proportionality of σ_x to a given by Eq. (45), gives the relationship of the order of σ_x to η_x as

$$0(\sigma_x) = 0(\eta_x) \tag{50}$$

Thus the $0(\sigma_x{}^{4/3})$ must be greater than the $0(\eta_x)$, and Eq. (43) is satisfied; consequently, a Rayleigh probability frequency function input that has a wide bandwidth power spectrum compared with the system transfer function leads to a Gaussian output.

In the application of the results presented herein for turbulence problems, the bandwidth of the input power spectrum will be large compared with the system transfer function if the system is only slightly damped. Such may be the case of an airplane component such as a tail buffeting near its flutter speed or if the airplane, while traversing atmosphere turbulence, experiences a large rearward center of gravity movement that substantially reduces the damping of its short-period oscillation. For these cases, experimental investigation of the character of the second moment and third absolute moment of the input probability functions appears desirable in view of the possible simplifications in describing the output probability functions if the input is non-Gaussian.

In the investigation of deducing the input characteristics from a measured output, it appears advisable that, in order to obtain the best estimate of the input characteristics, the system transfer function should have a bandwidth comparable with that of the input. If the bandwidth of the system transfer function is extremely narrow compared with the input, then the accuracy of the input power spectrums would be questionable at all frequencies except the natural frequency of the system transfer function; as an additional consequence, all the calculated moments of the input probability function would also be questionable.

Concluding Remarks

The higher order moments above the second of the probability functions for either the input forcing function or the output response of a linear system are determined from an extension of power-spectral methods of generalized harmonic analysis. Examination of the generalized expressions for determining any order moment indicates that the calculations necessary for determining moments higher than the fourth become extremely laborious. Methods are discussed for describing probability functions in terms of the moments with special interest to one that requires a minimum number. For the special case of a non-Gaussian forcing function that has a wide bandwidth compared with the bandwidth of the system transfer function, it is shown that for most cases the output response will be Gaussian. The final determination of whether the output response is Gaussian depends on the relative order of the second moment and the third absolute moment of the input probability functions.

Appendix (A)

Proof of Fourier transform pair:

$$G(f_1, f_2) = 2\int_{-\infty}^{\infty}\int_{-\infty}^{\infty} R(\tau_1, \tau_2)\, e^{-j2\pi(f_1\tau_1+f_2\tau_2)}\, d\tau_1 d\tau_2 \tag{A-1a}$$

$$R(\tau_1, \tau_2) = \frac{1}{2}\int_{-\infty}^{\infty}\int_{-\infty}^{\infty} G(f_1, f_2) e^{j2\pi(f_1\tau_1+f_2\tau_2)}\, df_1 df_2 \tag{A-1b}$$

Let

$$R(\tau_1, \tau_2) = \lim_{T\to\infty} C_T(\tau_1, \tau_2) \tag{A-2}$$

where

$$C_T(\tau_1, \tau_2) \equiv \frac{1}{2T}\int_{-\infty}^{\infty} y_T(t) y_T(t+\tau_1) y_T(t+\tau_2)\, dt \tag{A-3}$$

and where

$$y_T = y(t) \qquad (\text{for } -T \le t \le T)$$
$$y_T = 0 \qquad (\text{elsewhere})$$

The Fourier transform of C_T can be written as follows:

$$\int_{-\infty}^{\infty}\int_{-\infty}^{\infty} C_T(\tau_1, \tau_2) e^{-j2\pi(f_1\tau_1+f_2\tau_2)}\, d\tau_1 d\tau_2 = \frac{1}{2T}\int_{-\infty}^{\infty} e^{j2\pi(f_1+f_2)t}\, y_T(t) dt \cdot \int_{-\infty}^{\infty} e^{-j2\pi f_1(t+\tau_1)}\, y_T(t+\tau_1)\, d\tau_1 \cdot \int_{-\infty}^{\infty} e^{-j2\pi f_2(t+\tau_2)}\, y_T(t+\tau_2) d\tau_2 \tag{A-4}$$

Let $s_1 = t + \tau_1$ and $s_2 = t + \tau_2$, and Eq. (A-4) then becomes

$$\int_{-\infty}^{\infty}\int_{-\infty}^{\infty} C_T(\tau_1, \tau_2) e^{-j2\pi(f_1\tau_1+f_2\tau_2)}\, d\tau_1 d\tau_2 = \frac{1}{2T}\int_{-\infty}^{\infty} y_T(t) e^{j2\pi(f_1+f_2)t} dt \cdot \int_{-\infty}^{\infty} e^{-j2\pi f_1 s_1}\, y_T(s_1)\, ds_1 \cdot \int_{-\infty}^{\infty} e^{-j2\pi f_2 s_2}\, y_T(s_2)\, ds_2 \tag{A-5}$$

but

$$A_T^*(f_1 + f_2) = \int_{-\infty}^{\infty} y_T(t) e^{j2\pi(f_1+f_2)t}\, dt \tag{A-6}$$

$$A_T(f_1) = \int_{-\infty}^{\infty} y_T(s_1) e^{-j2\pi f_1 s_1} ds_1 \tag{A-7}$$

$$A_T(f_2) = \int_{-\infty}^{\infty} y_T(s_2) e^{-j2\pi f_2 s_2} ds_2 \tag{A-8}$$

where the asterisk denotes the complex conjugate. Substitution of Eqs. (A-6), (A-7), and (A-8) into Eq. (A-5) results in the following expression for the Fourier transform of $C_T(\tau_1, \tau_2)$:

$$\int_{-\infty}^{\infty}\int_{-\infty}^{\infty} C_T(\tau_1, \tau_2) e^{-j2\pi(f_1\tau_1 + f_2\tau_2)} d\tau_1 d\tau_2 = \frac{1}{2T} A_T^*(f_1 + f_2) A_T(f_1) A_T(f_2) \tag{A-9}$$

If we define the power spectrum function as

$$G(f_1, f_2) \equiv \lim_{T\to\infty} (1/T) A_T^*(f_1 + f_2) A_T(f_1) A_T(f_2)$$

then Eq. (A-9) becomes

$$\frac{G(f_1, f_2)}{2} = \lim_{T\to\infty} \int_{-\infty}^{\infty}\int_{-\infty}^{\infty} C_T(\tau_1, \tau_2) e^{-j2\pi(f_1\tau_1 + f_2\tau_2)} d\tau_1 d\tau_2 \tag{A-10}$$

Substitution of Eq. (A-2) into Eq. (A-10) gives Eq. (A-1a). Eq. (A-1b) is a direct consequence of the inverse Fourier transform and may easily be verified.

REFERENCES

[1] Press, H., and Mazelsky, B., *A Study of the Application of Power-Spectral Methods of Generalized Harmonic Analysis to Gust Loads on Airplanes*, NACA TN No. 2853, 1953.

[2] Clementson, G. C., *An Investigation of the Power Spectral Density of Atmospheric Turbulence*, Ph.D. Thesis, M.I.T., 1950.

[3] Liepmann, H. W., *On the Application of Statistical Concepts to the Buffeting Problem*, Journal of the Aeronautical Sciences, Vol. 19, No. 12, pp. 793–800, December, 1952.

[4] Fung, Y. C., *Statistical Aspects of Dynamic Loads*, Journal of the Aeronautical Sciences, Vol. 20, No. 5, pp. 317–329, May, 1953.

[5] James, H. M., Nichols, N. B., and Phillips, R. S., *Theory of Servomechanisms;* McGraw-Hill Book Company, Inc., New York, 1947.

[6] Pearson, K., *Contributions to the Mathematical Theory of Evolution,* Philosophical Transactions of the Royal Society, London, A., 185, 1894.

[7] Pearson, K., *Contributions to the Mathematical Theory of Evolution, IV: On the Probable Errors of Frequency Constants and on the Influence of Random Selection on Variation and Correlation*, Philosophical Transactions of the Royal Society, London, A., 191, 1898.

[8] Pearson, K., *On the Systematic Fitting of Curves to Observations and Measurements*, Philosophical Transactions of the Royal Society, London, B., 1 and 2, 1902.

[9] Shohat, J. A., and Tamarkin, J. D., *Problem of Moments*, American Mathematical Society, 1943.

[10] Cramér, H., *Mathematical Methods of Statistics;* Princeton University Press, Princeton, N.J., 1946.

An Authorized Binding for Journal of the Aeronautical Sciences

Arrangements have been made by the Institute of the Aeronautical Sciences for members and subscribers to have their Journals bound into distinctively designed books.

Twelve issues, January through December, bound in best grade blue washable buckram, imprinted with your name on cover, cost but $3.45 per volume.

Ship Journals parcel post insured. Within 30 days after receipt, bound volumes will be shipped prepaid in the U.S.A. Full remittance must accompany order.

Publishers' Authorized Bindery Service
(*Binders of all Journals*)

308 West Randolph St. Chicago 6, Ill.

Effect of Diffusion Fields on the Laminar Boundary Layer

JOHN W. SMITH*
Bell Aircraft Corporation

ABSTRACT

A theory is developed which describes the effect of a general diffusion field on the dynamic and thermal characteristics of a laminar boundary layer on a flat plate in steady compressible flow. Fluid properties are considered as functions of temperature and local concentration of the foreign gas. The diffusion field is described by a differential equation that relates convective and diffusion transfer and which considers diffusion currents arising from gradients of concentration and temperature. By means of the usual transformations the system is reduced to a set of ordinary differential equations, which in turn are transformed into a set of integral equations. The latter is amenable to solution by the method of successive approximations.

The theory and results have bearing on the problem of control and reduction of aerodynamic heating at hypersonic speeds. The special feature of this approach lies in the utilization of diffusion fields for the purpose of reducing the detrimental effects of viscous dissipation. Although the theory is adapted to a fuller investigation of this problem, the numerical examples considered involve mainly diffusion fields of helium, with which good results have been achieved at Mach Numbers 8 and 12. Whereas at the higher Mach Number the influx of heat was practically eliminated, a reversal in the direction of heat flow has been effected at the lower Mach Number.

LIST OF SYMBOLS

c_p = specific heat at constant pressure
C_i = constants of integration in Eq. (2.8)
$\vec{C}_i$ = average peculiar velocity (cf. reference 5)
D_{12} = coefficient of mutual diffusion
$f(\eta)$ = dimensionless stream function [cf. Eq. (3.10)]
F_n = functions defined by Eq. (3.18)
$\vec{J}_n$ = diffusion current
k = thermal conductivity
K_n = constants of integration
M = Mach Number
n = total particle density
n_1 = foreign particle density
n_{10} = (n_1/n)
p = pressure
P_r = Prandtl Number
t = (T/T_0)
T = absolute temperature
u, v = boundary-layer velocity components in x, y directions, respectively
x, y = coordinates parallel and perpendicular to flat plate surface, respectively
α = thermal diffusion constant
β_n = constants defined by Eq. (2.19)
γ = ratio of specific heats
η = independent variable introduced by Eqs. (2.10) and (3.10)
λ = (D_{12}/ν_0)
μ = coefficient of viscosity
ν = kinematic viscosity
ρ = density
ϕ_n = functions defined by Eq. (3.11)
ϕ_{ni} = functions defined by Eq. (3.23)
ψ = stream function
Ψ_n = functions defined by Eq. (3.18)

Subscript 0 generally refers to free-stream quantities.
Subscript aw refers to adiabatic wall conditions.
Primes indicate differentiation with respect to η.

Received September 22, 1953.

* Aerodynamicist. Present Address: 17 E. 94th St., New York 28, N.Y.

(1) INTRODUCTION

THE BASIC MATERIAL UNIT considered in standard theories of fluid mechanics is the fluid particle, which is conceived as a volume of fluid having the following properties: It is arbitrarily small compared with the macroscopic dimensions of the physical system, yet it encloses a sufficiently great number of molecules so that fluctuations in pressure, temperature, and density can be neglected. The fluid particle is considered to move with a velocity that at each point is equal to the macroscopic flow velocity described by the standard equations of fluid mechanics, and its trajectories are just the stream lines of laminar flow. Now let us suppose that the molecules constituting a fluid particle at a given instant are labeled in some way. One would then observe a diffusion current of these molecules flowing out of the fluid particle in all directions, until the given set of molecules has distributed itself throughout the entire system. This diffusion current is itself a macroscopic phenomenon, observable through ordinary instruments, and must not be confused with the Brownian motion executed by individual molecules. The reason that diffusion currents can be ignored in most discussions of fluid mechanics arises from the circumstance that the constituent molecules of the physical system are assumed to be dynamically equivalent, in which event the diffusion transfer does not affect the characteristics of the flow.

The local concentration of special molecules, defined either as a particle density or as a mole fraction, may be considered as a parameter defined at each point in the flow and constituting a field. This diffusion field can be determined theoretically by integration of a differential equation that is analogous to the continuity equation of ordinary fluid mechanics and which ex-

presses the conservation of special molecules. As was pointed out above, the special case of diffusion transfer involving dynamically equivalent molecules leads to great simplifications because the velocity, temperature, and pressure fields are unaffected by the diffusion transfer and can be calculated without recourse to the diffusion equation. Diffusion of active nitrogen into inert nitrogen and mutual diffusion of isotopes of a given element are instances of diffusion problems that may be considered in this fashion, since the condition of dynamic equivalence is closely satisfied. In general, however, such parameters as density, specific heat, viscosity, etc., which enter into the ordinary flow equations, depend strongly on the concentration of special molecules, for which reason the ordinary flow equations cannot be solved without recourse to the equation of diffusion.

The present paper concerns itself with steady-state diffusion fields of a foreign gas in the laminar boundary layer on a flat plate and its effect on the dynamic and thermal boundary-layer profiles. Apart from the theoretical interest attaching to the given problem, the theory has important bearing on boundary-layer control through fluid injection, a topic that has received considerable attention in recent literature.[1] Most theoretical treatments of fluid injection assume dynamically equivalent fluids and study effects that are entirely different from the effect considered in this paper. The now classical report of Schlichting and Bussmann,[2] for instance, studies the effect of maintaining a nonvanishing normal velocity at the wall on the velocity profiles of an incompressible boundary layer. Other reports have studied the cooling of a compressible boundary layer through injection of liquid air, which, in addition to the effect considered by Schlichting and Bussmann, involves energy transfer between the boundary layer and coolant. Although the present theory is fundamentally adequate to account for these various conditions, the sample problems given here have isolated for consideration the special effect of the diffusion field of a foreign gas on the velocity and temperature profiles of a laminar boundary layer.

This effect appears when the physical characteristics of the foreign gas, such as density, viscosity, heat conductivity, and specific heat, differ appreciably from those of the primary gas. The qualitative and quantitative character of the effect depends, of course, on the particular foreign gas selected. A thorough investigation of this problem would utilize hypothetical gases for which the combination of physical characteristics can be varied at will, and the influence of these characteristics on the boundary layer profiles could be studied systematically. In this fashion one could find criteria for the selection of particular foreign gases best suited for any given purpose of boundary-layer control. Because of the rather time-consuming nature of the numerical calculations, especially for the compressible case, we have adopted the simpler program of selecting for consideration one or two special gases that have interesting and possibly useful physical characteristics and for which empirical determinations of the relevant physical constants have been made. Hydrogen and helium, both notable for their low densities, high heat conductivities, and high specific heats, were considered in the isothermal (low-speed) problem, and helium alone was considered in the case of compressible (hypersonic) flow. As will be seen in Sections (3) and (4), helium gas holds great promise as a coolant to be applied in flight régimes where aerodynamic heating would become important.

The simpler case of isothermal boundary-layer flow has been investigated first, and the theory was later extended to the more complicated case of compressible flow with dissipation of kinetic energy. It was thought expedient, for reasons of clarity, to follow the same development in the present paper. Section (2), therefore, contains a brief account of the simpler problem, while the main theory is presented in Section (3).

(2) Isothermal Boundary Layers

(a) Basic Equations

The laminar dynamic boundary layer on a flat plate is described, as usual, by three differential equations, expressing conservation of mass, conservation of x-momentum, and conservation of y-momentum, respectively,

$$(\partial/\partial x)(\rho u) + (\partial/\partial y)(\rho v) = 0 \tag{2.1}$$

$$\rho u \frac{\partial u}{\partial x} + \rho v \frac{\partial u}{\partial y} = \frac{\partial}{\partial y}\left(\mu \frac{\partial u}{\partial y}\right) \tag{2.2}$$

$$\partial p/\partial y = 0 \tag{2.3}$$

Because of Eq. (2.3), the pressure must be constant throughout the field. The condition that the boundary layer be isothermal implies, therefore, that the density ρ and the coefficient of viscosity μ are functions of the concentration parameter only. Suppose n_1 denotes the particle density of foreign gas, and n denotes the total particle density. According to Avogadro's law, n is constant throughout the boundary layer, and we can dimensionalize n_1 by referring it to n. The quantity $n_{10} = n_1/n$, which is the local mole fraction of foreign gas, will be considered as the basic concentration parameter that defines the diffusion field.

The diffusion current $\vec{J}_1$ is defined as the total quantity of special molecules (expressed here in terms of mole fractions) flowing through unit area perpendicular to the flow direction in unit time. At constant temperature and pressure and in the absence of body forces, the diffusion current can be related to the diffusion field through the equation,

$$\vec{J}_1 = -D_{12} \operatorname{grad} n_{10} \tag{2.4}$$

where the coefficient of mutual diffusion D_{12} is largely independent of concentration. The differential equation expressing the conservation of special molecules is derived by balancing the convection and diffusion currents,

$$u(\partial n_{10}/\partial x) + v(\partial n_{10}/\partial y) = -\operatorname{div} \vec{J} \tag{2.5}$$

Using Eq. (2.4) and assuming that $\partial^2/\partial x^2 \ll \partial^2/\partial y^2$, the diffusion equation for the isothermal boundary layer becomes

$$u\frac{\partial n_{10}}{\partial x} + v\frac{\partial n_{10}}{\partial y} = D_{12}\frac{\partial^2 n_{10}}{\partial y^2} \tag{2.6}$$

(b) *Self-Diffusion*

The somewhat trivial case of self-diffusion deserves brief mention, because it is easily dealt with and has an interesting application. If the special molecules are dynamically equivalent to the primary molecules, then ρ and μ are constant, and the x-momentum equation can be written in the form

$$u(\partial u/\partial x) + v(\partial u/\partial y) = \nu(\partial^2 u/\partial y^2) \tag{2.7}$$

where ν is the kinematic viscosity. The coefficient of self-diffusion D_{11} has the dimensions of kinematic viscosity and, in fact, has roughly the same magnitude. To a first approximation, at least, D_{11} can be identified with ν. It is evident, then, from a comparison of Eqs. (2.6) and (2.7), that the solution for the concentration profile is obtained as a linear function of the velocity profile,

$$n_{10} = C_1 + C_2 u \tag{2.8}$$

C_1 and C_2 being constants of integration.

The fact that the concentration profile for self-diffusion coincides, roughly, with the velocity profile for isothermal flow over a flat plate could be utilized for the purpose of boundary-layer visualization. The obvious experiment that is suggested by this result consists in the use of active nitrogen to be introduced into an inert boundary layer through some permeable wall. It is supposed that this can be done in such a manner that the boundary-layer flow is virtually undisturbed. One can expect that an orange glow will appear in the boundary-layer region, the thickness of which is commensurate with the thickness of the dynamic boundary layer, and that the transition point should be conspicuous.

(c) *Mutual Diffusion: Method of Solution*

For mutual diffusion, the problem is complicated by the fact that the local density and viscosity become functions of the concentration parameter n_{10}. An important simplification is achieved by assuming that both u and n_{10} are functions of the similarity parameter η alone, where $\eta \sim yx^{-1/2}$. This assumption is justified so long as the boundary conditions permit all relevant quantities to remain constant at $y = 0$, with the exception of the normal velocity v. The latter may, in general, be permitted to vary inversely as the square root of x. When these conditions are satisfied, it is possible to reduce the given system of partial differential equations to a system of total differential equations, which is more amenable to numerical integration.

Let a stream function ψ, a similarity variable η, and a function $f(\eta)$ be introduced through the following relations:

$$u = \frac{\rho_0}{\rho}\frac{\partial \psi}{\partial y}; \qquad v = -\frac{\rho_0}{\rho}\frac{\partial \psi}{\partial x} \tag{2.9}$$

$$\eta = (1/2)y\sqrt{\rho_0 u_0/\mu_0 x} \tag{2.10}$$

$$\psi = \sqrt{\nu_0 x u_0}\, f(\eta) \tag{2.11}$$

where the subscript zero indicates free-stream conditions. The continuity equation is automatically satisfied through use of a stream function, and only Eqs. (2.2) and (2.6) remain to be considered. These can be transformed to the (x, η)-plane, using the transformation formulas,

$$\left.\begin{aligned} [\partial/\partial y]_x &= (1/2)\sqrt{\rho_0 u_0/\mu_0 x}\,(\partial/\partial \eta) \\ [\partial/\partial x]_y &= (\partial/\partial x) - (1/2)x^{-1}\eta(\partial/\partial \eta) \end{aligned}\right\} \tag{2.12}$$

When the given transformation formulas are applied to Eq. (2.9), there results the following expression for the velocity components:

$$\left.\begin{aligned} u &= (1/2)u_0(\rho_0/\rho)\,(df/d\eta) \\ v &= \frac{1}{2}\sqrt{\frac{\mu_0 u_0}{\rho_0 x}}\left(\frac{\rho_0}{\rho}\right)\left(\eta\frac{df}{d\eta} - f\right) \end{aligned}\right\} \tag{2.13}$$

Using Eqs. (2.12) and (2.13) and dropping terms that involve derivatives with respect to x at constant η, one can transform the x-momentum and diffusion equations into the following ordinary differential equations, respectively:

$$f(\phi_2^{-1}f')' + [\phi_1(\phi_2^{-1}f')']' = 0 \tag{2.14}$$

$$\lambda n_{10}'' + \phi_2^{-1} f n_{10}' = 0 \tag{2.15}$$

where

$$\phi_1 = \mu_0^{-1}\mu; \quad \phi_2 = \rho_0^{-1}\rho; \quad \lambda = \nu_0^{-1}D_{12} \tag{2.16}$$

and primes denote differentiation with respect to η.

Apart from the strongly nonlinear character of Eq. (2.14), it should be observed that the solutions are required to satisfy two-point boundary conditions—i.e., conditions at $\eta = 0$ and $\eta = \infty$. The method of solution most suitable to problems of this kind is one that has been utilized in several papers dealing with boundary-layer theory. Notable among these, perhaps, is the early paper by H. Schuh,[3] which describes the given

method of solution and also gives some consideration to the diffusion problem. The essential steps of the procedure are, first, to transform the differential equations to a set of integral equations; and, second, to solve the latter by the method of successive approximations [the specific advantages of which will be more fully discussed in Section (3)].

Eqs. (2.14) and (2.15) are easily converted into the required integral forms. Eliminate the square brackets of Eq. (2.14) by carrying out the differentiation, and divide both sides by $(\phi_2^{-1}f')'$. Integrate once and take the antilogarithm of both sides. After performing two further successive integrations, one obtains the following integral equation corresponding to Eq. (2.14):

$$f = [f]_0 + K_1 \int_0^\eta \phi_2 \int_0^\eta \phi_1^{-1} \times \exp\left\{-\int_0^\eta \phi_1^{-1} f \, d\eta\right\} d\eta \, d\eta \quad (2.17)$$

The integration constant K_1 can be adjusted through the condition that $\lim_{\eta \to \infty} f' = 2$, which means, according to Eq. (2.13), that the x-component of velocity approaches the free-stream value asymptotically. The integration constant $[f]_0$, which according to Eq. (2.13) is related to the normal velocity component at $\eta = 0$, may be left unspecified. The third integration constant has been set equal to zero, in accordance with the no-slip condition that is generally imposed upon the x-component of velocity at the wall.

In a similar manner one can derive the following integral form of the equation of diffusion:

$$n_{10} = [n_{10}]_0 + K_3 \int_0^\eta \exp\left\{-\frac{1}{\lambda}\int_0^\eta \phi_2^{-1} f d\eta\right\} d\eta \quad (2.18)$$

(*d*) *Sample Problems*

To illustrate the convergence of the successive approximations and to gain some insight into the nature of a diffusion field and its effect on the velocity profile, Eqs. (2.17) and (2.18) have been solved for two special cases: diffusion of hydrogen and helium into atmospheric air at standard (N.T.P.) thermodynamic conditions. All requisite physical data could be obtained from the International Critical Tables,[4] with the exception of D_{12} for helium-air mixtures. The latter was estimated from some data given in reference 8 [see Section (3)].

According to Avogadro's law, the density of a binary gas mixture is a linear function of the composition parameter. The same is not exactly true for viscosity coefficients and other transfer characteristics, but experimental data indicate that the deviations from linearity are generally small. For the purpose of this investigation it will be sufficiently accurate to represent the functions ϕ_n in the form

$$\phi_n = 1 + \beta_n n_{10} \quad (2.19)$$

where the β_n are constants.

From the appropriate experimental data, one can derive the following set of constants characterizing the two given problems:

	H_2 – Air	He – Air
β_1 =	−0.507	0.097
β_2 =	−0.931	−0.862
λ =	4.63	3.94

The subject of boundary conditions will be discussed in Section (4). Here we state only that the boundary conditions imposed in the given sample problems are as follows:

$$f = f' = 0; \quad n_{10} = 1 \text{ at } y = 0; \quad f' = 2; \quad n_{10} = 0 \text{ at } y = \infty \quad (2.20)$$

The zero-order solution for f, which may be taken to correspond to the case where foreign gas is entirely absent from the boundary layer, turns out to be the well-known Blasius function. The zero-order solution for n_{10}, corresponding to the same case, is identically zero. Convergence of the process of successive approximations, as illustrated in Fig. 1 for the hydrogen diffusion problem, is entirely satisfactory. The numerical calculation can be greatly shortened, of course, by antic-

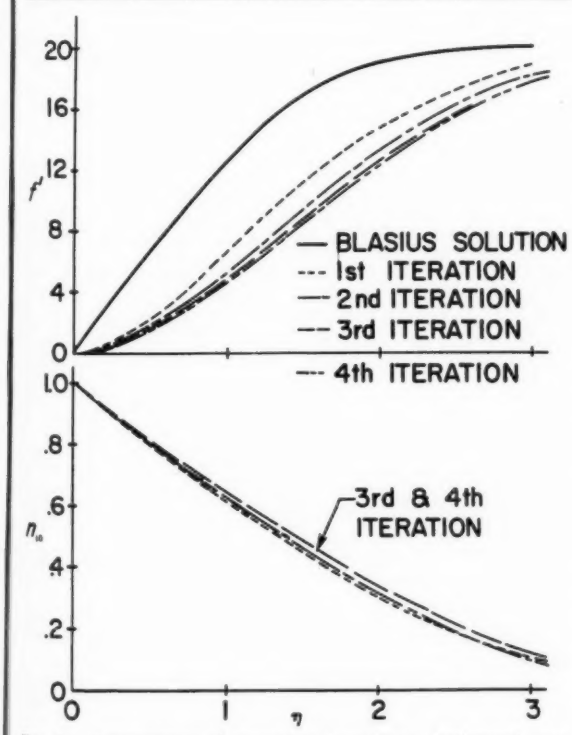

FIG. 1. Convergence of successive iterations: isothermal case (hydrogen diffusion field).

ipating the course of future iterations in order to pick a better trial function.

The velocity and concentration profiles for both hydrogen and helium diffusion are given in Fig. 2. It is interesting to note, in the first place, that the concentration profiles are almost identical. This fact is indicative of a certain insensitivity of the concentration profiles, which is also confirmed by the rapid convergence indicated in Fig. 1. So far as the velocity profiles are concerned, we can conclude (at least for the isothermal case considered here) that low density tends to lessen the velocity gradients, while low viscosity has the opposite effect.

(3) The General Theory

(a) *Basic Equations*

The fundamental boundary-layer equations for variable fluid properties and for vanishing external pressure gradient may be given in the form*

$$\rho u \frac{\partial u}{\partial x} + \rho v \frac{\partial u}{\partial y} = \frac{\partial}{\partial y}\left(\mu \frac{\partial u}{\partial y}\right) \qquad (3.1)$$

$$\partial p/\partial y = 0 \qquad (3.2)$$

$$(\partial/\partial x)(\rho u) + (\partial/\partial y)(\rho v) = 0 \qquad (3.3)$$

$$\rho u \frac{\partial}{\partial x}(c_p T) + \rho v \frac{\partial}{\partial y}(c_p T) = \frac{\partial}{\partial y}\left(k \frac{\partial T}{\partial y}\right) + \mu \left(\frac{\partial u}{\partial y}\right)^2 \qquad (3.4)$$

The first two equations express conservation of x- and y-momentum, respectively. The third equation expresses conservation of mass, while the last equation expresses conservation of energy. The quantities ρ, μ, k, and c_p depend on temperature and on the concentration parameter. For this reason it is necessary to introduce an additional differential equation describing the diffusion field before the given system can be integrated.

The diffusion equation that is applicable to the general case contemplated in this section is not identical with the diffusion equation for isothermal flow, the latter being a special case of it. This circumstance arises, in the first place, from the dependence of the total particle density n on temperature and, in the second place, from the fact that the diffusion current depends not only on concentration gradient but on temperature gradient as well. Let $\vec{C}_i$ represent the average peculiar velocity of molecules of type i, as defined by Chapman and Cowling.[5] We define the diffusion current $\vec{J}_1$ to be the number of foreign gas molecules flowing across a unit area perpendicular to $\vec{C}_1$ in unit time—viz.,

$$\vec{J}_1 = n_1 \vec{C}_1 \qquad (3.5)$$

* Neglecting diffusion thermo effect.

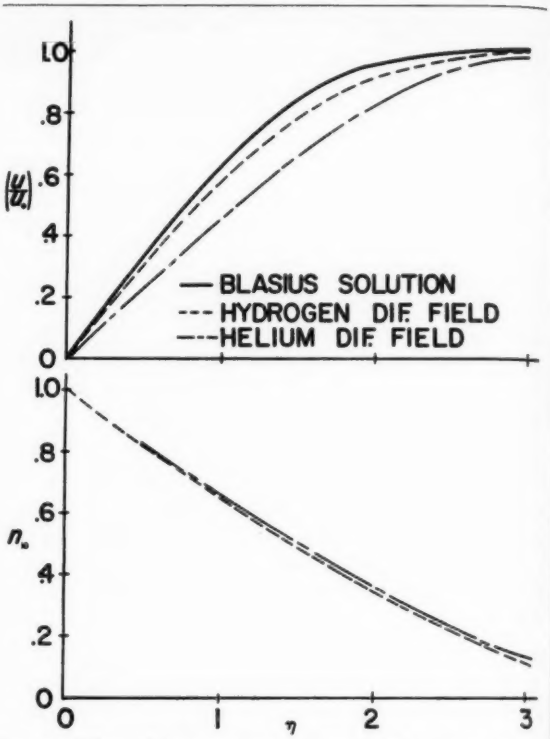

Fig. 2. Effect of hydrogen and helium diffusion fields in air: isothermal case.

where n_1 represents the particle density of foreign molecules. Conservation of foreign molecules implies that the number of foreign molecules entering a given volume in unit time through convection equals the number departing through diffusion. The general form of the diffusion equation is, therefore,

$$u(\partial n_1/\partial x) + v(\partial n_1/\partial y) = -\text{div } \vec{J}_1 \qquad (3.6)$$

The variability of n with temperature, as mentioned above, implies that it is no longer possible to replace n_1 by the dimensionless parameter $n_{10} = n_1/n$ in the convection term.

From the formulas given in reference 5, one can derive the following expression for the diffusion current:†

$$\vec{J}_1 = -nD_{12}\left\{\text{grad } n_{10} - \frac{\alpha n_{10} n_{20}}{T} \text{ grad } T\right\} \qquad (3.7)$$

where D_{12} again represents the coefficient of mutual diffusion and α is the thermal diffusion constant. The second term in Eq. (3.7) represents an additional diffusion current caused by the temperature gradient and expresses the tendency of lighter molecules to migrate into regions of high temperature. This process is known as "thermal diffusion," and the thermal diffusion constant is known for several binary gas mixtures.[5]

Substituting Eq. (3.7) into (3.6) and neglecting derivatives with respect to x, as usual, one obtains the

† Subscript 1 refers to the lighter molecules (cf. reference 6).

final form of the diffusion equation for the given problem,

$$u\frac{\partial n_1}{\partial x} + v\frac{\partial n_1}{\partial y} = \frac{\partial}{\partial y}\left\{nD_{12}\left[\frac{\partial n_{10}}{\partial y} - \frac{\alpha n_{10}n_{20}}{T}\left(\frac{\partial T}{\partial y}\right)\right]\right\} \tag{3.8}$$

(b) Method of Solution

The problem at hand consists in finding a solution to the system of differential equations constituted by Eqs. (3.01)–(3.4), together with Eq. (3.8), which satisfies a given set of boundary conditions. Eq. (3.2) has already been utilized through the implicit assumption that the pressure is everywhere constant and can therefore be neglected. The equation of continuity will be satisfied automatically through use of a stream function and can also be neglected.

We begin, as in Section (2), by introducing a stream function ψ, a new independent variable η, an f-function that is analogous to the Blasius function, and some dimensionless parameters through the following definitions:

$$u = \frac{\rho_0}{\rho}\frac{\partial \psi}{\partial y}; \qquad v = -\frac{\rho_0}{\rho}\frac{\partial \psi}{\partial x} \tag{3.9}$$

$$\eta = \frac{1}{2}\sqrt{\frac{\rho_0 u_0}{\mu_0 x}}; \qquad \psi = \sqrt{\gamma_0 x u_0}\, f(\eta) \tag{3.10}$$

$$\left.\begin{aligned} \mu &= \phi_1\mu_0; \qquad \rho = \phi_2\rho_0; \qquad k = \phi_3 k_0 \\ c_p &= \phi_4 c_{p_0}; \quad nD_{12} = \phi_5 n_0 \nu_0; \quad n = \phi_6 n_0 \\ T &= tT_0 \end{aligned}\right\} \tag{3.11}$$

Again we transform the differential equations to the (x, η)-plane by means of the transformation formulas.

$$\left.\begin{aligned} \left[\frac{\partial}{\partial y}\right]_x &= \frac{1}{2}\sqrt{\frac{\rho_0 u_0}{\mu_0 x}}\frac{\partial}{\partial \eta} \\ \left[\frac{\partial}{\partial x}\right]_y &= \frac{\partial}{\partial x} - \frac{1}{2}x^{-1}\eta\frac{\partial}{\partial \eta} \end{aligned}\right\} \tag{3.12}$$

One finds, as before, that the velocity components are given by the expressions

$$\left.\begin{aligned} u &= (1/2)u_0[\phi_2^{-1}f'] \\ v &= \frac{1}{2}\sqrt{\frac{\mu_0 u_0}{\rho_0 x}}\,\phi_2^{-1}\,[\eta f' - f] \end{aligned}\right\} \tag{3.13}$$

Using this result, together with the transformation formulas given in Eq. (3.12), and setting partial derivatives with respect to x at constant η equal to zero, one obtains the following system of ordinary differential equations, expressing conservation of x-momentum, conservation of energy, and conservation of foreign molecules, respectively:

$$f[\phi_2^{-1}f']' + [\phi_1(\phi_2^{-1}f')']' = 0 \tag{3.14}$$

$$f[\phi_4 t]' + Pr_0^{-1}[\phi_3 t']' + 1/4(\gamma_0 - 1) \times M_0^2\phi_1[(\phi_2^{-1}f')']^2 = 0 \tag{3.15}$$

$$\phi_2^{-1}f[\phi_6 n_{10}]' + [\phi_5(n_{10}' - \alpha n_{10}(1 - n_{10})t^{-1}t')]' = 0 \tag{3.16}$$

where the free-stream Prandtl and Mach Numbers have been introduced through the identities

$$\left.\begin{aligned} Pr_0 &= c_{p_0}\mu_0/k_0 \\ (1/4)\,(\gamma_0 - 1)M_0^2 &= u_0^2/4c_{p_0}T_0 \end{aligned}\right\} \tag{3.17}$$

The next step will be to transform Eqs. (3.14)–(3.16) into integral equations that lend themselves readily to the process of successive approximation. This is accomplished by the "method of variation of parameters" as described, for instance, by Ince.[7] Let there be given a second order nonhomogeneous linear differential equation of the form

$$L(\eta)u_n = F_n$$

and let the solution to the associated homogeneous equation be

$$u_n = [u_n]_0 + K_n\int_0^\eta \Psi_n\, d\eta$$

where $[u_n]_0$ and K_n are constants of integration. It can be shown, in this particular case, that the solution to the complete equation has the form

$$u_n = [u_n]_0 + K_n\int_0^\eta \Psi_n\, d\eta + \int_0^\eta \Psi_n\left[\int_0^\eta F_n\Psi_n^{-1}\, d\eta\right] d\eta \tag{3.18}$$

This mathematical theorem is readily applicable to the given problem. Since the resulting system of integral equations will ultimately be solved by the method of successive approximations, there is some freedom in selecting terms to be included in the general term F_n representing the nonhomogeneous component of the differential equation. As will be seen below, the F-terms appearing in the present development include mainly terms that are peculiar to the diffusion problem, while the Ψ-functions correspond essentially to the terms considered in standard theories of the compressible boundary layer.

Let the variable u_n occurring in Eq. (3.18) represent the quantities f, t, and n_{10} for $n = 1$, 2, and 3, respectively. By means of elementary calculations one obtains the following expressions for F_n and Ψ_n:

$$\left.\begin{aligned} \Psi_1 &= \phi_2\int_0^\eta \phi_1^{-1}\exp\left\{-\int_0^\eta \phi_1^{-1}f\, d\eta\right\} d\eta \\ F_1 &= 0 \end{aligned}\right\} \tag{3.19}$$

$$\left.\begin{aligned} \Psi_2 &= \phi_3^{-1}\exp\left\{-Pr_0\int_0^\eta \phi_3^{-1}\phi_4 f\, d\eta\right\} \\ F_2 &= -Pr_0\phi_3^{-1}\{(1/4)\,(\gamma_0 - 1) M_0^2\phi_1[(\phi_2^{-1}f')']^2 + f\phi_4' t\} \end{aligned}\right\} \tag{3.20}$$

$$\left.\begin{aligned} \Psi_3 &= \phi_5^{-1} \exp\left\{ - \int_0^\eta \phi_2^{-1}\phi_5^{-1}\phi_6 f \, d\eta \right\} \\ F_3 &= -\phi_5^{-1}\left\{ \phi_2^{-1}\phi_6' f n_{10} - [\alpha\phi_5 n_{10}(1 - n_{10})t^{-1}t']' \right\} \end{aligned}\right\} \quad (3.21)$$

The given set of integral equations is amenable to solution by the method of successive approximations. One of the advantages of the present formulation lies in the fact that explicit constants of integration are available which can be readily adjusted to satisfy the two-point boundary conditions. Other advantages are the comparative ease with which the requisite numerical operations can be carried out and the possibility of detecting and controlling numerical errors. The calculation can be performed by a subsidiary worker with the aid of a manual calculating machine and requires approximately 10 hours for each iteration.

(c) *Sample Problems*

The sample problems considered in this section were chosen to illustrate the effect of a diffusion field of helium atoms on the dynamic and thermal characteristics of a compressible boundary layer at high Mach Numbers. To render the solutions fully determinate, the following conditions must be specified: (a) boundary conditions; (b) exact functional dependence of ϕ_n on t and n_{10}, and the numerical values of Pr_0, M_0, γ_0, and α.

The following boundary conditions are assumed:

$$\begin{aligned} f = f' = 0; \quad t = 6; \quad n_{10} = 1 \quad \text{at } y = 0 \\ f' = 2; \quad t = 1; \quad n_{10} = 0 \quad \text{at } y = \infty \end{aligned} \quad (3.22)$$

In particular, it is supposed that the concentration of helium near the wall is constant, while the normal component of velocity vanishes there. Possible objections to this supposition, based on the question as to whether conditions of this nature are physically feasible, will be answered in the next section, where the practical significance of the given theory is discussed.

To facilitate the numerical calculation, the ϕ-functions are represented as a product of two factors, depending, respectively, on n_{10} and t,

$$\phi_n = \phi_{n1}(n_{10})\phi_{n2}(t) \quad (3.23)$$

The functions ϕ_{n1}, which express dependence of a given property on the local concentration of helium, can be represented with sufficient accuracy by linear expressions. The constants entering into these linear expressions are assumed to be independent of temperature and are usually evaluated at N.T.P. conditions. The resulting functional relationships are given in the following list, together with the sources from which relevant empirical data were obtained:

$\phi_{11} = 1 + 0.097n_{10}$	Reference 4
$\phi_{12} = t^{1/2}\left(\dfrac{1.505}{1 + 0.505t^{-1}}\right)$	Sutherland law
$\phi_{21} = 1 - 0.862n_{10}$	Reference 4
$\phi_{22} = t^{-1}$	Gas law

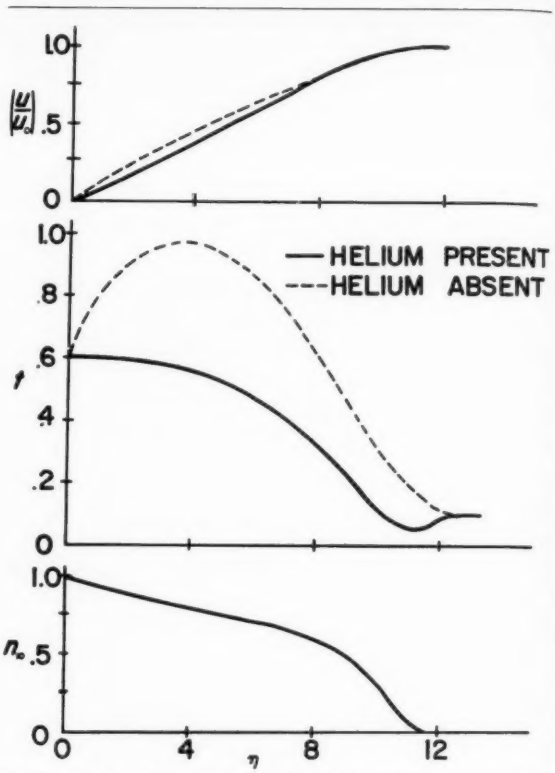

FIG. 3. Effects of a helium diffusion field: $M_0 = 12$; $[t]_0 = 6$.

$\phi_{31} = 1 + 4.87n_{10}$	Reference 4
$\phi_{32} = \phi_{12}$	Assuming constant c_p and constant Prandtl Number
$\phi_{41} = 1 + 4.18n_{10}$	Reference 5
$\phi_{42} = 1$	Usual approximation
$\phi_{51} = 1$	n and D_{12} both independent of concentration
$\phi_{52} = 2.98t^{3/4}$	Estimated from data for $H_2 - A$, He-A and H_2-air mixtures given in references 4 and 8, and assuming a free-stream temperature $T_0 = 392°$R.
$\phi_{61} = 1$	Avogadro's law
$\phi_{62} = \phi_{22}$	Gas law

We further assume

$$Pr_0 = 0.75, \quad \gamma_0 = 1.40, \quad \alpha = 0.36^5$$

Only the free-stream Mach Number remains now to be specified. Two sample calculations have been carried out, corresponding to the conditions $M_0 = 12$ and 8, respectively. The resulting velocity, temperature, and concentration profiles are indicated in Figs. 3 and 4, together with the corresponding velocity and temperature profiles that obtain in the absence of a diffusion field and which have been calculated by Van Driest.[9] The theoretical and practical significance of these results will be discussed in the following section. Here we shall only state that approximately three iterations are required to achieve sufficient convergence.

provided one uses Van Driest's velocity and temperature profiles for the first trial functions. Faster convergence can of course be achieved through the use of more suitable trial functions.

(4) Results and Applications

(a) *Interpretation of Results*

The most striking effect of the helium diffusion fields is observed in the temperature profiles, as indicated by Figs. 3 and 4. The normal peaks in the temperature profile, which obtain whenever the wall temperature is kept at a value less than adiabatic or equilibrium temperature, are caused by the dissipation of kinetic energy. It is evident that these peaks are greatly diminished by the admixture of helium, and in particular instances they may be altogether eliminated. This result is mainly due to three contributing factors, the first two of which act to reduce the temperature rise caused by dissipation of kinetic energy, while the third factor tends to reduce all temperature gradients in the boundary layer. It was pointed out in Section (1) that helium is notable for its low density, high specific heat, and high heat conductivity. The first of these properties tends to reduce the velocity gradient in the boundary layer, as was shown by the results obtained in Section (2). In view of the fact that the dissipation of kinetic energy varies as the square of this gradient, one can conclude that low density tends to reduce viscous heating. For a given rate of dissipation of kinetic energy, the resulting temperature rise will be reduced by the presence of helium, because the latter has a very high specific heat. Finally, all temperature gradients in the boundary layer tend to be reduced on account of the high thermal conductivity contributed by the helium atoms. In this manner each of the three most unusual physical properties of helium gas plays a part in reducing the peaks and gradients of hypersonic temperature profiles.

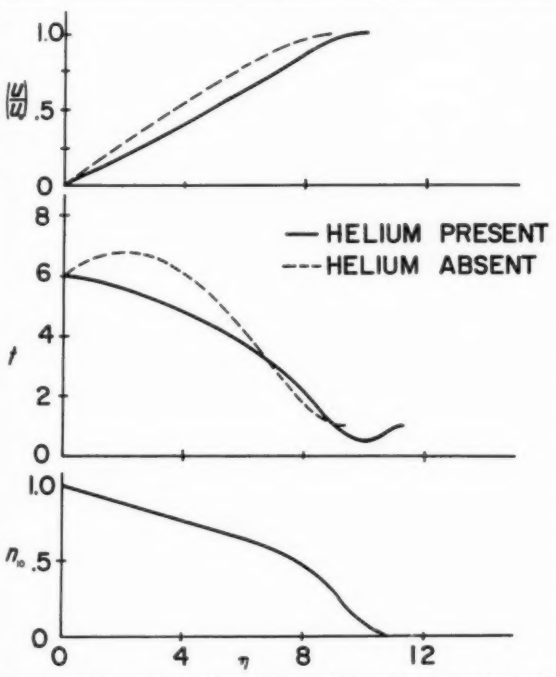

FIG. 4. Effects of a helium diffusion field: $M_0 = 8$; $[t]_0 = 6$.

The two sample problems of Section (3) differ in the following respect: While the magnitude of the initial gradient of the temperature profile at $M_0 = 12$ is greatly reduced by the admixture of helium, its sign is unchanged. This means that heat still flows into the wall, though the rate at which this takes place may be greatly reduced. At $M_0 = 8$, however, the sign of the initial temperature gradient has changed, causing a reversal in the direction of heat flow. These results are easily interpreted by means of the well-known expression for adiabatic wall temperature, which is applicable to any chemically homogeneous boundary layer with Prandtl Number approximately equal to 1:

$$T_{aw} = T_0[1 + (1/2)(\gamma - 1)\sqrt{Pr}\, M^2]_0 \quad (4.1)$$

This formula enables one to express the adiabatic wall temperature of an all-helium boundary layer in terms of the adiabatic wall temperature in air, corresponding to the same free-stream temperature and velocity. For this condition $(\gamma - 1)M^2$ varies inversely as the specific heat, which implies, according to Eq. (4.1), that

$$\frac{(T_{aw} - T_0)_{\text{He}}}{(T_{aw} - T_0)_{\text{air}}} = \frac{(\sqrt{Pr}\, c_p^{-1})_{\text{He}}}{(\sqrt{Pr}\, c_p^{-1})_{\text{air}}} \cong \frac{(c_p)_{\text{air}}}{(c_p)_{\text{He}}} = 0.193 \quad (4.2)$$

Applying this result to the first problem, for which $M_0 = 12$, one finds that the adiabatic wall temperature would be reduced from its value $25.9T_0$ in air to $5.82T_0$ in an all-helium boundary layer. Assuming an "average concentration" of helium equal to 80 per cent, the estimated adiabatic wall temperature becomes $7.02T_0$, which is greater than wall temperature for the given problem. This explains the small but positive temperature gradient at the wall which has been calculated. At a free-stream Mach Number of 8, however, the adiabatic wall temperature is reduced from $12.1T_0$ in air to $3.14T_0$ in an all-helium boundary layer. Assuming, as before, an average concentration of helium equal to 80 per cent, this value is increased to $3.68T_0$, which is still considerably less than wall temperature. This explains the reversal in heat flow noted above.

One further point of interest concerning the temperature profiles must be explained. It is somewhat remarkable that there could occur a pronounced dip in the temperature curve near the outer edge of the boundary layer, where temperatures below the free-stream value are maintained. At least to the present author's knowledge, such a phenomenon is not indicated by other theories of the laminar boundary layer, but its appearance in the present context is readily ex-

plainable. An inspection of the numerical calculation discloses that the phenomenon is caused by the term $(f\varphi_4' l)$ occurring in Eq. (3.20). It arises from the convection term of the original energy equation and expresses the effect of variable specific heat on convection of enthalpy. From the given concentration profiles it is evident that strong negative gradients of specific heat exist near the temperature minimum. The following simplified argument indicates how these gradients account for the unusual behavior of the temperature profiles: Consider a small rectangle fixed in the outermost region of the boundary layer, where the velocity gradient is effectively zero. Two of its sides are taken to coincide with the local stream lines, and the remaining sides are perpendicular to the flow direction. Let the upstream and downstream sides be referred to as A and B, respectively. A fluid particle traversing the given rectangle moves in the direction of decreasing η. Suppose the temperature in the rectangle were maintained at its free-stream value. Then, because of the negative gradient of specific heat, the fluid particle would gain enthalpy while traversing the rectangle. Since dissipation of kinetic energy can be neglected in this region, the temperature within this rectangle will naturally drop. In this way a positive temperature gradient is set up which opposes the convection of enthalpy caused by the variation of specific heat.

Two remarks should be made in conclusion. A comparison of numerical values indicates that the thermal diffusion term contributes only a small correction to the concentration and could be neglected in the given instances without causing undue errors in the result. This is partially due to the fact that the presence of helium in the boundary layer has greatly reduced the strength of temperature gradients, thereby causing the thermal diffusion term to be smaller than an initial estimate would disclose. Further, it appears from the figures that the velocity profiles are not greatly affected by the admixture of helium, although the initial gradients are somewhat reduced.

(*b*) *Concerning the Boundary Conditions*

A few words should be said concerning the particular boundary conditions that have been assumed in the sample problems. The objection may be raised that it is not physically feasible to maintain a constant nonvanishing concentration of foreign gas near the wall without maintaining, at the same time, a nonvanishing normal velocity through the wall.

One may reply, in the first place, that questions relating to the physical feasibility of the given boundary conditions need not concern us at all. They have been selected for the purpose of investigating the effect that the presence of a foreign gas can have on boundary-layer profiles, unmasked by any additional disturbances, such as the existence of a nonvanishing normal velocity near the wall. If this condition should be an idealization that is physically unattainable, it nevertheless describes trends and tendencies of general significance. Moreover, the assumption of vanishing normal velocity near the wall is accidental not only to the effect of diffusion fields on the boundary layer but also to the theory and method of solution presented in this paper, which is directly applicable to the more general case.

On the other hand, the conditions that have been stipulated in the sample problems are by no means experimentally inconceivable. Let us suppose the wall to be a surface that is perfectly permeable to both primary and special molecules. Such a surface would prohibit the existence of a discontinuity in composition. If the gas pressure inside the surface is maintained at the free-stream value, there will be no net flow of gas through the wall. In this case the concentration of special molecules in the boundary layer is maintained by means of a pure diffusion current through the wall, in keeping with the stipulated boundary conditions.

(*c*) *Applications and Conclusions*

The theory and results presented in this paper have bearing on the problem of control and reduction of aerodynamic heating at hypersonic speeds. The special feature of the present approach to this problem lies in the utilization of diffusion fields for the purpose of reducing the detrimental effects of viscous dissipation, a procedure that may be compared with the application of a lubricant between two surfaces. Although the given theory and method of solution are adapted to a fuller investigation of this problem, the numerical examples presented in this report are mainly concerned with diffusion fields of helium, with which highly satisfactory results have been achieved at the free-stream Mach Numbers of 8 and 12. Whereas at the higher Mach Number the influx of heat was practically eliminated, a reversal in the direction of heat flow has been effected at the lower Mach Number.

References

[1] Broadwell, J. E., and Sherman, P., *Survey of Porous-Wall Heat-Transfer Literature*, WADC Contract No. AF18(600)-51, E. O. No. 462 Br-1, April, 1953.

[2] Schlichting, H., and Bussmann, K., *Exakte Loesungen fuer die Laminare Grenzschicht mit Absaugen und Ausblasen*, Schrift. d. Deutschen Akademie d. Luftfahrtforschung, Vol. 7B, No. 2, 1943.

[3] Schuh, H., *The Solution of the Laminar Boundary Layer Equation for the Flat Plate for Velocity and Temperature Fields for Variable Physical Properties and for the Diffusion Field at High Concentration*, NACA TM No. 1275, May, 1950.

[4] *International Critical Tables of Numerical Data, Physics, Chemistry, and Technology;* McGraw-Hill Book Company, Inc., New York, 1929.

(*Continued on page 178*)

Problems and Results of Investigations on Cascade Flow *,†

HERMANN SCHLICHTING‡

Institute of Fluid Mechanics, Technical University of Braunschweig, Germany

SUMMARY

A summarizing report is given of the research work on the flow through cascades of airfoils which has been conducted in recent years at the Institute of Fluid Mechanics at the Technical University of Braunschweig. The theoretical investigations led to a simple solution of the "Indirect Problem" and the "Direct Problem" for the two-dimensional incompressible frictionless flow through cascades. By an extensive computation of "Cascade Downwash Tables," the amount of calculation for any special case has been reduced to such an extent that a systematic theoretical investigation of the cascade problem has become possible.

Two-dimensional viscous flow through cascades has been treated by applying boundary-layer theory, thus giving for the first time theoretical data for the loss coefficients. An extensive theoretical program, which aims to explore the relations between the geometric and aerodynamic parameters of cascades, including loss coefficients, has been started and partly completed.

For the two-dimensional compressible flow through cascades at high subsonic velocities, a convenient method of computation has been given which is based on the Prandtl-Glauert rule. In this way, the above-mentioned solution of the "Direct Problem" for incompressible flow has become applicable also to compressible subsonic flow.

The theoretical results have been checked by some systematic experiments on two-dimensional cascades. Special attention has been given to obtain two-dimensional flow by means of boundary-layer slots at the walls and by applying suction. Pressure distributions, as well as loss coefficients, as obtained from experiments are in good agreement with theory.

Furthermore, numerous experiments have been done with cylindrical axial-flow cascades having various hub ratios and untwisted blades. These cascades were tested with axial inflow, thus giving a considerable swirl of the outflow. By comparison with tests on two-dimensional cascades with blades of the same profile, it has become evident that for cylindrical cascades the effects of radial divergence—i.e., the variation of the solidity ratio over the radius—on the pressure distribution over the blade and on the local loss coefficients generally are extremely small. Also, some research has been done on two-dimensional cascades with clearance.

Received July 1, 1953. Revised and received September 24, 1953.

* From a lecture held at the Conference of the Committee for Fluid Motion Research of the "Verein Deutscher Ingenieure" in Karlsruhe, Germany, on March 19–21, 1953. The full German text has been published in *Zeitschrift für Flugwissenschaften*, Vol. I, No. 5, pp. 109–122, October, 1953. For this English translation I am indebted to Dipl.-Ing. E. S. Krauss, AFRAeS, London, and to Prof. J. Weske, of the University of Maryland.

† These investigations have been conducted with the assistance of the "Deutsche Forschungsgemeinschaft," Bad Godesberg, and of several German industrial firms. Among the staff of the Institute, Dr.-Ing. N. Scholz, Dr.-Ing. L. Speidel, Dipl.-Ing. H. Schäffer, and Ing. H. Goldmann prominently participated in the work.

‡ Professor.

(1) INTRODUCTION

A SUCCESSFUL INVESTIGATION of the cascade problem only by systematic experimental research, as it was done for the single airfoil by extensive wind-tunnel tests in U.S.A. during the last decades, seems to be quite hopeless in view of the much greater number of parameters and also because of heavy experimental difficulties. Real progress beyond occasionally measured special cases can therefore only be achieved by extensive theoretical investigations, which, however, require a careful supervision by experiment. From these considerations the Institute of Fluid Mechanics at the Technical University of Braunschweig decided to carry out closely interrelated theoretical and experimental investigations.

The leading idea of our research work is that a deeper knowledge of the flow phenomena, as they occur in turbomachines in a most complex manner, will only be possible by an extensive analysis. This analysis must extend to theory, as well as to experiment. The basis of all investigations of the flow through cascades is the incompressible flow through a two-dimensional cascade. Only if this basic problem is fully understood, will it be profitable to attack the problems involved in the remaining parameters.

The most important of these other parameters are:

(1) Three-dimensional effects (a) along the walls and (b) due to clearance.

(2) Radial divergence of cylindrical cascades.**

(3) Compressibility effects (Mach Number).

(4) Centrifugal forces (for the rotating unit).

Systematic research on incompressible flow through a cascade seems to be unavoidable if a sound knowledge of the physical process is to be acquired instead of being satisfied with purely empirical results.

Therefore, at the beginning, we have confined our investigations mainly to the incompressible flow through two-dimensional cascades, since so many unsolved problems exist in this particular field.

Among the other parameters mentioned before which complicate the problem of cascades, up to now we have

** Variation of the solidity ratio with radius.

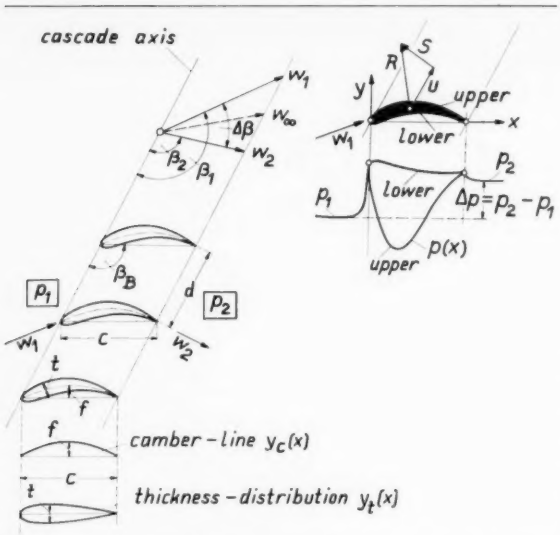

FIG. 1. Geometric and aerodynamic parameters of a two-dimensional cascade.

only dealt with a few and to a moderate extent. Therefore I should like to report at first on the investigations of two-dimensional cascades and later on some of the other problems—in particular, the effect of Mach Number; three-dimensional effects, especially end losses and radial divergence as occurring in cylindrical cascades.

(2) INVESTIGATIONS OF TWO-DIMENSIONAL CASCADES

Whereas in earlier papers the flow through cascades has been treated as a flow through a passage, all modern investigations are based on the concepts of airfoil theory. Each blade is treated as an airfoil and the mutual interference of the blades plays a most important role. The main problem in investigations of the two-dimensional cascade is to find the relation between the geometric and aerodynamic parameters of the cascade. The main *geometric parameters* are, as shown in Fig. 1, the profile of the blade:

with the maximum camber, f/c
thickness chord ratio, t/c
camber line, $y_c(x)$
thickness distribution, $y_t(x)$

and the geometry of the cascade as given by:

solidity ratio, d/c
angle of stagger (or blade angle), β_B

The first parameters that define the profile of the blade are known from the airfoil alone. The two additional parameters defining the geometry of the cascade depend on the arrangement of the blades in the cascade.

The *aerodynamic parameters* of the cascade are:

inflow and outflow velocity, w_1, w_2
angle of inflow and angle of outflow, β_1, β_2 or α_1, α_2
deflection of flow deviation, $\Delta\beta = \beta_1 - \beta_2$
pressure difference across the cascade, $\Delta p = p_2 - p_1$
chordwise pressure distribution over the blade, $p(x)$
resultant aerodynamic force on the blade, $R(U, S)$
with the tangential component, U
and the thrust component, S
loss of total head in the cascade, Δh

The establishment of the relation between these geometric and aerodynamic parameters is the aim of these investigations. This relation is greatly affected by the Reynolds Number and Mach Number. For the single airfoil, the relation between the geometric and aerodynamic parameters has been established, to a large extent, by aeronautical aerodynamics. But with regard to cascades, our knowledge is far from being satisfactory. The reason is that, because of the greater number of geometric and aerodynamic parameters, the problem of the cascade is much more difficult than that of the single airfoil.

(2.1) *Theoretical Investigations*

In all previous theoretical investigations of the flow through cascades a frictionless fluid has been assumed throughout.[1] From the very beginning of our investigations, we have taken into account the friction of the fluid for the first time.[2, 3] Thus, a theoretical calculation of the loss coefficients has become possible. This is of particular importance because these losses determine the quality of the cascade and thus the efficiency of the turbomachine.

(*2.1.1*) *Incompressible Flow.*—But before we could start with the investigations of the cascade flow with friction we had to deal with extensive basic problems in the field of frictionless flow through cascades.

For the calculation of the boundary layer, it is necessary to know the pressure distribution according to potential flow theory. Unfortunately, the existing methods available for calculating this pressure distribution proved to be unsuitable for our purpose of systematic investigations of the cascade flow, since they are either too elaborate or they do not satisfy one requirement—which is to be able to vary the geometric parameters of the cascade separately. The possibility of varying the geometric parameters separately—e.g., variation of solidity ratio with the remaining parameters—the blade angle and the blade profile being constant, proves to be of predominating importance in order to obtain clear information on the relation between the geometric and aerodynamic parameters.

The two most important basic problems of the theory of cascades in frictionless fluid are the so-called "Indirect Problem" and the "Direct Problem."

In the "*Indirect Problem*" the known quantities are the directions of the inflow and outflow—i.e., the velocity diagram—and the unknown quantities are the

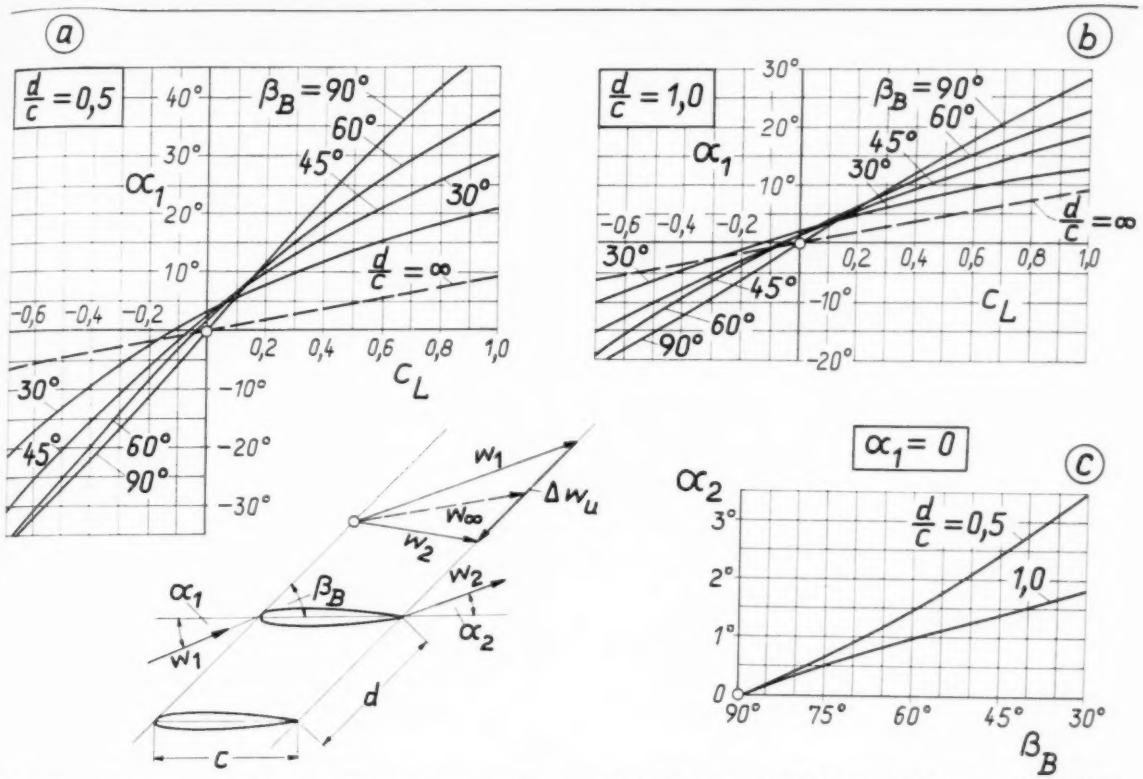

FIG. 2. Aerodynamic coefficients of cascades as functions of solidity ratio d/c and angle of blade β_B: blade section NACA 0010.

Lift coefficient $c_L = \dfrac{L}{(1/2)\rho w_\infty^2 c} = 2\dfrac{d}{c}\dfrac{\Delta w_u}{w_\infty}$; L = lift of one blade, normal to w_∞.

geometry of the cascade and the geometry of the blade section and also the pressure distribution on the blade.

In the "*Direct Problem*" the known quantities are the geometry of the cascade and the geometry of the blade profile, and the unknown quantities are the resulting aerodynamic force on the blade, the pressure distribution and the direction of the outflow—all of these as functions of the direction of the inflow.

In the "Indirect Problem" the aerodynamics of the cascade are given and the geometry is asked for. The "Direct Problem" is the reverse of the "Indirect Problem."

We have succeeded in finding a convenient method for solving these two problems. The solution is based on the method of singularities, which replaces the blade by a distribution of sources, sinks, and vortices—a method already suggested earlier by Schilhansl[4] and Ackeret.[5] A solution for the "Indirect Problem" has been given by Scholz[18] and a solution for the "Direct Problem" by Schlichting.[19]

With the aid of a catalog that compiles universally tabulated functions, the amount of computational work has been reduced considerably as compared with the work involved previously. For instance, the work required for the "Direct Problem" of a given cascade with ten different angles of inflow can now be completed in about 20 hours instead of 20 days.[6, 7] Hence, a systematic theoretical investigation of the cascade problem seems to have become possible and we have started with it.

A primary result of such a systematic computation is shown in Fig. 2. The lift coefficient c_L is plotted against the angle of inflow α_1, for a series of cascades with blades of the NACA 0010 profile. The solidity ratios are $d/c = 0.5$ and 1.0 and the blade angles $\beta_B = 90°$, 60°, 45°, and 30°. The corresponding values for the single airfoil, $d/c = \infty$, are included, thus confirming the well-known fact that the slope of the lift curve of the blade in cascade is only a fraction of the lift slope of the single airfoil.

It is of particular interest to note that, except for the case of the unstaggered cascade, $\beta_B = 90°$, the curves of c_L plotted against α_1 do not pass through the origin. This means that, at an inflow parallel to the chord, $\alpha_1 = 0$, the lift coefficient is different from zero. In a staggered cascade of symmetrical profiles of finite thickness with inflow parallel to the blade chord, the flow is deflected toward the cascade axis, which was found first by Ruden[8] and later by Marcinowski.[9] In Fig. 2c, the angle of deflection α_2 is plotted against the

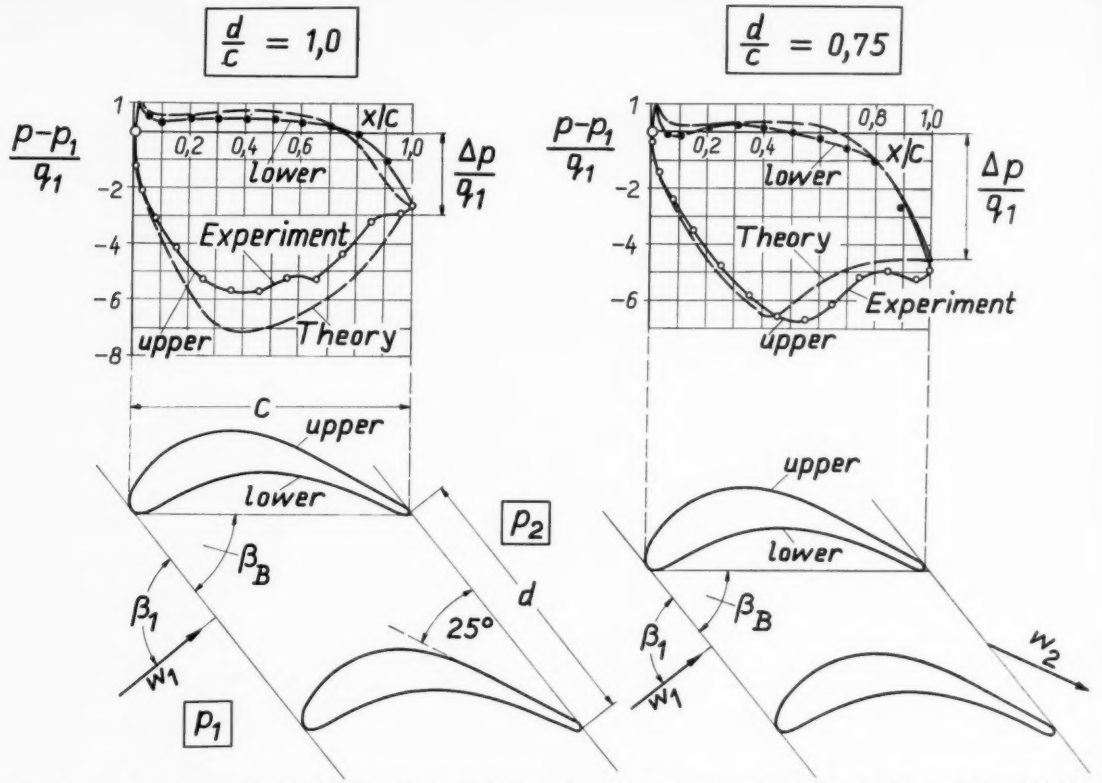

FIG. 3. Pressure distribution of turbine blade sections with large camber in two-dimensional cascades; theory according to Richter;[20] blade section GHH-B; $\beta_B = 51°$; $\beta_1 = 90°$; $Re = w_1 c/\nu = 6 \times 10^4$; $q_1 = (\rho/2)w_1^2$.

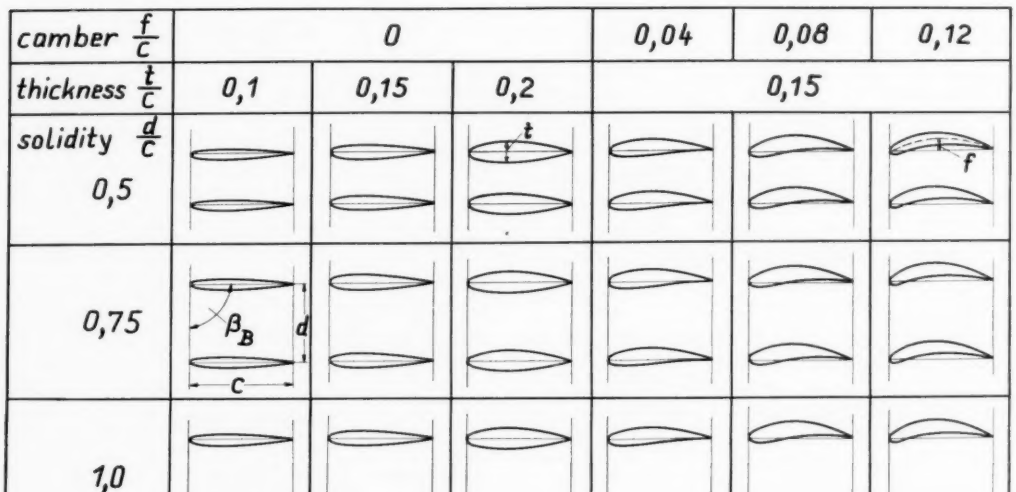

FIG. 4. Unstaggered cascades: $\beta_B = 90°$. Thickness distribution: NACA standard four digit airfoils, camber line—parabolic.

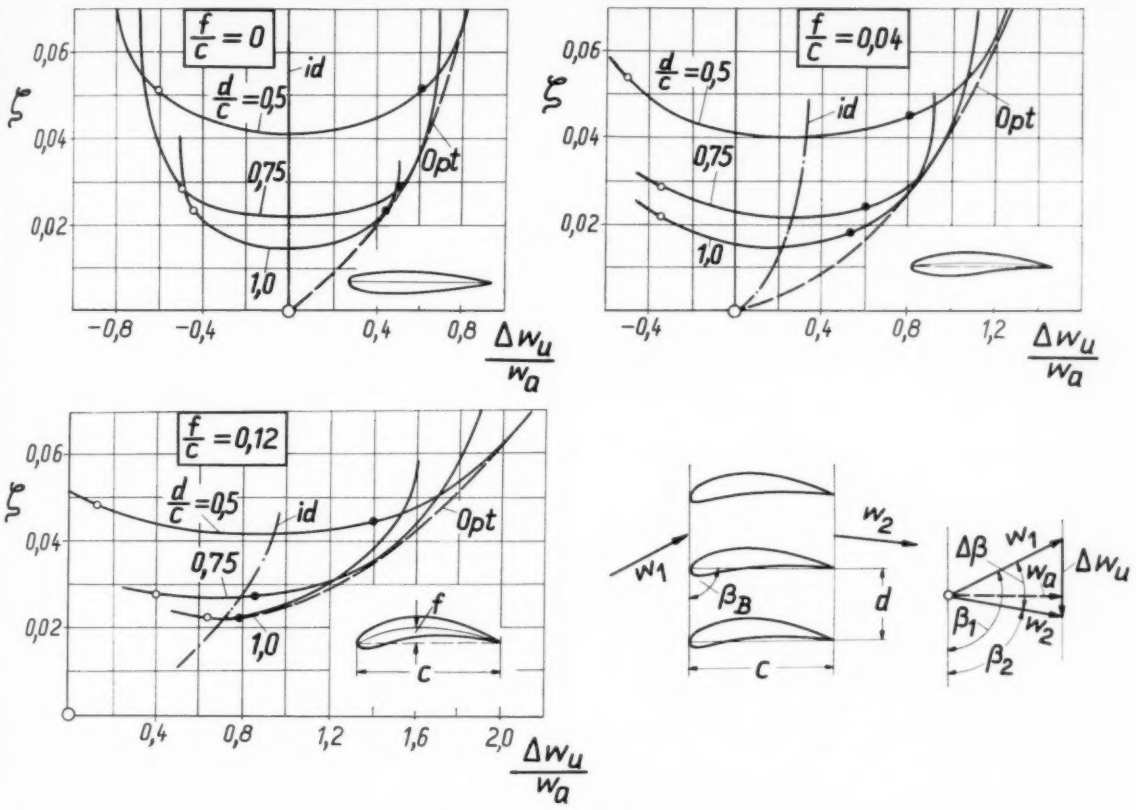

FIG. 5. Theoretical loss coefficients ζ according to Eq. (1) for unstaggered two-dimensional cascades of Fig. 4 for various values of maximum camber f/c, according to Speidel.[10] Blade angle $\beta_B = 90°$; thickness $t/c = 0.15$; Reynolds Number $Re = w_a c/\nu = 10^6$, boundary layer fully turbulent. ●○ first occurrence of separation on upper and lower surface, respectively. *id* = ideal angle of entry.

blade angle β_B for various values of the solidity ratio d/c for an inflow parallel to the chord of the blade.

In the course of our systematic investigations on cascades we have made extensive calculations of pressure distributions, because these are the basis for all theoretical computations of the loss coefficients. Our method of calculation is most suitable for blades of moderate thickness and of moderate camber. As, however, blades with large values of maximum camber occur in steam turbines, we have extended our method to such cases. In Fig. 3, the theoretical pressure distributions of a turbine cascade, having blades with large values of maximum camber and large deflections of flow, are compared with experimental pressure distributions for two different values of the solidity ratio. The agreement is good, particularly in view of the discrepancy one would have expected to exist between theoretical and experimental values due to the neglect of the effect of friction. The rapid change of curvature of the contour of the upper surface of the airfoil section considered is reflected in the pressure distribution in form of a sudden change of the pressure for the cascade with the smaller solidity. Further pressure distributions, together with their correlation with theory, will be given later.

Viscous flow, loss coefficients: The main objective of our investigations is to find the most favorable cascades with regard to losses of flow energy. The method of calculating the losses is basically that of the boundary-layer theory applied to the cascade. We have embarked on an extensive program on these lines, which is partly completed.

In Fig. 4, a survey is given of a number of cascade configurations, the losses of which have been calculated by Speidel.[10] This first part of our program refers to unstaggered cascades only—i.e., the solidity ratio being the only parameter of the geometry of the cascade. All blade sections are NACA sections, with varying thickness chord ratios and varying maximum camber. From the numerous results, only one diagram about loss coefficients may be given here, Fig. 5. One of the most important aerodynamic parameters of a cascade is the velocity difference Δw_u in the tangential direction across the cascade. It is desirable to design cascades with the greatest possible deflection of the flow at a minimum of losses. In Fig. 5 the loss coefficient

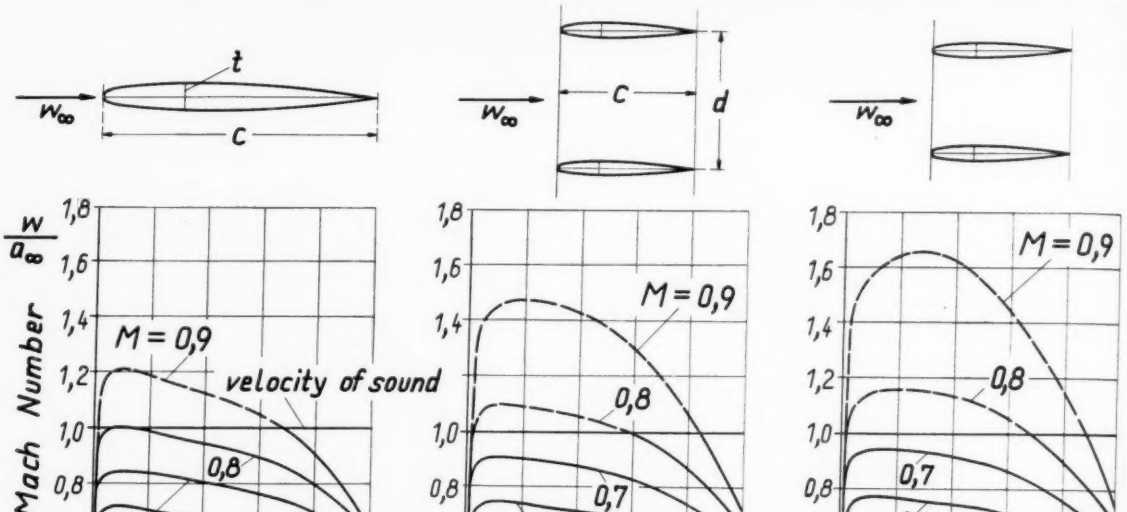

FIG. 6. Local Mach Number of two-dimensional cascades in subsonic flow. Blade section NACA 0010.

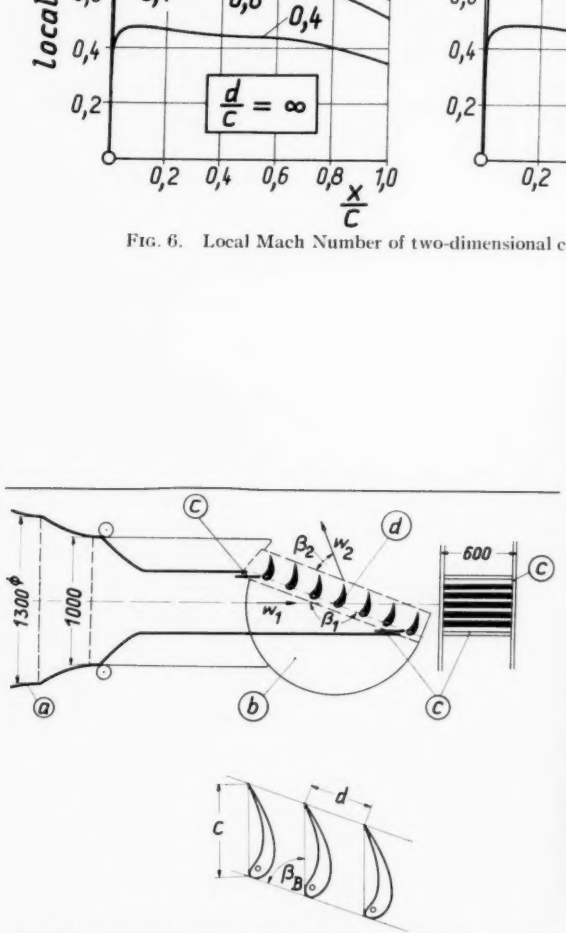

FIG. 7. Schematic presentation of two-dimensional cascade wind-tunnel; blade chord c = 200 mm. approximately. (a) Wind-tunnel nozzle; (b) mounting discs for angular adjustment; (c) boundary-layer suction slots; and (d) blade with pressure taps for pressure distribution measurements. The figures 600, . . ., mean millimeters.

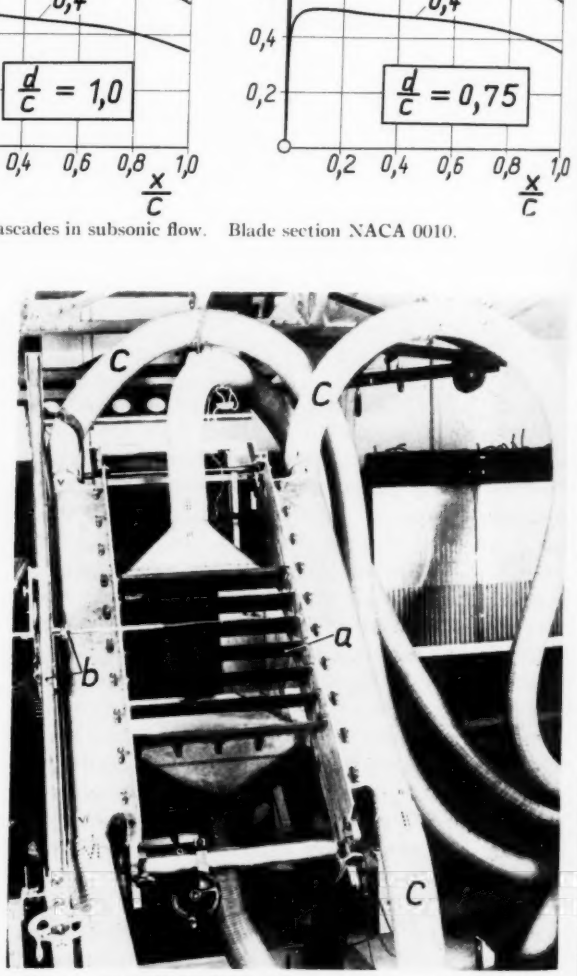

FIG. 8. Two-dimensional cascade wind tunnel with suction slots. (a) Cascade; (b) traverse mechanism for measuring probes; and (c) suction ducts.

$$\zeta = \Delta h/(\rho/2)w_{2id}^2 = \Delta h/q_{2id} \qquad (1)$$

based on the theoretical outflow velocity w_{2id} is plotted against the velocity ratio $\Delta w_u/w_a$, which corresponds substantially to the angle of deflection of the flow $\Delta\beta$. Each of the three diagrams refers to a constant value of maximum camber and three different solidities of the cascade, $d/c = 0.5, 0.75$, and 1.00.

For moderate deflections of flow, the minimum losses are associated with the largest values of cascade spacing, because the losses are essentially proportional to the number of blades for small blade loadings. For larger angles of deflection, however, a closer spacing is more favorable. The reason for this behavior is that, at greater angles of deflection, the lift loading of the individual blade is becoming too large. For excessive loadings, the flow separates and the losses increase rapidly. The curve referred to as "Optimum" is the envelope of the three d/c curves and indicates the minimum of losses associated with a given angle of deflection and solidity ratio. The symbols ● and ○ indicate the beginning of separation on the upper and lower surface of the blade, respectively. Only in the region between ○ and ● is the flow attached on both surfaces. It is of particular interest to note that the optimum values (envelope) are throughout on the right-hand side of ●, which means that the flow on the upper surface is slightly separated. This is in good agreement with experiments but is completely different from the behavior of the single airfoil. Whereas in the case of the single airfoil an increase in lift coefficient is always associated with a considerable increase in drag particularly in the range of partly separated flow, in the case of the cascade it is possible to obtain a reduction of the losses by increasing the spacing which corresponds to an increase in blade loading at constant angle of deflection. The reason is that the increase in drag of the individual blade is more than compensated by the decrease in the number of blades.

(*2.1.2*) *Compressible Flow* (*Subsonic*).—In the majority of practical cases, the velocity of flow through cascades is so high that the compressibility effects cannot be neglected. The methods known for calculating the frictionless compressible flow through cascades[23–25] are too complicated to be suitable for the systematic investigations that are most urgently needed. It is therefore feasible also to apply the Prandtl-Glauert rule, which for the single airfoil has proved most satisfactory, to the cascade in the range of subsonic velocities. The important assumption for the applicability of the Prandtl-Glauert rule—that the deviations from a parallel flow are small—also remains valid for the flow through cascades. This assumption therefore corresponds to a restriction to small angles of deflection of the flow. For the present analysis, the most convenient form of the Prandtl-Glauert rule is that for which the blade section is the same in the compressible flow and in the corresponding incompressible flow. In this case, therefore, the reduction in density due to the expansion of the gas corresponds to a smaller spacing, which in turn causes greater velocities. According to Scholz,[18] the calculation of the compressible flow through a cascade with a given spacing and a given stagger at a given Mach Number can be reduced to the calculation of an incompressible flow through a cascade with a different spacing and a different angle of stagger. For the unstaggered cascade, the relations are extremely simple.

In this case a cascade in compressible flow at a Mach Number $M = w_\infty/a_\infty$ and a solidity d_c/c corresponds to a cascade in incompressible flow with a smaller solidity ratio d_i/c, which is given by the equation

$$d_i/c = (d_c/c)\sqrt{1 - M^2} \qquad (2)$$

The equations for the transformation of the velocities and pressures are

$$u_c\left(x; \frac{d_c}{c}, M\right) = u_i\left(x; \frac{d_i}{c}\right)\Big/\sqrt{1 - M^2} \qquad (3)$$

$$p_c\left(x; \frac{d_c}{c}, M\right) = p_i\left(x; \frac{d_i}{c}\right)\Big/\sqrt{1 - M^2} \qquad (4)$$

By virtue of reducing the compressible subsonic flow through cascades to an incompressible flow, the method for solving the "Direct Problem" in incompressible flow can be readily used.

As an example, the velocity distributions of unstaggered cascades with NACA 0010 blade section are shown in Fig. 6, the inflow being parallel to the blade chord and therefore with zero deflection.

This diagram permits direct information regarding the chordwise position of the point at which the velocity of sound is first reached with increasing free-stream Mach Number. The local Mach Number $M_{\text{local}} = w/a_\infty$, which is obtained by

$$M_{\text{local}} = \frac{w}{a_\infty} = \frac{w}{w_\infty}\frac{w_\infty}{a_\infty} = \frac{w}{w_\infty}M \qquad (5)$$

is shown for the single airfoil and also for the cascades with the solidity ratios $d/c = 1$ and 0.75. Whereas for the single airfoil the velocity of sound is at first attained at a Mach Number of $M = 0.8$, for the solidity of $d/c = 1$ the velocity of sound is first reached at a Mach Number of $M = 0.75$ and for the solidity of 0.75 at a Mach Number of $M = 0.72$. The curves shown in Fig. 6 are only valid for completely subsonic flow. As soon as the velocity of sound is reached locally at Mach Numbers near $M = 1$ in the smallest cross section of the passage between the blades, compression shocks occur, and the passage is chocked and supersonic velocities will occur aft of the smallest cross section. In Fig. 6, the curves in the supersonic region are therefore shown in dotted lines. These conditions have been investigated more closely in theory and ex-

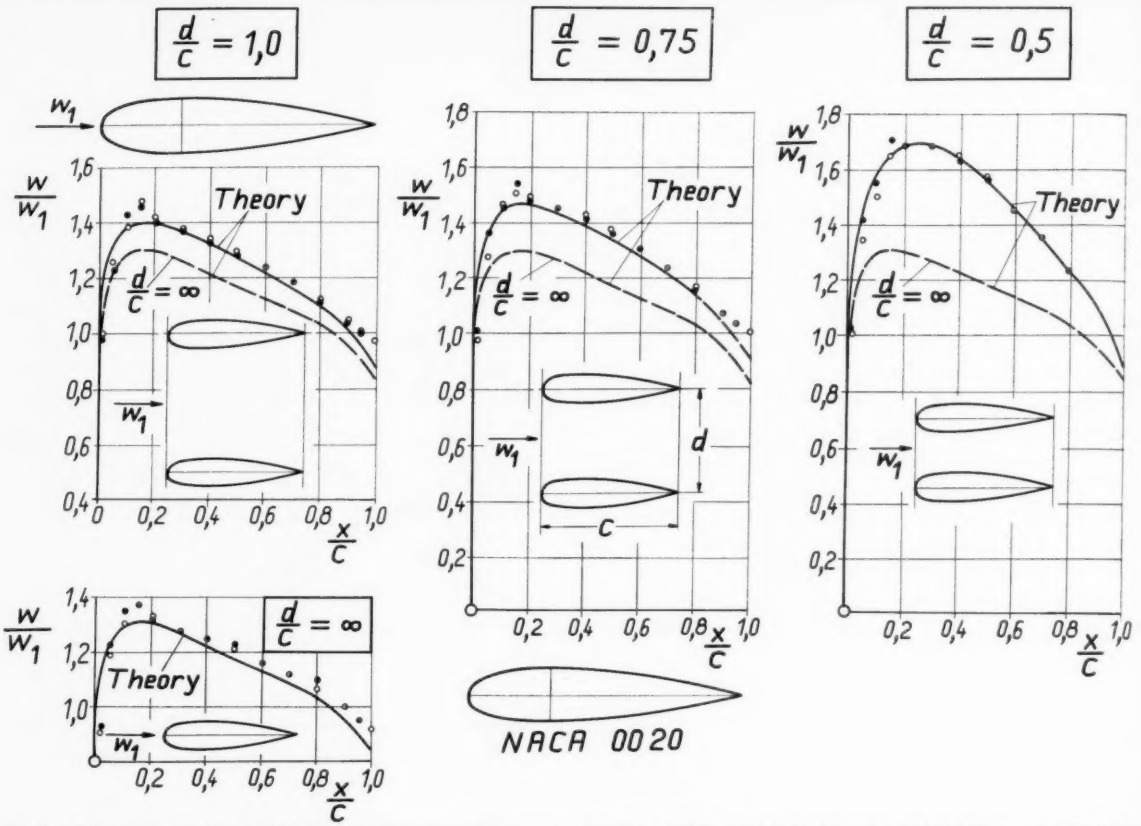

FIG. 9. Chordwise velocity distributions over unstaggered cascades of various solidity ratios d/c for symmetrical inflow. Comparison of theory and experiment: ○● measured velocities along the upper surface and lower surface, respectively.

periment by Ackeret and Rott.[11] It can be generally stated that a blade in cascades is more sensitive to compressibility effects than the single airfoil.

(2.2) *Experimental Investigations*

I shall now deal with our experiments on two-dimensional cascades. Apart from the extreme difficulties of experimental investigations of two-dimensional cascades associated with obtaining fully two-dimensional flow conditions, there is the additional fundamental difficulty of the immense amount of experimental work required if a clear concept of the effects of various parameters upon the cascade is desired.

Experimental investigations of two-dimensional cascades therefore should be carried out, in my opinion, first and foremost for checking systematic theoretical investigations apart from supplying practical data in special cases (e.g., roughness and special blade sections).

(*2.2.1*) *The Two-Dimensional Cascade Tunnel.*—Our two-dimensional cascade tunnel, which was constructed after some years of preliminary research by Dr. N. Scholz and Ing. H. Goldmann, is particularly suited for such experiments. The experience gained with other tunnels has, of course, been used, in particular the experience—insofar as it has been published—of Erwin and Emery[12] in the NACA Laboratory at Langley Field.

In Fig. 7, a schematic presentation of this cascade tunnel is shown. The tunnel is of rectangular cross section and can be attached to the nozzle of a wind tunnel with a diameter of 1.3 m. The main dimensions are shown in Fig. 7. The number of blades is seven; thus, according to our experience, the flow corresponding to an infinite number of blades is obtained for the middle blade. The following parameters can be set at any required value within a satisfactory range:

solidity ratio, d/c
blade angle, β_B
inflow velocity, w_1
direction of inflow, β_1

The following quantities are measured as functions of these parameters:

(1) Pressure distribution on the blade (pressure taps), $p(x)$.
(2) Direction of outflow behind the cascade, β_2.
(3) Outflow velocity, w_2.
(4) The total head behind the cascade, h_2.

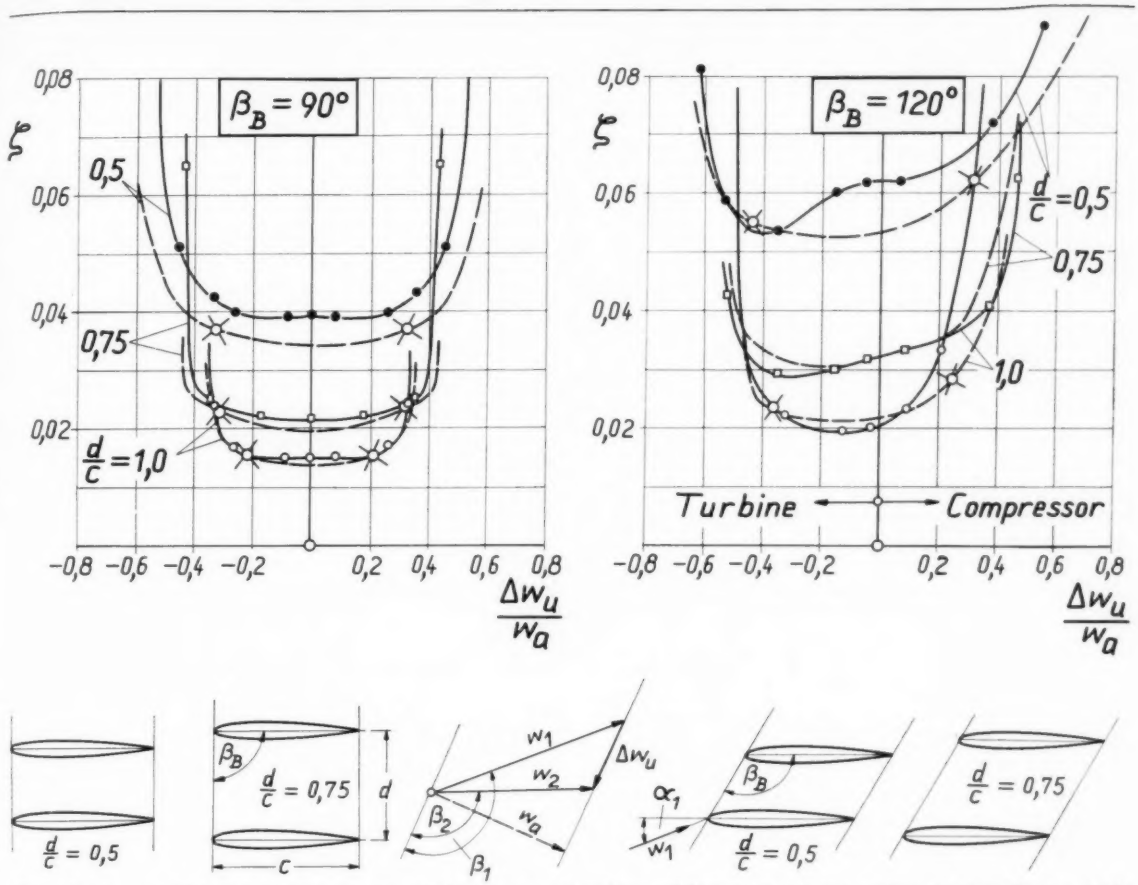

FIG. 10. Loss coefficient ζ according to Eq. (6) for cascades of various solidity ratios d/c and various blade angles β_B; blade section NACA 0010; $Re = w_2 c/\nu = 5 \times 10^5$, fully turbulent boundary layer. Solid lines represent experiments by Scholz; dashed lines represent theory by Speidel[10]; and the circles with projected lines mark the position of separation point at $x/c = 0.95$.

The distributions of the last three quantities have been measured in a plane behind the cascade parallel to the cascade axis extending at least over one spacing. A special instrument was developed which made it possible to take the readings of all quantities in one survey, thus reducing considerably the time required for the tests. The greatest inflow velocity of 60 *m* per sec. is in the range of incompressible flow. The chord of the blade is $c = 200$ mm., and the Reynolds Number based on the outflow velocity is

$$Re = w_2 \cdot c/\nu = 5 \times 10^5$$

Special care has been taken to obtain two-dimensional flow through the cascade, which is rather difficult because of the boundary layers on the walls. But the verification of a good two-dimensional flow is of extreme importance, particularly with respect to the comparison of theory and experiment.

In order to remove the boundary layer, slots are arranged at the four walls ahead of the cascade which are used for removing the boundary layer by suction. The cascade tunnel with this arrangement for suction is shown in Fig. 8. The two slots of each sidewall are connected by means of two ducts and each slot of the upper and lower wall by means of one duct, a total of six ducts in form of flexible tubes with an axial blower with an installed power of approximately 33 hp. With this two-dimensional cascade tunnel we have obtained a large number of results, some of which I will now discuss briefly.

(*2.2.2*) *Some Experimental Results as Compared with Theory.*—The first series of tests was done with cascades of blades of NACA 0020 profile. Though the thickness chord ratio of this section is comparatively large, $t/c = 0.2$, making this profile of limited practical value, it was chosen in order to test the interference effects due to some contraction of the flow resulting from the boundary layers along the walls which were not completely removed by the suction. Furthermore, this profile allowed for a comparison with theoretical calculations.

A comparison of the experimental pressure distribution with theory is shown in Fig. 9 for an unstaggered cascade with solidity ratios $d/c = 1.0$, 0.75, and 0.50;

in each case the direction of the inflow was parallel to the chord of the blade. The theoretical pressure distribution over the single airfoil, $d/c = \infty$, is also shown for comparison. The difference between the pressure distribution of the blade in cascade and the single airfoil naturally increases with closer spacing. For all solidity ratios, the agreement between theory and experiment is very good indeed.

Some of the results on loss coefficients are shown in Fig. 10, where the loss coefficient

$$\zeta = \Delta h/(\rho/2)w_a^2 = \Delta h/g_a \qquad (6)$$

based on the velocity head of the effective flow $g_a = (\rho/2)w_a^2$ is plotted against the deflection $\Delta w_u/w_a$ for three solidity ratios $d/c = 1.0, 0.75$, and 0.50. In the case of the unstaggered cascade, $\beta_B = 90°$, all cascades are compressor cascades. For the staggered cascades, $\beta_B = 120°$, the negative values of Δw_u correspond to turbine cascades and the positive values of Δw_u to compressor cascades. The theoretical loss coefficients are also shown for comparison with the experimental values. The agreement is good. Particularly, the rapid increase of the loss coefficients with increasing deflection $\Delta w_u/w_a$ due to separation is well reproduced by theory.

So far, only two-dimensional flow problems in cascades have been discussed. From the practical point of view, the three-dimensional losses due to the sidewalls of the passage and due to the clearance are of equal importance. For normal values of the ratio of blade height b to blade chord c, of $b/c = 2$ to 3, the two-dimensional losses—so-called blade losses—are about half the total losses. The other half is due to the three-dimensional effects at the walls and the clearance. Extensive results about the three-dimensional losses at the walls have been obtained earlier by Carter.[21] Some contributions about the losses due to the clearance have been given in a report by Schäffer.[13] Some results are given in the German version of this paper.

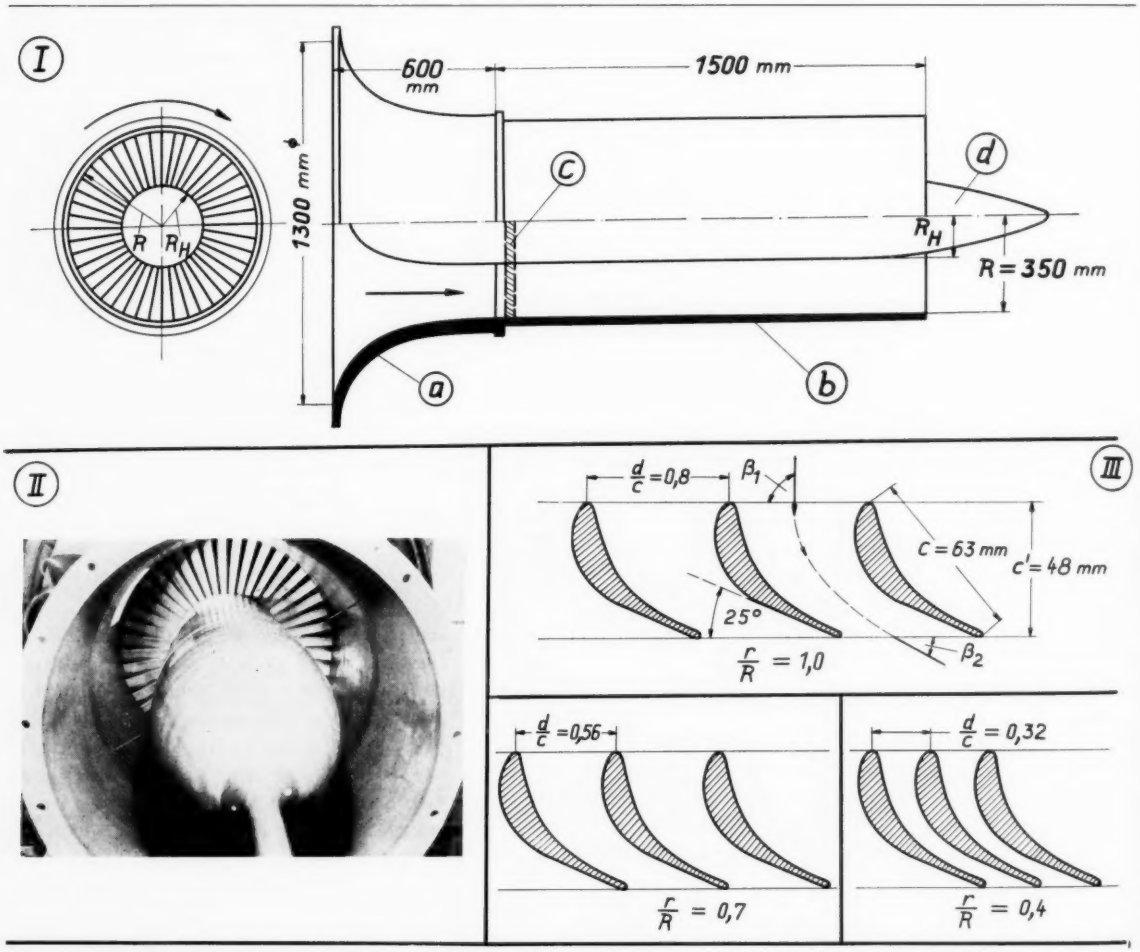

FIG. 11. Experimental setup for cylindrical cascades. (I) General view: (a) inlet nozzle; (b) outer ring; (c) cascade, number of blades, $z = 44$; and (d) hub, various R_H. (II) View in upstream direction. (III) Cross section of blades at various radial stations r/R; blade section GHH-B.

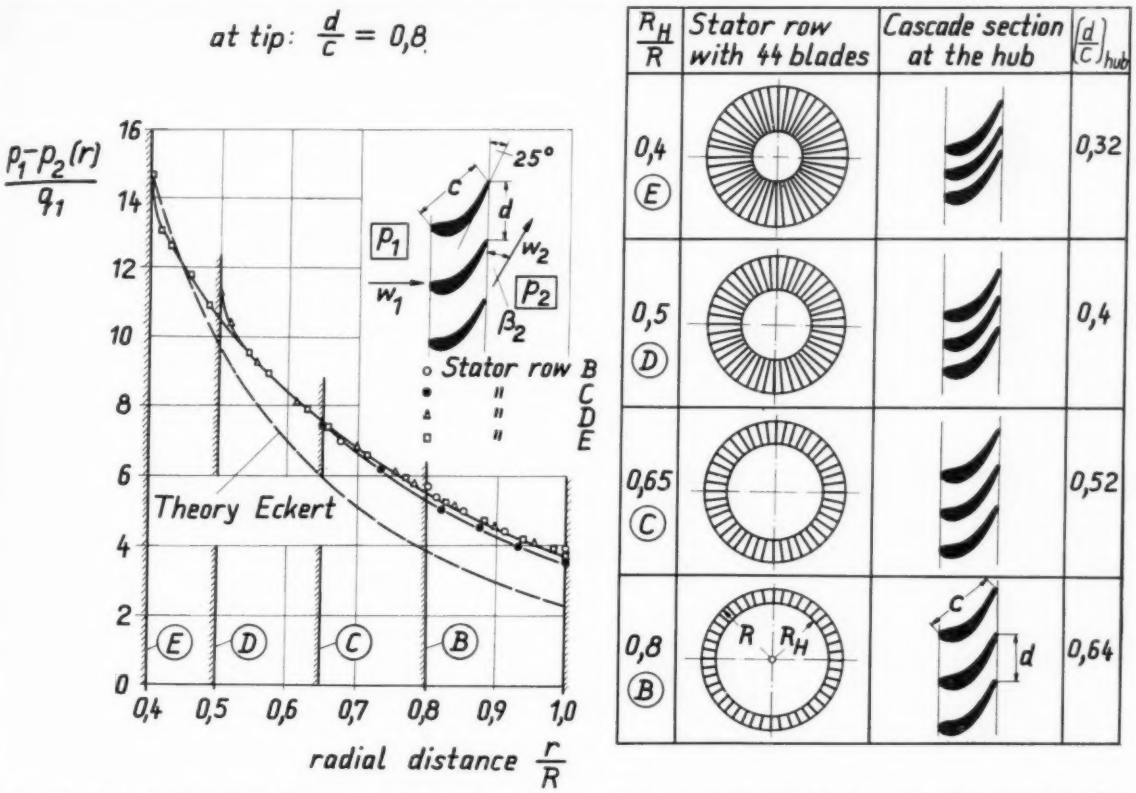

FIG. 12. Radial distribution of pressure difference $p_1 - p_2(r)$ across the cascade for cylindrical cascades of various hub atiosr R_H/R; blade section GHH-B. $R = 350$ mm.; $c = 63$ mm.; $Re = w_1 c/\nu = 6 \times 10^4$. Theory according to E. Eckert[17] assuming constant angle of flow at outlet, $\beta_2 = 24°$.

(3) Investigations on Cylindrical Axial-Flow Cascades

Extensive experimental investigations have been carried out on cylindrical axial-flow cascades in order to clarify the problems of three-dimensional cascade flow. Scholz[14] has reported on this subject in greater detail, and Schäffer[15] has extended this work. These investigations, extending over some years, had originally been conducted in order to verify experimentally the theory of the dead flow region near the hub in a rotating flow as given by Bammert.[16] I do not want to give any details about this point but want only to report on the relation between two-dimensional and three-dimensional cascade flow, which we have drawn from these experiments.

The test arrangement is shown in Fig. 11. The flow is confined to the annular space between the hub (radius R_H) and the outer tube (radius R). The stator contains 44 untwisted blades radially arranged. At the entry to the stator, the flow is purely axial, the angle of inflow being $\beta_1 = 90°$, whereas the angle of the outflow is about $\beta_2 = 24°$. Thus there is a considerable deflection of the flow. The flow leaves the stator with a swirl of such a magnitude that, in the annular space behind the stator, the circumferential velocity of the flow is a multiple of the axial component. Four different cylindrical cascades have been tested. The outer radius, the number of blades, and the blade profile being the same, the radius of the hub R_H and, hence, the hub ratio R_H/R were varied, as follows (Fig. 12):

$$R_H/R = 0.8;\ 0.65;\ 0.5;\ 0.4$$

The solidity ratio at the outer radius remained constant with a value of $d/c = 0.8$, whereas the solidity ratio at the hub varied from $d/c = 0.64$ to 0.32. In the annular space behind the stator the distributions of the static pressure, of the magnitude of the velocity, and the direction of the velocity were measured over the blade spacing and the radial distance. Also pressure distribution measurements over the blade surface over the whole annular space were carried out.

In Fig. 12 the radial distribution of the pressure difference across the cascade is shown for the four different hub ratios. The pressure difference across the cascade, $\Delta p = p_1 - p_2$, is considerably greater near the hub than near the outer wall, because the pressure p_2 behind the cascade increases from the inner part toward the outer part because of the radial pressure

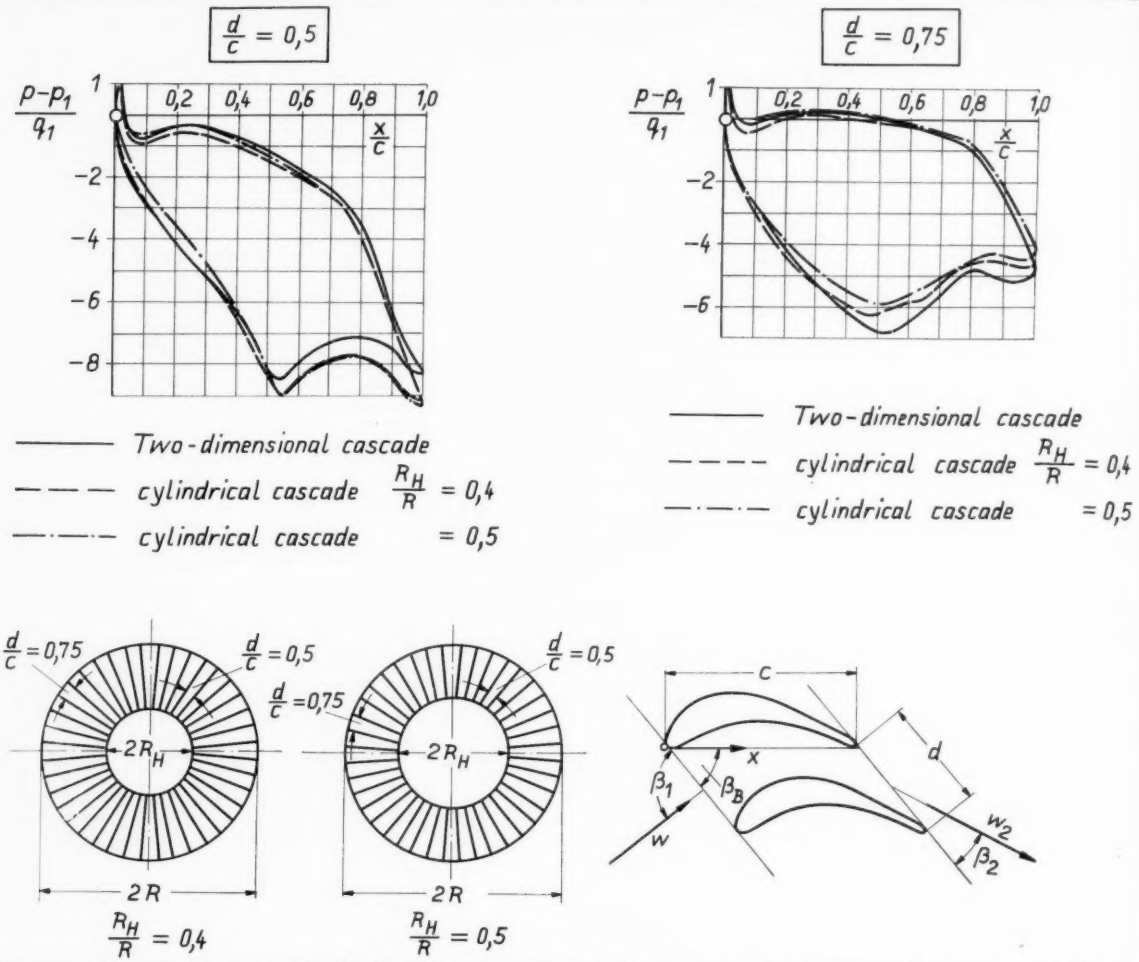

FIG. 13. Comparison of pressure distributions for the two-dimensional and the cylindrical cascade. Parameters as in Fig. 12. $\beta_B = 51°$; $\beta_1 = 90°$; $Re = w_1 c/\nu = 6 \times 10^5$.

distribution, which is connected with the rotational flow; whereas the pressure p_1 in front of the cascade is constant over the radius. The presentation in Fig. 12 shows the remarkable fact that the radial distribution of the pressure difference across the cascade is independent of the hub ratio. It can therefore be concluded that the rotational flow is of the same type for all hub ratios. For comparison, the theoretical curve according to Eckert and Korbacher[17] is included, which was calculated for an outflow angle of $\beta_2 = 24°$ corresponding to two-dimensional cascade flow. This theoretical curve is somewhat below the experimental values of the cylindrical cascade. The difference between the two curves represents the additional pressure difference due to friction. This additional pressure difference is approximately constant along the radius.

With the aid of the pressure distribution measurements it is possible to throw some light on the "radial divergence," this meaning the variation of the solidity ratio along the radius. For this purpose also, pressure distributions on the two-dimensional cascade with the same blade section and with different solidity ratios have been taken. A comparison of the pressure distributions of the two-dimensional cascade and the cylindrical cascade is shown in Fig. 13. The pressure distributions for two values of the solidity ratio, $d/c = 0.75$ and 0.50, of the two-dimensional cascade are compared with those of the cylindrical cascade at such a radial station, for which the solidity ratio is just the same as that of the two-dimensional cascade. The pressure distribution of the two-dimensional cascade is in excellent agreement with that of the cylindrical axial-flow cascade. It can therefore be concluded that the effect of "radial divergence" on the pressure distribution and, hence, on the boundary layer is negligible. It can further be concluded that for a stator row cascade the local loss coefficients are independent of the "radial divergence" due to the absence of the centrifugal forces.

In Fig. 14 the local loss coefficient $\zeta = \Delta h/(\rho/2)\, w_1^2$ (based on the inflow velocity) is plotted against the radial distance for a cascade with the hub ratio $R_H/R = 0.5$. Except for the region very near to the hub and the outer wall of the annular space, the loss coefficient of the two-dimensional cascades is in full agreement with that of the cylindrical cascade. The additional end losses are confined to the vicinity of the inner and the outer walls. In the present case, where the ratio of blade height b to blade chord c is $b/c = 2.8$, the total loss, including three-dimensional losses, is $\zeta_{\text{total}} = 0.480$, while the losses of the two-dimensional cascade are 0.391. The additional end losses therefore are 19 per cent of the total losses.

Finally, a few remarks may be made about the radial distribution of the velocity components behind the cylindrical cascade. The radial distribution of the angle of outflow β_2 and the radial distribution of all three velocity components—i.e., the circumferential component w_{2u} due to rotation; the axial component w_{2a}, which gives the mass flow; and also the radial component w_{2r}—are shown in Fig. 15 as measured in a plane $0.03R$ behind the cascade, with a hub ratio $R_H/R = 0.5$. The radial component is scaled up by a factor of ten, and all quantities are averaged over one spacing in the circumferential direction.

For the axial and circumferential components of the velocity, theoretical values are given which have been calculated according to Eckert[17] for the measured distribution of the outlet angle β_2. This theory shows satisfactory agreement with measurements. As the radial component of the velocity is comparatively small, the correct measurement of these values is rather difficult. In the present case the radial velocity component is directed toward the center throughout the entire radial distance of the annular space. The sign of the radial velocity component is easy to realize. Because of the radial pressure increase due to the rotating flow (Fig. 12), there is a greater pressure difference at the inner parts of the cascade than at its outer parts. Consequently, the amount of the outflow velocity w_2 is greater at the inner part than at the outer part of the cascade. Since the direction of the outflow velocity w_2 is almost constant over the radial distance due to the untwisted blades, the axial component w_{2a} giving the mass flow is also greater at the inner part than at the outer part. As the axial component in front of the cascade is constant over the radius, a transportation of fluid must take place inside the cascade from the outer part toward the inner part. This transportation of fluid is associated with an inward radial component of the velocity inside the cascade, which is still persisting shortly behind the cascade, as can be seen from our experiments. A theoretical curve of the radial velocity distribution is also given which is based on the concept of the flow just discussed and which was calculated by applying the equation of continuity to the w_{2a} distribution.

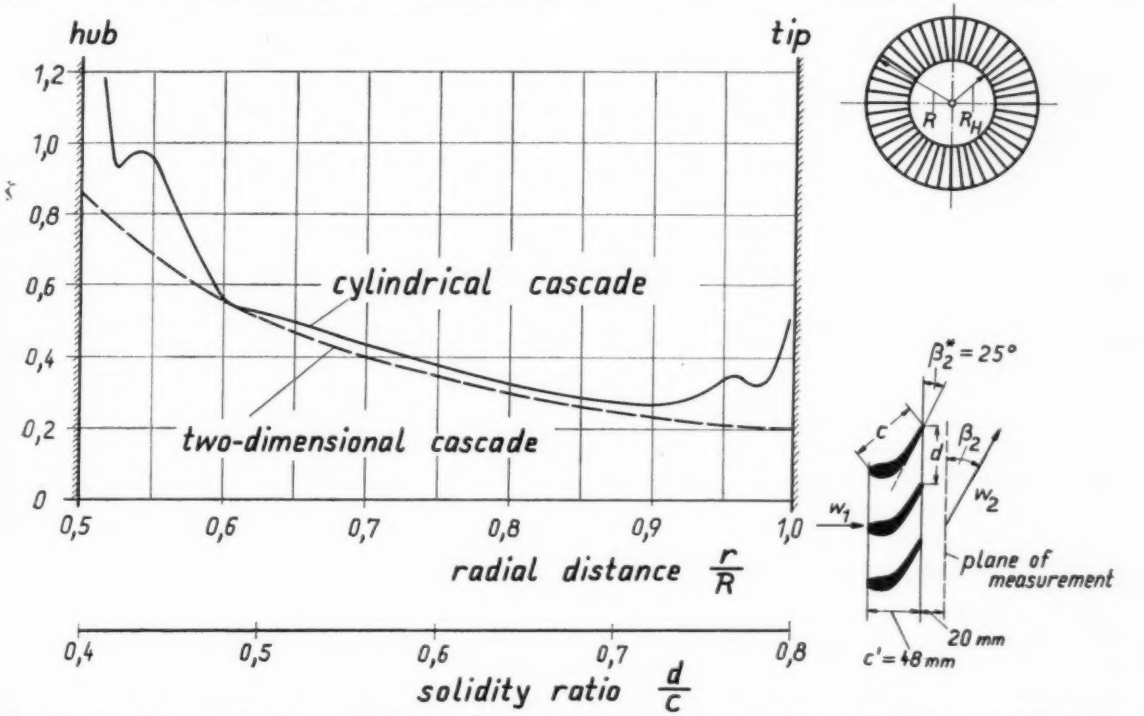

FIG. 14. Local loss coefficient ζ for a cylindrical cascade (cascade D of Fig. 12). Experiments by Schäffer.[18] $\zeta = \Delta h/(\rho/2)w_1^2$.

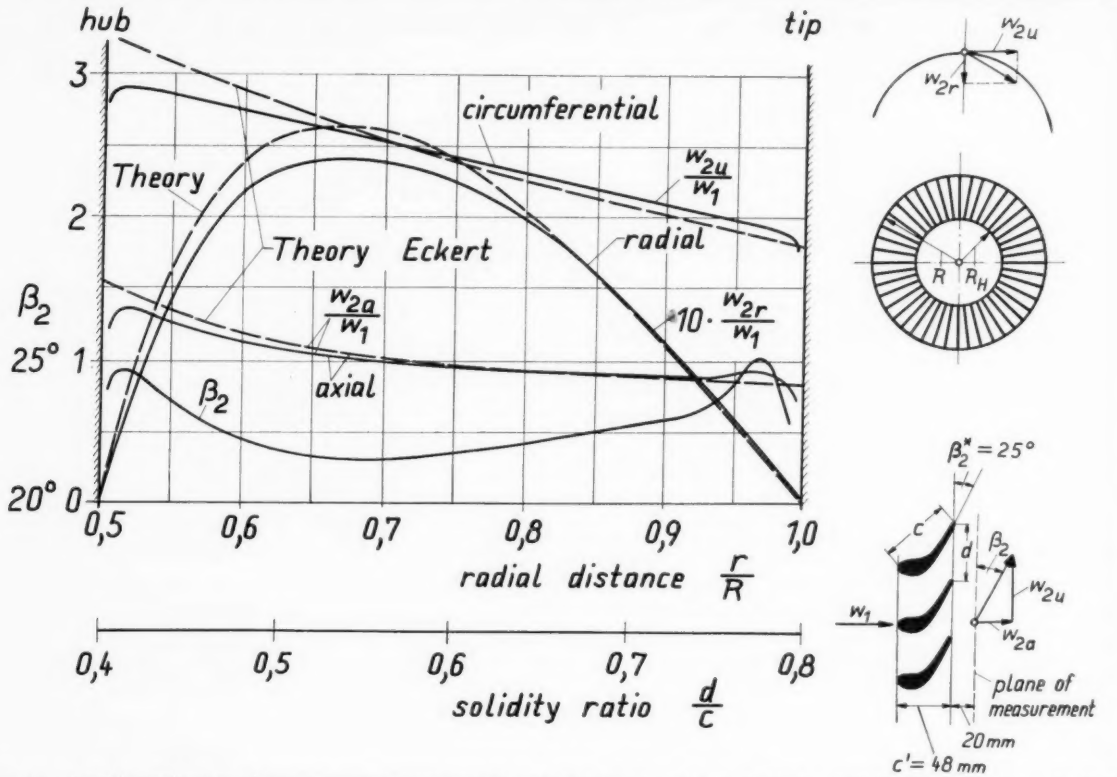

FIG. 15. Radial distribution of velocity components and of angle of flow at outlet, β_2, behind a cylindrical cascade (cascade D of Fig. 12). Solid lines represent experiments by Schäffer,[16] and dashed lines represent theory for w_{2u} and w_{2a} according to E. Eckert.[17]

(4) CONCLUSIONS

The results of the investigations of the flow through cascades are now summarized, and a few suggestions are given for further research in this particular field.

Systematic investigations of cascade flow carried out at the Institute of Fluid Mechanics at the Technical University of Braunschweig were primarily done for two-dimensional cascades in incompressible flow including viscosity effects, because we think that the effects of compressibility and the effects due to three-dimensional flow (end losses, losses due to clearance, and effects due to radial divergence) can be attacked successfully only if the two-dimensional incompressible cascade flow is sufficiently well understood. With regard to this problem we have succeeded in making some remarkable contributions. Some results have also been obtained for the three-dimensional cascade flow.

These are the main results of our investigations:

Two-Dimensional Cascade Flow

(1) *Theoretical.*—Simple methods for solving the "Indirect Problem" and the "Direct Problem" have been worked out for the two-dimensional incompressible frictionless flow through cascades. By this method the time for calculating the pressure distribution for a given cascade, for ten different angles of inflow, has been reduced to about 20 hours.

(2) *Theoretical.*—Extensive systematic investigations of the loss coefficients have been carried out for unstaggered cascades in two-dimensional incompressible viscous flow. The theoretical calculation of the loss coefficients leads to cascades of best efficiency—i.e., cascades with a minimum loss coefficient at a given angle of deflection. These cascades in most cases have a comparatively large value of the solidity ratio and are associated with a flow that is slightly separated.

(3) *Theoretical.*—By applying the Prandtl-Glauert rule, a method has been developed for calculating the compressible frictionless two-dimensional flow through cascades with small angles of deflection of the flow through cascades. It has been shown by some examples that at a constant blade section and constant solidity ratio the velocities at the blade in cascade are increasing more rapidly with increasing Mach Number than the velocities on the single airfoil.

(4) *Experimental.*—A two-dimensional cascade tunnel for incompressible flow has been constructed primarily for checking the results of theoretical cascade calculations, but it also was constructed for investigating special cascade problems of practical importance. Special care has been taken to obtain conditions

of two-dimensional flow. By means of boundary-layer slots and by applying suction, this has been achieved satisfactorily. Measurements in this cascade tunnel are in good agreement with theoretical results.

Cylindrical Axial-Flow Cascades

(5) *Radial Divergence.*—The radial divergence of the blades has a very small influence on the flow through cylindrical cascades. The pressure distribution over a blade in a cylindrical cascade was found to be exactly the same as in the two-dimensional cascade of the same solidity ratio.

(6) *Radial Velocity Components.*—For a cylindrical cascade with untwisted blades and a purely axial inflow, there exists a radial velocity component immediately behind the cascade directed toward the center with a maximum value of about 25 per cent of the axial velocity component for hub ratio $R_H/R = 0.5$.

Further Investigations

For *further investigations* in the field of cascade flow the following problems seem to be the most important.

(1) *Experimental Investigation of Compressible Flow Through Cascades.*—Some careful two-dimensional compressible cascade experiments are needed as the basis for theoretical work in this field. These measurements should start from Mach Numbers in the incompressible flow range and go up to supersonic flow, thus giving a link between incompressible and compressible two-dimensional cascade flow.

(2) *Theoretical Investigations of Compressible Flow Through Cascades.*—It is desirable to enlarge considerably upon the calculations of the compressible frictionless two-dimensional flow through cascades, first in the subsonic range. The Prandtl-Glauert rule applies to purely subsonic flow and to moderate angles of deflection of the flow only. However, for turbine cascades large angles of deflection are required.

(3) *Three-Dimensional Losses.*—Apart from the losses in two-dimensional cascades, a considerable contribution to the total losses results from the three-dimensional losses that are due to the clearance and to the sidewalls of the blade passage. Having analyzed the two-dimensional losses, a systematic investigation of the three-dimensional losses is urgently required.

(4) *Investigations on Rotating Cascades.*—Experiments with rotating cascades are of prominent importance, first in the region of subsonic flow. These experiments are necessary for the investigation of the effects of centrifugal forces on the flow through the cascade.

References

[1] Weinig, F., *Die Strömung um die Schaufeln von Turbomaschinen;* Leipzig, 1935.

[2] Schlichting, H., *Grenzschicht-Theorie;* Karlsruhe, Germany, 1951.

[3] Schlichting, H., and Scholz, N., *Ueber die theoretische Berechnung der Strömungsverluste eines ebenen Schaufelgitters,* Ingenieur-Archiv, Vol. 19, p. 42, 1951.

[4] Schilhansl, M., *Näherungsweise Berechnung von Auftrieb und Druckverteilung in Flügelgittern,* Jahrbuch d. Wissenschaftlichen Gesellschaft für Luftfahrt, p. 151, 1927.

[5] Ackeret, J., *Zum Entwurf dichtstehender Schaufelgitter,* Schweizer Bauzeitung, Vol. 60, p. 120, 1942.

[6] Traupel, W., *Die Berechnung der Potentialströmung durch Schaufelgitter,* Sulzer Technische Rundschau, No. 1, 1945.

[7] Garrick, J. E., *On the Plane Potential Flow Past a Lattice of Arbitrary Airfoils,* NACA Report No. 788, 1944.

[8] Ruden, P., *Untersuchungen über einstufige Axialgebläse,* Luftfahrtforschung, Vol. 14, p. 325, 1937.

[9] Marcinowski, H., *Messungen an axialen Schaufelgittern,* Sonderheft "Versuchswesen der Firma Voith"; Heidenheim, Brenz, 1949.

[10] Speidel, L., *Berechnung der Strömungsverluste von ungestaffelten ebenen Schaufelgittern,* Doctor thesis, Braunschweig, 1953, to be published shortly in the *Ingenieur Archiv.*

[11] Ackeret, J., and Rott, N., *Ueber die Strömung von Gasen durch ungestaffelte Schaufelgitter,* Schweizer Bauzeitung, Vol. 67, pp. 40–41, 58–61, 1949.

[12] Erwin, J. B., and Emery, J. C., *Effect of Tunnel Configuration and Testing Technique on Cascade Performance,* NACA TR No. 1016, 1951.

[13] Schäffer, H., *Messungen der Spaltverluste eines ebenen Schaufelgitters,* Report No. 52/17 of the Institute of Fluid Mechanics of the Technical University of Braunschweig, 1952.

[14] Scholz, N., *Experimentelle Untersuchungen an Drallströmungen durch axiale Schaufelgitter,* Report No. 53/1 of the Institute of Fluid Mechanics of the Technical University of Braunschweig, 1953. To be published shortly as aVDI-Forschungsheft.

[15] Schäffer, H., *Untersuchungen an einem axialen Schaufelgitter mit dem Nabenverhältnis $R_N/R_A = 0.5$,* Report No. 53/5 of the Institute of Fluid Mechanics of the Technical University of Braunschweig, 1953.

[16] Bammert, K., and Kläukens, H., *Nabentotwasser hinter Leiträdern von axialen Strömungsmaschinen,* Ingenieur-Archiv, Vol. 17, p. 367, 1949. See also Zeitschrift des Vereins Deutscher Ingenieure, Vol. 92, p. 777, 1950.

[17] Eckert, E., and Korbacher, G., *Die Strömung durch Axialturbinenstufen von grosser Schaufelhöhe,* Forschungsbericht der ZWB (*Zentrale für wissenschaftliches Berichtswesen der deutschen Luftfahrtforschung*), No. 1750, 1943.

[18] Scholz, N., *Ein Berechnungsverfahren zum Entwurf von Schaufelgitterprofilen,* Report No. 52/27 of the Institute of Fluid Mechanics of the Technical University of Braunschweig, 1952. To be published shortly as a VDI-Forschungsheft.

[19] Schlichting, H., *Berechnung der reibungslosen Strömung für ein vorgegebenes ebenes Schaufelgitter in inkompressibler Strömung,* Report No. 52/18 of the Institute of Fluid Mechanics of the Technical University of Braunschweig, 1952.

[20] Richter, W., *Berechnung der Potentialströmung ebener Gitter mit beliebig vorgegebenen Profilen* (unpublished report), Braunschweig, 1952.

[21] Carter, A. D. S., *Three-Dimensional-Flow Theories for Axial Compressors and Turbines,* Proc. Inst. Mech. Eng., Vol. 159, p. 255, 1948.

[22] Howell, A. R., *The Present Basis of Axial Flow Compressor Design—Part I, Cascade Theory and Performance,* British ARC R. & M. 2095, 1942.

[23] Spur, R. A., and Allen, H. J., *A Theory of Unstaggered Airfoil Cascades in Compressible Flow,* NACA TR No. 888, 1947.

[24] Costello, G. R., *Method of Designing Cascade Blades with Prescribed Velocity Distribution in Compressible Potential Flows*, NACA TR No. 978, 1950.

[25] Costello, G. R., Cummings, R. L., and Sinette, J. T., *Detailed Computational Procedure for Design of Cascade Blades with Prescribed Velocity Distributions in Compressible Potential Flow*, NACA TN No. 2281, 1951.

[26] Scholz, N., *Two-Dimensional Correction of the Outlet Angle in Cascade Flow*, Readers' Forum, Journal of the Aeronautical Sciences, Vol. 20, No. 11, pp. 786–787, November, 1953.

Effect of Diffusion Fields on the Laminar Boundary Layer

(*Continued from page 162*)

[5] Chapman, S., and Cowling, T. G., *The Mathematical Theory of Non-Uniform Gases;* Cambridge University Press, 1952.

[6] Jost, W., *Diffusion in Solids, Liquids, and Gases;* Academic Press, Inc., New York, 1952.

[7] Ince, E. L., *Integration of Ordinary Differential Equations;* Interscience Publishers, New York, 1952.

[8] Strehlow, R. A., *The Temperature Dependence of the Mutual Diffusion Coefficients for Four Gaseous Systems*, University of Wisconsin, Naval Research Laboratory, Department of Chemistry, CM-776, February, 1953.

[9] Van Driest, E. R., *Investigation of the Laminar Boundary Layer in Compressible Fluids Using the Crocco Method*, NACA TN No. 2597, January, 1952.

Changes of Address

Since the Post Office Department does not as a rule forward magazines to forwarding addresses, it is important that the Institute be notified of changes in address 30 days in advance of publishing date to ensure receipt of every issue of the JOURNAL and REVIEW.

Notices should be printed legibly and sent directly to:

Institute of the Aeronautical Sciences, Inc.

2 East 64th Street, New York 21, New York

Applications of Hypersonic Small-Disturbance Theory

MILTON D. VAN DYKE*

Ames Aeronautical Laboratory, NACA

SUMMARY

When slender objects fly at high supersonic speeds, linearized theory breaks down because nonlinearity becomes an essential feature of the flow. A study is made of the simplest inviscid theory retaining the essential nonlinearity, which is that underlying the hypersonic similarity rule of Tsien and Hayes. The accuracy is greater than in the transonic or supersonic small-disturbance theories and can be further increased by interpreting results in conformity with Newtonian impact theory.

Because of a coincidence, this hypersonic small-disturbance theory can be reinterpreted so as to yield a first approximation also in the range of linearized theory. Thus a single theory and a single similarity rule cover the entire supersonic range from just above the transonic zone to infinite Mach Number.

To illustrate that the theory can serve both as a simplified model of the full equations and as a practical approximation, several problems relating to bodies of revolution are solved. An anomaly in an earlier solution for slender cones is found to result from computational errors rather than any shortcoming of the theory. The initial flow gradients at the nose of an ogive are determined, and a troublesome singularity encountered in the full problem by other investigators is found to be illusory. Lighthill's technique of rendering solutions uniformly valid is then used to calculate the third term in the power series for surface pressure.

SYMBOLS

b	= ratio of cone slope to shock-wave slope
B	= function defining body shape
C_p	= pressure coefficient
f	= conical stream function for cone
g, h	= subsequent terms in series expansion of stream function for ogive
M	= free-stream Mach Number
p	= pressure
r	= radial coordinate
$R(x)$	= radius of meridian curve of ogive of revolution
$s(x)$	= function defining shock wave on body of revolution
S	= function defining shock-wave surfaces
u, v, w	= Cartesian velocity components with u in free-stream direction
x, y, z	= Cartesian coordinates with x in free-stream direction
β	= $\sqrt{M^2 - 1}$
γ	= adiabatic exponent of gas (1.405 in examples)
δ	= local slope of two-dimensional body
θ	= conical coordinate, $\bar{r}/\bar{x}$
ρ	= density
σ	= semivertex angle of cone
τ	= thickness parameter of body; in examples, initial slope of shock wave
ψ	= stream function for body of revolution
ω	= reduced entropy function, $\bar{p}/\bar{\rho}^\gamma$
$(\quad)_\infty$	= free-stream value
$(\quad)_0$	= value at tip of ogive
$(\overline{\quad})$	= reduced form [see Eq. (2)]
$[\quad]$	= jump in quantity through shock wave

Presented at the Aerodynamics Session, Annual Summer Meeting, IAS, Los Angeles, July 15–17, 1953. Revised and received November 26, 1953.

* Aeronautical Research Scientist.

INTRODUCTION

AERODYNAMIC SHAPES ARE ordinarily most efficient when they cause the least flow disturbance. For this reason, linearized theory, based on the assumption of small disturbances due to thin or slender bodies, has been of great practical value in analyzing both subsonic and supersonic flows. However, when the flight Mach Number of even a very slender object greatly exceeds unity, linearized theory breaks down because nonlinearity becomes an essential feature of the flow. At such speeds, just as in the transonic range, linearized theory must be abandoned in favor of an approximation that retains the essential nonlinearity.

If viscosity can be neglected (or accounted for separately), the velocity disturbances produced by a thin body remain small compared with its flight speed no matter how great the Mach Number. The pressure disturbances are also small compared with the stagnation pressure, though perhaps large compared with the static pressure. In this sense, the flow field involves only small disturbances. Consequently, the full equations of motion can be simplified to provide a useful approximation at arbitrarily high flight speeds.

An investigation is made here of the simplest approximation to the full equations which retains the nonlinearity essential at Mach Numbers large compared with unity. The resulting theory is that which underlies the hypersonic similarity rule of Tsien[1] and Hayes.[2] Although the similarity rule has already been thoroughly explored, the underlying theory has, in fact, never been written down except for plane flow in a restricted range of Mach Number,[3] and applications have been limited to the few special cases that are strictly irrotational or can be assumed approximately so. Here other examples are studied in which flow rotation is important. It is shown that the small-disturbance theory serves as a helpful guide to the full theory and as a useful approximation for practical calculations.

A more detailed exposition of some parts of this paper is given in reference 4.

Hypersonic Small-Disturbance Theory

Consider a thin or slender three-dimensional body fixed in a uniform supersonic stream. The motion will be assumed steady for simplicity, the extension to slightly unsteady flow being straightforward.[4] Let the thickness of the body be described by the parameter τ, which is small compared with unity. (For example, τ may be taken as the maximum streamwise slope of the body.) It is known that linearized theory yields an adequate description of the flow only when the free-stream Mach Number M is some moderate multiple of unity, so that $M\tau \ll 1$. As M increases, so that $M\tau$ approaches and exceeds unity, linearized theory breaks down in general (and so do higher approximations based upon it, such as second-order theory). Thus nonlinearity becomes essential, and the flow will be termed *hypersonic* if the free-stream Mach Number is so great that $M\tau$ is not small. (It may be very large, as when $M \to \infty$.)

Mathematically, it is convenient to regard the various small-disturbance theories as approximations that become exact for vanishing thickness. From this point of view, we seek a simplified theory that provides a first approximation as

$$\left.\begin{matrix}\tau \to 0 \\ M \to \infty\end{matrix}\right\} \text{ with } 1/M\tau = 0(1)^*$$

Small-Disturbance Problem

A first approximation to the full equations of motion is to be found by retaining only leading terms in the thickness parameter τ. This is accomplished by introducing new variables that are of order unity.

The full equations of motion, expressing the conservation of mass, momentum, and energy, may be written as

$$(\rho u)_x + (\rho v)_y + (\rho w)_z = 0 \tag{1a}$$

$$uu_x + vu_y + wu_z + (p_x/\rho) = 0 \tag{1b}$$

$$uv_x + vv_y + wv_z + (p_y/\rho) = 0 \tag{1c}$$

$$uw_x + vw_y + ww_z + (p_z/\rho) = 0 \tag{1d}$$

$$u(p/\rho^\gamma)_x + v(p/\rho^\gamma)_y + w(p/p^\gamma)_z = 0 \tag{1e}$$

where subscripts indicate differentiation.

An appropriate transformation of variables is suggested by the known facts that lateral velocities must be proportional to the body slope, that at high Mach Numbers the lateral extent of the disturbance field is a moderate multiple of the body thickness, that according to Newtonian impact theory the surface pressure coefficient is proportional to the square of the inclination, etc. Thus, choosing the x axis in the free-stream direction, we introduce new (barred) variables according to

$$\left.\begin{aligned} u &= u_\infty[1 + \tau^2\bar{u}(\bar{x}, \bar{y}, \bar{z})] \\ v &= u_\infty\tau\bar{v}(\bar{x}, \bar{y}, \bar{z}) \\ w &= u_\infty\tau\bar{w}(\bar{x}, \bar{y}, \bar{z}) \\ p &= p_\infty(\gamma M^2\tau^2)\bar{p}(\bar{x}, \bar{y}, \bar{z}) \\ \rho &= \rho_\infty\bar{\rho}(\bar{x}, \bar{y}, \bar{z}) \\ x &= \bar{x} \\ y &= \tau\bar{y} \\ z &= \tau\bar{z} \end{aligned}\right\} \tag{2}$$

We *assume* that the new dependent variables ($\bar{u}$, $\bar{v}$, $\bar{w}$, $\bar{p}$, $\bar{\rho}$) are $0(1)$ as $\tau \to 0$ for fixed $M\tau$ and that the reciprocals of the new independent variables ($1/\bar{x}$, $1/\bar{y}$, $1/\bar{z}$) are also $0(1)$. This assumption will be justified by the complete internal consistency of the resulting approximate problem.

If we introduce these new variables and discard terms that contain τ^2 explicitly, Eqs. (1) reduce to

$$\bar{u}_{\bar{x}} + \bar{v}\bar{u}_{\bar{y}} + \bar{w}\bar{u}_{\bar{z}} + (\bar{p}_{\bar{x}}/\bar{\rho}) = 0 \tag{3}$$

and

$$\bar{\rho}_{\bar{x}} + (\bar{\rho}\bar{v})_{\bar{y}} + (\bar{\rho}\bar{w})_{\bar{z}} = 0 \tag{4a}$$

$$\bar{v}_{\bar{x}} + \bar{v}\bar{v}_{\bar{y}} + \bar{w}\bar{v}_{\bar{z}} + (\bar{p}_{\bar{y}}/\bar{\rho}) = 0 \tag{4b}$$

$$\bar{w}_{\bar{x}} + \bar{v}\bar{w}_{\bar{y}} + \bar{w}\bar{w}_{\bar{z}} + (\bar{p}_{\bar{z}}/\bar{\rho}) = 0 \tag{4c}$$

$$(\bar{p}/\bar{\rho}^\gamma)_{\bar{x}} + \bar{v}(\bar{p}/\bar{\rho}^\gamma)_{\bar{y}} + \bar{w}(\bar{p}/\bar{\rho}^\gamma)_{\bar{z}} = 0 \tag{4d}$$

Upstream and laterally far away from the body, the flow quantities must attain free-stream values,

$$\left.\begin{aligned} \bar{u} = \bar{v} = \bar{w} &= 0 \\ \bar{p} &= 1/\gamma M^2\tau^2 \\ \bar{\rho} &= 0 \end{aligned}\right\} \text{ in the free stream} \quad \begin{matrix}(5a)\\(5b)\\(5c)\end{matrix}$$

If the body is described in reduced coordinates by $B(\bar{x}, \bar{y}, \bar{z}) = 0$, the condition of tangent flow at the surface becomes, neglecting terms of $0(\tau^2)$,

$$B_{\bar{x}} + \bar{v}B_{\bar{y}} + \bar{w}B_{\bar{z}} = 0 \quad (\text{at } B = 0) \tag{6}$$

If the full system of shock waves is described by $S(\bar{x}, \bar{y}, \bar{z}) = 0$, the shock-wave relations become, to the same approximation,

$$[\bar{u}]/S_{\bar{x}} = [\bar{v}]/S_{\bar{y}} = [\bar{w}]/S_{\bar{z}} \tag{7a}$$

$$[\bar{\rho}(S_{\bar{x}} + \bar{v}S_{\bar{y}} + \bar{w}S_{\bar{z}})] = 0 \tag{7b}$$

$$[\bar{\rho}(S_{\bar{x}} + \bar{v}S_{\bar{y}} + \bar{w}S_{\bar{z}})^2 + (S_{\bar{y}}^2 + S_{\bar{z}}^2)\bar{p}] = 0 \tag{7c}$$

$$\left[\frac{1}{2}(S_{\bar{x}} + \bar{v}S_{\bar{y}} + \bar{w}S_{\bar{z}})^2 + \frac{\gamma}{\gamma - 1}(S_{\bar{y}}^2 + S_{\bar{z}}^2)\,\bar{p}\,\bar{\rho}\right] = 0 \tag{7d}$$

$$[\bar{p}/\bar{\rho}^\gamma] \geq 0 \tag{7e}$$

at $S = 0$. Here square brackets denote the increase in a quantity across the shock wave.

The assumptions regarding orders of magnitude are now justified by the complete internal consistency of the reduced problem when $1/(M\tau) = 0(1)$. However, the consistency argument breaks down when $M\tau \ll 1$ [formally, when $M\tau = o(1)$], because then the require-

* Here the order symbols are used in the conventional sense: $f(\tau) = 0(1)$ as $\tau \to 0$ means that $f(\tau)$ remains bounded as $\tau \to 0$, and $f(\tau) = 0(g[\tau])$ means that $f(\tau)/g(\tau)$ is $0(1)$. Similarly, $f(\tau) = o(1)$ means that $f(\tau)$ vanishes as $\tau \to 0$.

ment of Eq. (5b) that $\bar{p} = (\gamma M^2\tau^2)^{-1}$ in the free stream contradicts the assumption that $\bar{p} = 0(1)$. This is an automatic warning that the reduction breaks down in the range of linearized theory.

A significant feature of the reduced equations is that the cross-flow problem for $(\bar{v}, \bar{w}, \bar{p}, \bar{\rho})$ does not involve the streamwise velocity $\bar{u}$. Hence the cross-flow problem can be solved independently; then u (if required) is given by the reduced Bernoulli equation,

$$\bar{u} + \frac{1}{2}(\bar{v}^2 + \bar{w}^2) + \frac{\gamma}{\gamma - 1}\frac{\bar{p}}{\bar{\rho}} = \text{const.} \qquad (8)$$

Therefore Eq. (3) and the first terms of Eqs. (5a) and (7a) are superfluous and can be disregarded hence forth.

The cross-flow problem is completely equivalent to the full problem of unsteady motion in the $\bar{y}$-$\bar{z}$ plane due to a moving solid boundary described by $S(\bar{x}, \bar{y}, \bar{z}) = 0$, $\bar{x}$ being the time.* This analogy was pointed out by Hayes in his extension of the hypersonic similarity rule.[2]

Because terms of order τ^2 have been disregarded in the reduction, flow quantities determined from the small-disturbance equations will differ from their full values by $0(\tau^2)$. This more general result agrees with Goldsworthy's conclusion[3] that in the special case of plane flow with $M\tau \sim 1$ the error is $0(1/M^2)$. The present estimate applies, however, even at $M = \infty$.

Combined Supersonic-Hypersonic Small-Disturbance Theory

It is known that transonic small-disturbance theory embraces linearized subsonic and supersonic theory as a special case, so that the awkward question of delimiting the transonic zone need not arise.[5] Likewise, a combination of hypersonic small-disturbance theory with linearized supersonic theory can be effected[6] but only through a coincidence. An immediate obstacle to such combination is the fact that the approximations leading to the two theories are mutually exclusive. The difficulty arises in the continuity equation, Eq. (1a), which in hypersonic theory reduces to

$$u_\infty \rho_x + (\rho v)_y + (\rho w)_z = 0$$

but in linearized theory reduces instead to

$$u_\infty \rho_x + \rho_\infty(u_x + v_y + w_z) = 0$$

The term $\rho_\infty u_x$ must be retained in linearized theory, whereas it must be dropped in hypersonic theory in order to achieve similitude.

However, comparison of the similarity rules in the two cases indicates that the two theories may be artificially combined simply by reinterpreting the solutions of the hypersonic theory. According to the hypersonic similarity rule, the reduced variables of Eq. (2) depend upon M and τ only in the combination $M\tau$. It can be shown that solutions of hypersonic small-disturbance theory remain valid for small values of $M\tau$ (which is the domain of linearized theory), provided that $M\tau$ is replaced by $\beta\tau$ and the results are interpreted in terms of physical variables according to

$$\begin{aligned}
u &= u_\infty[1 + \tau^2\bar{u}(\bar{x}, \bar{y}, \bar{z};\ \beta\tau)] \\
v &= u_\infty\tau\bar{v}(\bar{x}, \bar{y}, \bar{z};\ \beta\tau) \\
w &= u_\infty\tau\bar{w}(\bar{x}, \bar{y}, \bar{z};\ \beta\tau) \\
p &= p_\infty\left[1 + \gamma M^2\tau^2\left\{\bar{p}(\bar{x}, \bar{y}, \bar{z};\ \beta\tau) - \frac{1}{\gamma\beta^2\tau^2}\right\}\right] = p_\infty\left[\gamma M^2\tau^2\bar{p} - \frac{1}{\beta^2}\right] \\
\rho &= \rho_\infty\left[1 + \frac{M^2}{\beta^2}\{\bar{\rho}(\bar{x}, \bar{y}, \bar{z};\ \beta\tau) - 1\}\right] = \rho_\infty\left(\frac{M^2}{\beta^2}\bar{\rho} - \frac{1}{\beta^2}\right)
\end{aligned} \qquad (9)$$

rather than according to Eq. (2). This means, for example, that the hypersonic similarity rule for C_p/τ^2 covers the entire range of supersonic flows if $M\tau$ is replaced by $\beta\tau$.

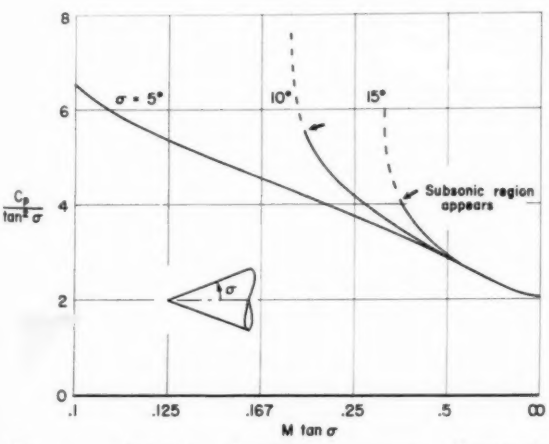

FIG. 1a. Correlation of pressure on cones. Hypersonic similarity rule.

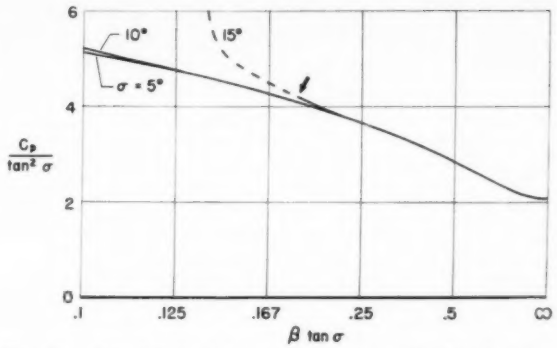

FIG. 1b. Correlation of pressure on cones. Combined supersonic-hypersonic similarity rule.

* The undisturbed fluid having density $\bar{\rho}_\infty = 1$ and pressure $\bar{p}_\infty = (\gamma M^2\tau^2)^{-1}$.

The error in hypersonic small-disturbance theory is $0(\tau^2)$, and that in linearized theory is $0(\tau/\beta)$ for shapes such as flat wings but only $0(\tau^2/\beta^2)$ for slender objects such as bodies of revolution. Hence the error in the combined theory is $0(\tau^2, \tau/\beta)$* for wings and $0(\tau^2, \tau^2/\beta^2)$ for fusiform shapes.

The obvious advantage of the combined theory and its associated similarity rule is demonstrated in Fig. 1. The pressure on cones of various thicknesses[7] is correlated first according to the original hypersonic similarity rule and then according to the combined rule, which is seen to extend the range of correlation down to the transonic zone.

Optimum Use of Hypersonic Small-Disturbance Theory

The error in hypersonic small-disturbance theory is only $0(\tau^2)$ compared with $0(\tau)$ for linearized theory and $0(\tau^{2/3})$ for transonic small-disturbance theory. Hence the need to correct for higher order terms in thickness is less in the hypersonic range than at lower speeds. Nevertheless, the accuracy of hypersonic small-disturbance theory can be strikingly improved simply by interpreting its results in conformity with Newtonian impact theory.

Newtonian impact theory assumes that fluid particles striking the body lose the normal component of their free-stream momentum, with the result that surface pressures are proportional to the square of the sine of the streamwise inclination. Although this result is not exact even in the limit as $M \to \infty$ (and $\gamma \to 1$), it holds approximately at high supersonic speeds. This suggests that the pressures predicted by hypersonic small-disturbance theory be extrapolated to thicker shapes by assuming a sine-squared variation.

Fig. 2 shows that in the limit of $M = \infty$ this idea extends the utility of the hypersonic correlation to cones of semivertex angles as extreme as 50°. Another illustration arises in correlating the lift on inclined bodies of revolution. Hypersonic small-disturbance theory cannot distinguish between lift and normal force. However, assuming a sine-squared variation of pressure indicates that, whereas the initial lift and normal-force slopes both vary considerably with body thickness, the modified component that is rotated twice as far behind the lift vector as is the normal-force vector (see sketch on Fig. 3a) should be independent of thickness. Fig. 3 shows that for cones[8] this is so nearly true that the accuracy of correlating hypersonic lift can be increased many fold.

* Whichever is the greater.

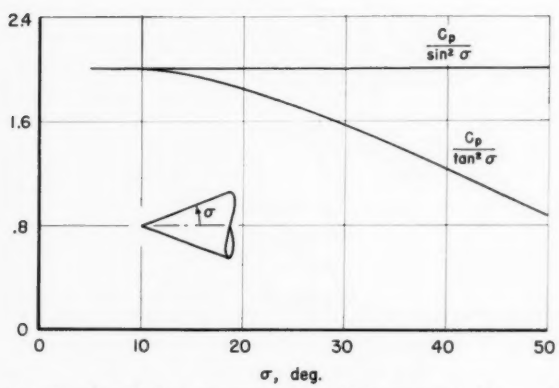

FIG. 2. Correlation of pressure on thick cones at $M = \infty$.

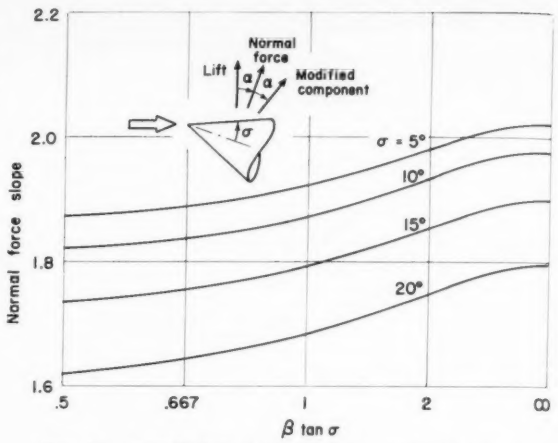

FIG. 3a. Correlation of lift of cones. Normal force.

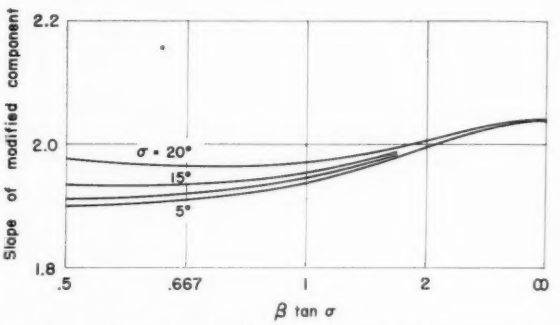

FIG. 3b. Correlation of lift of cones. Modified component.

APPLICATIONS TO BODIES OF REVOLUTION

The utility of hypersonic small-disturbance theory will now be illustrated by applying it to three related problems connected with pointed bodies of revolution. The first of these problems has been completely solved for the full equations, so that comparison will indicate the accuracy to be expected from small-disturbance theory; in the second problem the small-disturbance theory has recently served as a guide to the full solution; and in the third problem useful results are obtained which have not yet been attempted with the full theory.

For axially symmetric flows it is convenient to satisfy the reduced continuity equation [Eq. (4a)] by introducing a stream function ψ,

$$\left.\begin{aligned}\psi_{\bar r} &= \bar r\bar p \\ \psi_{\bar x} &= -\bar r\bar p\bar v\end{aligned}\right\} \tag{10}$$

Then Eq. (4d) states that $\bar p/\bar\rho^\gamma$ is a function only of ψ (that is, entropy is constant along stream lines between shock waves). Substituting into the momentum equations gives

$$\psi_{\bar r}{}^2\psi_{\bar x\bar x} - 2\psi_{\bar x}\psi_{\bar r}\psi_{\bar x\bar r} + \psi_{\bar x}{}^2\psi_{\bar r\bar r} = \gamma\frac{\psi_{\bar r}{}^{(\gamma+1)}}{\bar r^{(\gamma-1)}}\left[\left(\psi_{\bar r\bar r} - \frac{\psi_{\bar r}}{\bar r}\right)\omega + \frac{\psi_{\bar r}{}^2}{\gamma}\omega'\right] \tag{11a}$$

where

$$\omega(\psi) = \bar p/\bar\rho^\gamma \tag{11b}$$

The problems to be considered involve a single bow shock wave, which may be described in reduced coordinates by $\bar r = s(\bar x)$. Then the shock-wave relations obtained from Eqs. (7) (or simply by reducing the convenient results of reference 9) are

$$\left.\begin{aligned}\bar v &= \frac{2}{\gamma+1}\frac{M^2\tau^2s'^2 - 1}{M^2\tau^2s'} && (12a)\\ \bar p &= \frac{2\gamma M^2\tau^2s'^2 - (\gamma-1)}{\gamma(\gamma+1)M^2\tau^2} && (12b)\\ \bar\rho &= \frac{(\gamma+1)M^2\tau^2s'^2}{2+(\gamma-1)M^2\tau^2s'^2} && (12c)\end{aligned}\right\} \text{ at } \bar r = s(\bar x)$$

Circular Cone

Consider flow past a slender circular cone of semivertex angle σ. It is convenient to regard the Mach Number and shock-wave angle as given and to identify the thickness parameter τ with the slope of the shock wave, letting $\sigma = b\tau$, where the constant b must be found.

The flow field is conical, so that the stream function has the form

$$\psi(\bar x, \bar r) = \bar x^2 f(\theta) \tag{13a}$$

where

$$\theta = \bar x/\bar r \tag{13b}$$

is a conical variable varying from b on the cone surface to unity at the shock wave. Then Eq. (11a) becomes the nonlinear ordinary differential equation,

$$4f^2f'' - 2ff'^2 = \gamma\omega_0\frac{f'^{(\gamma+1)}}{\theta^{(\gamma-1)}}\left(f'' - \frac{f'}{\theta}\right) \tag{14a}$$

where ω_0 is the constant value of $\bar p/\bar\rho^\gamma$ behind the shock wave given, according to Eqs. (12b) and (12c), by

$$\omega_0 = \frac{2\gamma M^2\tau^2 - (\gamma-1)}{\gamma(\gamma+1)M^2\tau^2}\left[\frac{2+(\gamma-1)M^2\tau^2}{(\gamma+1)M^2\tau^2}\right]^\gamma \tag{14b}$$

The boundary conditions at the shock wave are found, from Eqs. (12a) and (12c), to be

$$\left.\begin{aligned}f(1) &= 1/2\\ f'(1) &= \frac{(\gamma+1)M^2\tau^2}{2+(\gamma-1)M^2\tau^2}\end{aligned}\right\} \tag{14c}$$

The constant b, which gives the cone surface, is determined by the requirement that the stream function vanish on the surface,

$$f(b) = 0 \tag{14d}$$

The nonlinear equation, Eq. (14a), is readily integrated numerically, starting at the shock wave ($\theta = 1$) and proceeding inward until f vanishes. The pressure coefficient is given in terms of f' by

$$\frac{C_p}{\sigma^2} = 2\left[\frac{\omega_0}{b^2}\left(\frac{f'}{\theta}\right)^\gamma - \frac{1}{\gamma M^2\sigma^2}\right] \tag{15}$$

In this way the surface pressure has been determined for values of the similarity parameter greater than $^1/_3$. (Below this range, linearized theory becomes accurate.) These results, expressed in the combined supersonic-hypersonic form, are compared in Fig. 4 with the full solution[7] for cones of various thicknesses. The fractional differences between the approximate and full solutions are nearly equal to τ^2, which suggests that the estimate of the error as $0(\tau^2, \tau^2/\beta^2)$ can be relied upon quantitatively. (The differences could, of course, be considerably reduced by interpreting the results in conformity with Newtonian impact theory.)

This approximate solution for cones was previously sought by Shen,[10] whose result is also shown in Fig. 4. It appears that his solution must involve computational errors.

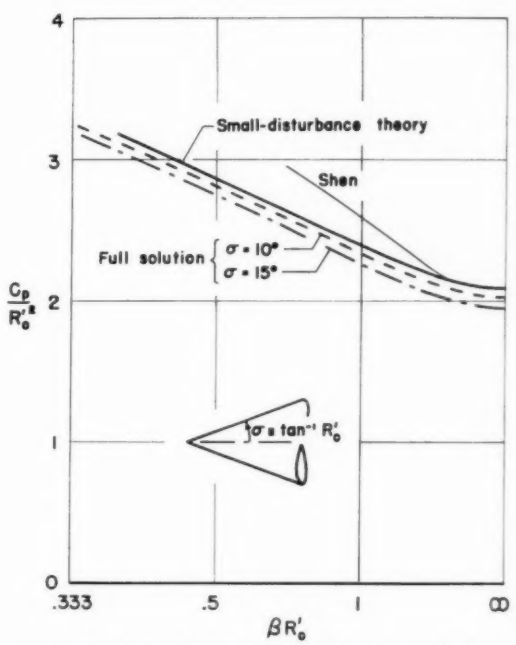

FIG. 4. Comparison of full and small-disturbance solutions for pressures on cones.

Initial Gradients on Ogives

The initial gradients of flow quantities at the tip of an ogival body of revolution can be determined by perturbing the solution for a cone. It is clear that the stream function will then consist of that for the cone plus an additional term,

$$\psi(\bar{x}, \bar{r}) = \bar{x}^2 f(\theta) + \bar{x}^3 g(\theta) \qquad (16)$$

Substituting into the equation of motion, Eq. (11a), yields a linear ordinary differential equation for the perturbation function g, with nonconstant coefficients depending upon the basic function f. Specifying the initial curvature of the shock wave provides initial conditions upon g. The equation can then be integrated numerically, and thus the initial pressure gradient and the ratio of shock wave to body curvature are determined.

A complication arises near the body surface, because $\theta = b$ is a singular point of the differential equation for g. As a consequence, it is found that g is not analytic near the surface but includes a term proportional to $(\theta - b)^{5/2}$. This term arises from the fact that the pencil of fluid striking the tip of the ogive is spread thin over the entire surface, and the linear entropy gradient at the tip due to a curved shock wave is thus intensified to a square-root gradient normal to the surface elsewhere.

This problem has recently been considered for the full equations by Cabannes[11] and by Shen and Lin.[12] The exceptional behavior of the solution near the surface was glossed over by Cabannes. On the other hand, Shen and Lin claimed to have found a logarithmic singularity. In addition to other difficulties, this would imply that the initial pressure gradient is infinite, although numerical solutions by the method of characteristics give no such indication. If the present small-disturbance theory is a faithful model of the full equations, the absence from it of any logarithmic singularity means that none can actually appear in the full problem. This conclusion has been confirmed by the authors of reference 12, who find upon re-examination that the logarithmic singularity was in fact illusory.*

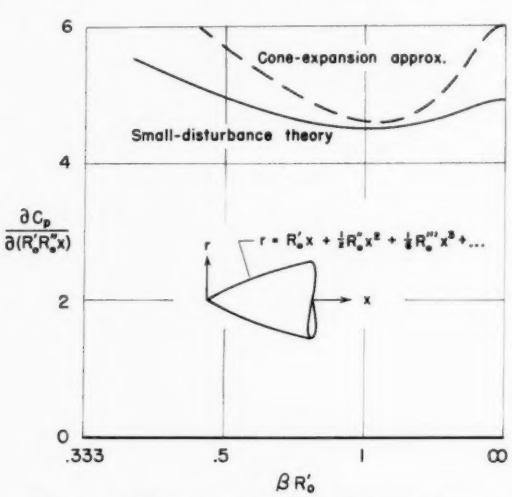

FIG. 5. Initial surface pressure gradients on ogives.

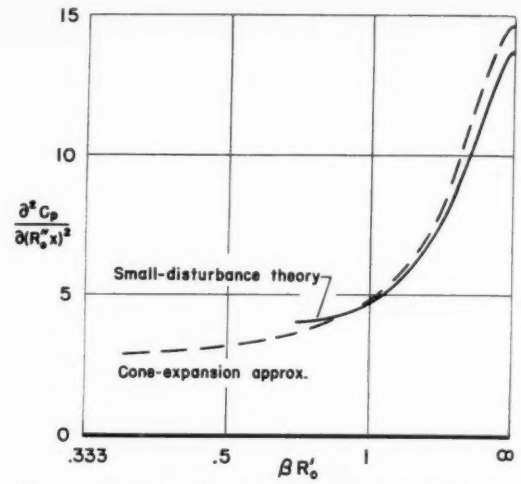

FIG. 6a. Initial surface pressure curvatures on ogives.

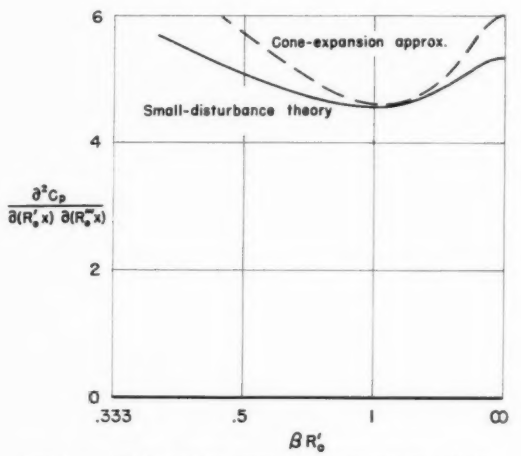

FIG. 6b. Initial surface pressure curvatures on ogives.

The initial pressure gradient is shown in Fig. 5 for values of the combined similarity parameter (based on initial slope) greater than $1/3$.

Further Terms in Series for Ogives

It might be supposed that, for an ogive described by a power series, further terms in a power series expansion for surface pressure could be found by retaining additional terms in Eq. (16),

$$\psi(\bar{x}, \bar{r}) = \bar{x}^2 f(\theta) + \bar{x}^3 g(\theta) + \bar{x}^4 h(\theta) + \ldots \qquad (17)$$

However, complications arise at this stage because of

* Private communication; see also Addendum No. 1 to reference 12.

the nonanalytic behavior of the stream function near the surface. Whereas $g(\theta)$ contains an authentic $^3/_2$-power branch point, $h(\theta)$ is found to contain a spurious $^1/_2$-power branch point, the next term an inverse $^1/_2$-power singularity, and so on. Hence, straightforward continuation of the procedure breaks down.

The difficulty arises from the fact that in the first perturbation the branch point in g arises at the basic cone ($\theta = b$) rather than at its proper location on the ogive surface. Although this discrepancy is negligible in the first perturbation, it is compounded in subsequent terms so as to be catastrophic. The remedy is to choose a slightly curvilinear coordinate system such that for each term the $^3/_2$-power branch point appears precisely at the body surface. Both the difficulty and the remedy are just those considered by Lighthill in his discussion of a technique for rendering approximate solutions uniformly valid.[13, 14]

With this modification, the procedure can, in principle, be continued indefinitely. It can therefore be concluded that an analytic body of revolution is accompanied by an analytic bow shock wave at supersonic speeds and an analytic pressure distribution.

Calculation of the next term in the series for surface pressure has been carried out,[4] and the results are presented in Fig. 6. Two functions arise, the surface pressure being given by

$$C_p = R_0'^2\left[\frac{C_p}{R_0'^2}\right] + R_0'R_0''\left[\frac{\partial C_p}{\partial(R_0'R_0''x)}\right]x + \frac{1}{2}\left\{R_0''^2\left[\frac{\partial^2 C_p}{\partial^2(R_0''x)^2}\right] + R_0'R_0'''\times\left[\frac{\partial^2 C_p}{\partial(R_0'x)\partial(R_0'''x)}\right]\right\}x^2 + \cdots \quad (18)$$

where R_0', R_0'', and R_0''' are the actual slope, second derivative, and third derivative at the tip of the ogive.

Newtonian impact theory, which was seen to be a useful qualitative guide, suggests that this number of terms suffices to predict the entire pressure distribution over circular-arc ogives. Accordingly, Rossow's accurate numerical solutions for circular-arc ogives[15] at a similarity parameter of unity are compared in Fig. 7 with the small-disturbance series. Three terms are seen to describe the pressure distribution with good accuracy over less than half the ogive length; at least one more term would be required to give the entire distribution.

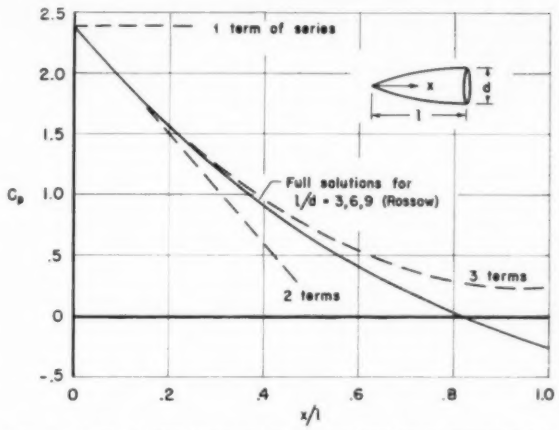

FIG. 7. Small-disturbance series approximation to pressure distributions over circular-arc ogives, $MR_0' \approx \beta R_0' = 1$.

CONCLUDING REMARKS

It has been seen that hypersonic small-disturbance theory serves both as a simple guide to the full theory and as a useful approximation for obtaining practical results. It appears that any extensive solution of supersonic flow using the full equations should be preceded by a pilot solution according to small-disturbance theory.

The small-disturbance equations are still inherently difficult to solve, because they are essentially nonlinear. Further approximations are desirable for simplifying the theory. In the case of plane flow, two extremely simple and accurate approximations are available: the reduced shock-expansion theory,[16, 17] and the even simpler tangent-wedge approximation which, when written in combined supersonic-hypersonic form, gives

$$C_p = \delta^2\left[\frac{\gamma+1}{2} + \sqrt{\left(\frac{\gamma+1}{2}\right)^2 + \frac{4}{\beta^2\delta^2}}\right] \quad (19)$$

if δ is the local slope (cf. reference 18). Hence, in plane flow the inviscid hypersonic problem is solved for practical purposes.

For general three-dimensional shapes, a promising approximation of comparable simplicity has been advanced by Eggers and his colleagues[17, 19, 20] and independently (for bodies of revolution) by Zienkiewicz and Bolton-Shaw.[21, 22] This "cone-expansion" method consists in applying the Prandtl-Meyer relations behind the tip of a pointed body as if the flow were plane. Thus, for a body of revolution, the surface pressure and Mach Number at the tip are taken from the solution for a cone, and the subsequent pressure distribution is calculated according to a Prandtl-Meyer expansion. This approximation yields surprising accuracy at sufficiently high Mach Numbers, and Eggers has discussed the reasons for this.[20] Zienkiewicz and Bolton-Shaw extend the approximation to lower Mach Numbers by using an empirically determined fraction of the full planar expansion. As an indication of the accuracy obtainable, the dashed curves in Figs. 6 and 5 show the coefficients calculated according to the cone-expansion procedure (with the full planar expansion). The full capabilities and limitations of this approximation have yet to be determined.

REFERENCES

[1] Tsien, H. S., *Similarity Laws of Hypersonic Flows*, Jour. Math. Phys., Vol. 25, No. 3, pp. 247–251, October, 1946.

[2] Hayes, Wallace D., *On Hypersonic Similitude*, Quart. Appl. Math., Vol. 5, No. 1, pp. 105–106, April, 1947.

[3] Goldsworthy, F. A., *Two-Dimensional Rotational Flow at High Mach Number Past Thin Aerofoils*, Quart. Jour. Mech. Appl. Math., Vol. 5, Part 1, pp. 54–63, March, 1952.

[4] Van Dyke, Milton D., *A Study of Hypersonic Small-Disturbance Theory*, forthcoming NACA paper.

[5] Spreiter, John R., *On the Application of Transonic Similarity Rules*, NACA TN No. 2726, June, 1952.

[6] Van Dyke, Milton D., *The Combined Supersonic-Hypersonic Similarity Rule*, Journal of the Aeronautical Sciences, Vol. 18, No. 7, pp. 499–500, July, 1951.

[7] Anon., *Tables of Supersonic Flow Around Cones*, Tech. Rep. No. 1, Dept. Elec. Eng., M.I.T., 1947.

[8] Anon., *Tables of Supersonic Flow Around Yawing Cones*, Tech. Rep. No. 3, Dept. Elec. Eng., M.I.T., 1947.

[9] Ames research staff, *Equations, Tables, and Charts for Compressible Flow*, NACA TR No. 1135, 1953.

[10] Shen, S. F., *Hypersonic Flow Over a Slender Cone*, Jour. Math. Phys., Vol. 27, No. 1, pp. 56–66, April, 1948.

[11] Cabannes, Henri, *Étude de l'Onde de Choc Attachée dan les Écoulements de Révolution, Première Partie: Cas d'un Obstacle Terminé par une Ogive*, La Recherche Aéronautique, No. 24, pp. 17–23, November-December, 1951.

[12] Shen, S. F., and Lin, C. C., *On the Attached Curved Shock in Front of a Sharp-Nosed Axially Symmetrical Body Placed in a Uniform Stream*, NACA TN No. 2505, October, 1951.

[13] Lighthill, M. J., *A Technique for Rendering Approximate Solutions to Physical Problems Uniformly Valid*, Phil. Mag., Ser. 7, Vol. 40, pp. 1179–1201, December, 1949.

[14] Lighthill, M. J., *The Shock Strength in Supersonic "Conical Fields,"* Phil. Mag., Ser. 7, Vol. 40, pp. 1202–1223, December, 1949.

[15] Rossow, Vernon J., *Applicability of the Hypersonic Similarity Rule to Pressure Distributions which Include the Effects of Rotation for Bodies of Revolution at Zero Angle of Attack*, NACA TN No. 2399, June, 1951.

[16] Linnell, Richard D., *Two-Dimensional Airfoils in Hypersonic Flows*, Journal of the Aeronautical Sciences, Vol. 16, No. 1, pp. 22–30, January, 1949.

[17] Eggers, A. J., Jr., and Syvertson, Clarence A., *Inviscid Flow About Airfoils at High Supersonic Speeds*, NACA TN No. 2646, March, 1952.

[18] Ivey, H. Reese, and Cline, Charles W., *Effect of Heat-Capacity Lag on the Flow Through Oblique Shock Waves*, NACA TN No. 2196, October, 1950.

[19] Eggers, A. J., Jr., and Savin, Raymond C., *Approximate Methods for Calculating the Flow About Nonlifting Bodies of Revolution at High Supersonic Airspeeds*, NACA TN No. 2579, December, 1951.

[20] Eggers, A. J., Jr., *On the Calculation of Flow About Objects Traveling at High Supersonic Speeds*, NACA TN No. 2811, October, 1952.

[21] Zienkiewicz, H. K., *A Method for Calculating Pressure Distributions on Circular Arc Ogives at Zero Incidence at Supersonic Speeds, Using the Prandtl-Meyer Flow Relations*, English Electric Co. Rep. No. L.A.t. 024, January, 1952; also British A.R.C. 14,790, 1953.

[22] Zienkiewicz, H. K., and Bolton-Shaw, B. W., *The Rapid, Accurate Prediction of Pressure on Non-Lifting Ogival Heads of Arbitrary Shape, at Supersonic Speeds*, English Electric Co. Rep. No. L.A.t. 034, June, 1952.

Conference on Supersonic Flow

An unclassified conference on Supersonic Flow will be held in the Mathematics Building, University of Maryland, from 9:30 a.m. to 5:00 p.m. on March 19–20, 1954.

Information concerning the conference may be obtained from Dr. E. L. Resler, Associate Research Professor, Institute of Fluid Dynamics and Applied Mathematics, University of Maryland, College Park, Md.

Energy Approach to the General Aircraft Performance Problem

EDWARD S. RUTOWSKI*

Douglas Aircraft Company, Inc.

ABSTRACT

The general aircraft performance problem is considered from the point of view of the balance that must exist between the potential and kinetic energy change of the aircraft, the energy dissipated against the drag, and the energy derived from the fuel.

This approach yields as one result a basic equation for the rate of change of the sum of the potential and kinetic energies of an aircraft. The form of the equation points to the use of aircraft total energy rather than altitude as the significant independent variable in the climb performance of high-speed aircraft. Using this equation, a method is outlined which permits finding either the path of minimum time or minimum fuel to change from one combination of speed and altitude to another.

The energy balance approach yields as another result a form of the aircraft range equation which incorporates a correction for the total energy change during the cruising portion of the flight. This form of the range equation shows that the dimension and the order of magnitude of aircraft range are given by the heat content of the fuel. Finally, the parameters of the range equation are examined to obtain an indication of the range capabilities of aircraft at supersonic speeds relative to those at subsonic speeds.

INTRODUCTION

SEVERAL NEW PROBLEMS HAVE ARISEN in the performance analysis of high-speed aircraft which cannot easily be solved by textbook or the conventional performance methods. One of the more important of these problems is the determination of the optimum path for an aircraft to reach speed and altitude, where optimum may imply either minimum time or minimum fuel. For low-speed aircraft, it was possible to state the problem simply as one of achieving a given altitude. Now, however, particularly with the wide range of speed of supersonic aircraft, the speed change in getting to altitude is significant relative to the altitude change so that the problem is how to attain both speed and altitude. The conventional methods of aircraft climb analysis using altitude as the independent variable are adequate for the problem of simply getting to an altitude but are not well suited for the more general problem. A method using an independent variable that combined speed and altitude would be better suited, since the problem is how to attain a combination of the two. Since speed can just as well be expressed by a level of kinetic energy and altitude by a level of potential energy, one means of describing a combination of speed and altitude is suggested. Represented as energies, speed and altitude can then essentially be added so that the problem can be stated as one of attaining a level of the sum of a kinetic and a potential energy, which can be defined as the total energy of the aircraft. The total energy would therefore seem to be a significant quantity in the climb analysis of an aircraft and suggested an approach to the problem from an energy point of view. This approach was tried and found to give a relatively simple solution to the problem of how to attain speed and altitude. Furthermore, it was found that, not only was this approach fruitful in problems of climb, but it also had application to problems of aircraft range as the result of its better exhibiting the basic elements that determine aircraft performance.

The purpose of this paper is to describe this energy approach, at first in general and, then, its application to problems of climb and range.

Presented at the Aerodynamics Session, Annual Summer Meeting, IAS, Los Angeles, July 15–17, 1953. Revised and received September 14, 1953.

* Aerodynamics Engineer, Santa Monica Division.

SYMBOLS

C_0, C_1, C_2, C_3	=	arbitrary constants
C_L	=	airplane lift coefficient
D	=	airplane drag, lbs.
E	=	airplane total energy, ft.lbs.
E/W	=	airplane specific energy, ft.lbs. per lb.
$f, f_1, \ldots, f_5$	=	arbitrary functions
g	=	acceleration due to gravity, ft. per sec.^{2}
h	=	altitude, ft.
H_c	=	heat content of the fuel, B.t.u. per lb.
L	=	airplane lift, lbs.
M	=	Mach Number
p	=	atmospheric pressure, lbs. per sq.ft.
R	=	airplane range, ft.
R_0	=	gas constant for air, ft.^{2}/sec.^{2}°R.
S	=	airplane wing area, sq.ft.
S.F.C.	=	specific fuel consumption, lbs./sec.lb.
t	=	time, sec.
T	=	engine net thrust, lbs.
T_0	=	atmospheric temperature, °R.
V	=	airplane velocity, ft. per sec.
V_i	=	indicated air speed, ft. per sec.
W	=	airplane gross weight, lbs.
W_0	=	initial airplane gross weight, lbs.
W_1	=	final airplane gross weight, lbs.
W_f	=	fuel weight, lbs.
x, y	=	arbitrary variables
γ	=	ratio of specific heats
η_0	=	overall powerplant efficiency
ρ	=	atmospheric density, slugs per cu.ft.

The Energy Balance Relationship

The energy approach to the general performance problem logically starts with a consideration of the source of the energy for propulsion. This source is the power-plant fuel, which is characterized by a heat content, H_c, which is essentially an energy content per pound of fuel. The stored energy of the fuel is converted into work of propulsion by the power plant at some overall efficiency, η_0, which is the product of its thermal and propulsive efficiencies. The energy per pound of fuel delivered by the power plant—that is, the product of the overall power-plant efficiency and the heat content—is expended in dissipation against the drag and in increasing the total energy of the aircraft. The sum of its kinetic and potential energies makes up the total energy of the aircraft and may be written as

$$E = Wh + \frac{WV^2}{2g} = W\left(h + \frac{V^2}{2g}\right) = \left(\frac{E}{W}\right)W \quad (1)$$

where

$$(E/W) = h + (V^2/2g)$$

The application of the principle of conservation of energy over a time interval dt, yields the following equation:

$$dE = \eta_0 H_c dW_f - (E/W)dW_f - DV\,dt$$

which describes the basic energy balance that must exist between the total energy change of the aircraft, the energy derived from the fuel, the total energy change due to a weight change in the airplane, and the energy dissipated against the drag. The terms involving the change in the total energy of the aircraft can be combined by use of the equation obtained by the differentiation of Eq. (1).

$$dE = Wd(E/W) + (E/W)dW$$

or

$$dE = Wd(E/W) - (E/W)dW_f$$

since

$$dW = -dW_f$$

The energy balance relationship then reduces to

$$Wd(E/W) = \eta_0 H_c dW_f - DV\,dt \quad (2)$$

This equation is here written in terms of the change in energy per pound of aircraft weight or what may be called the specific energy of the aircraft. The specific energy is a function only of the speed and altitude of the aircraft, and it, rather than the energy itself, which is a function of gross weight also, is the item of primary interest in the usual performance problems. It should be made clear, however, that Eq. (2) does properly take into account the energy change due to the change in gross weight as fuel is burned. Eq. (2) is the basic relationship from which the remaining equations in the paper are obtained. In fact, this general relationship will yield most of the equations used in the calculation of specific performance problems. In the present paper, it is used to obtain the classical form of the climb and range equations, as well as alternate forms that are considered to be better adapted to the treatment of some performance problems of high-speed aircraft.

This relationship is particularly useful in that it permits a common approach to several performance problems—for example, climb and range—which are usually treated as completely independent problems.

The Classical Climb Equation

The climb equation in its classical form will now be obtained from the energy balance relationship by first deriving the more fundamental equation of the rate of change of specific energy of an aircraft. To accomplish this derivation, Eq. (2) is rewritten to obtain

$$\frac{d(E/W)}{dt} = \frac{\eta_0 H_c}{W}\frac{dW_f}{dt} - \frac{DV}{W} \quad (3)$$

Remembering that $\eta_0 H_c$ represents the useful work of propulsion done per pound of fuel, this quantity may be expressed in terms of the power-plant thrust, T, and the fuel rate as

$$\eta_0 H_c = \frac{\text{work}}{\text{lb. of fuel}} = \frac{\text{work/time}}{\text{lb. of fuel/time}} = \frac{TV}{(dW_f/dt)} \quad (4)$$

Using this expression in Eq. (3), the following relationship is obtained:

$$d(E/W)/dt = (V/W)(T - D) \quad (5)$$

This equation states simply that the rate of change of specific energy is given by the excess power per pound of aircraft weight. It is to be distinguished from the commonly used relation,

$$dE/dt = (T - D)V$$

which is only approximate, since it neglects the energy change due to the changing weight of the aircraft. The full expression, using Eqs. (4) and (5),

$$\frac{dE}{dt} = (T - D)V\left[1 - \frac{(E/W)}{H_c[1 - (D/T)]\eta_0}\right]$$

shows that this effect becomes increasingly important as the specific energy capability, or essentially the speed and altitude capability of aircraft increases relative to the specific energy content of the fuel. The fact that the specific energy concept yields as simple an expression as Eq. (5) leaves little, if any, reason for neglecting the effect of changing gross weight. This relationship can be used to obtain the so-called "fundamental" performance equation of classical aerodynam-

ics. The derivation is accomplished by first differentiating Eq. (1) to obtain

$$\frac{d(E/W)}{dt} = \frac{dh}{dt} + \frac{V}{g}\frac{dV}{dt}$$

Using this expression in Eq. (5) and solving for the rate of climb,

$$\left[\frac{dh}{dt} = \frac{V}{W}(T - D)\right] - \frac{V}{g}\frac{dV}{dt} \qquad (6)$$

The portion of the equation in the brackets is the so-called "fundamental" performance equation. As shown by Eq. (6), it is based on the assumption that the climb speed be constant ($dV/dt = 0$). In this particular case, the "fundamental" equation and Eq. (5) are identical, so that the excess power per pound of weight can be interpreted as giving either the rate of change of specific energy or the rate of climb at constant speed. Regarding it as a rate of change of specific energy, the excess power per pound of weight can also be interpreted as giving the longitudinal acceleration at constant altitude. In the early days of aviation when speeds were low, this approximate equation did not introduce appreciable error even in the case of a changing speed during a steady climb. The form of the correction can be seen by a rewriting of Eq. (6) to obtain

$$\frac{dh}{dt} = \frac{V}{W}(T - D)\left[\frac{1}{1 + (V/g)(dV/dh)}\right] \qquad (7)$$

The magnitude of this correction factor is shown in Fig. 1 for the simple cases of climb at constant indicated speed and constant Mach Number. Although small for low climbing speed, the correction factor indicated in the figure rapidly becomes appreciable as the climb speed increases. In fact, for climb at a constant Mach Number of 2.0, the correction factor exceeds 2.0. The correction factor is well known, so that climb calculations of high climbing speed aircraft are generally made using the complete expression given by Eq. (7).

Although Eq. (7) is adequate for the calculation of climb performance once the climb technique is known, its form is unwieldy for the more general problem of finding the optimum technique. The difficulty arises from the fact that the rate of climb is given by a function of the type

$$dh/dt = f(h, V, dV/dh)$$

The dependence of the rate of climb on dV/dh makes it necessary to consider the climb as a whole in a problem such as minimizing the time to a given altitude. The common procedure of considering the rate of climb independently at each altitude is not strictly valid. The problem of minimizing time to climb with a function of the above type is a typical calculus of variations problem. However, the lack of a simple analytical expression for thrust makes such an approach difficult. Simplification of the problem is generally accomplished by assuming that (dV/dh) can be neglected. A first approximation can be thus obtained which can be adjusted to give a path closer to the optimum. However, this adjustment requires judgment so that some other means of simplification leading to a direct answer is desirable. It is here argued that Eq. (5), using the concept of specific energy, provides the desired simplification with no loss in accuracy compared to the use of Eq. (7).

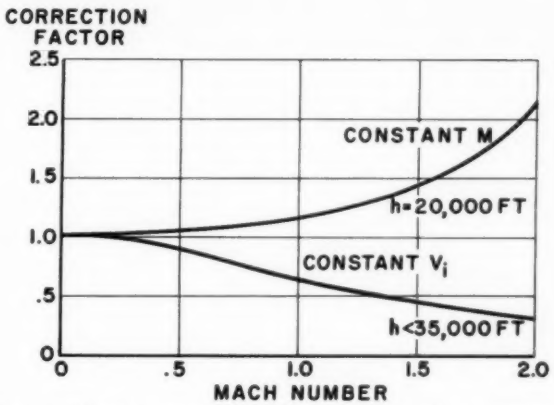

FIG. 1. Kinetic energy correction to rate of climb at constant speed.

THE USE OF THE SPECIFIC ENERGY CONCEPT IN CLIMB PROBLEMS

The rate of change of specific energy of an aircraft, at a fixed gross weight, is a function only of altitude and velocity.

$$d(E/W)/dt = f(h, V)$$

The use of Eq. (5) therefore provides the desired simplification by the elimination of the derivative, dV/dh. This equation does not specify the form in which the energy is added but rather gives an expression for the rate of increase of the sum of the kinetic and potential energies of the aircraft per pound of weight. Unlike the "fundamental" performance equation and Eq. (7), the climb technique, or essentially the proportions in which the kinetic and potential energies are added, does not have to be specified in any calculation using the concept of specific energy. The simplicity of Eq. (5) would therefore recommend its use in preference to Eq. (7) if specific energy could be shown to be a useful and a usable concept.

It is to be noted that Eq. (5) is exactly the "fundamental" performance equation except that the altitude is replaced by the specific energy. Because this specific energy has the semblance of an altitude, the suggestion has been made[1,2] that it be called an "energy height." It has, in fact, the dimension of a length and is the sum of the geometric altitude and the altitude equivalent of the kinetic energy were it all converted

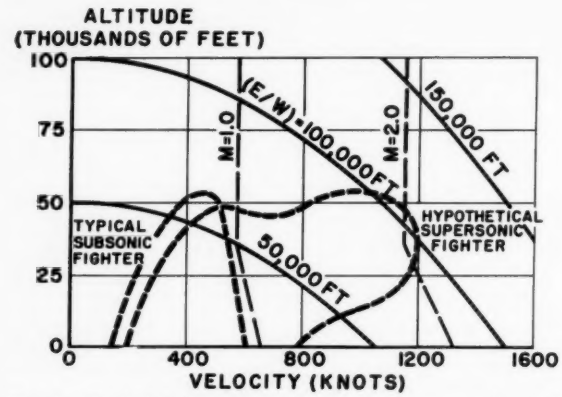

FIG. 2. Typical fighter speed-altitude envelopes superimposed on contours of constant specific energy.

into potential energy. The significance of the use of the specific energy rather than altitude as the independent variable may be seen in Fig. 2. The contours of constant specific energy are the locus of all points having a given sum of kinetic and potential energies per pound of weight. Also shown in Fig. 2 superimposed on the specific energy contours are the speed-altitude envelopes representative of a present-day fighter and a hypothetical supersonic fighter. From these envelopes, it is evident that the final altitude in itself is no longer adequate in the specification of climb problems, since this altitude may be achieved over a wide range of speeds. The problem is more often to achieve some combination of both speed and altitude rather than simply an altitude. Therefore, since any combination of speed and altitude determines a level of specific energy, the problem can be stated as one of achieving a final energy level from some initial value of specific energy. While it is true that a specific energy does not determine a unique combination of speed and altitude, the exact proportion of kinetic and potential energy may generally not be important, except perhaps at the final condition desired. Furthermore, if it is important, the desired proportion can generally be achieved readily, since only a redistribution rather than an increase in energy is required. Because of this possibility of ready interchanges of kinetic and potential energy by means of a dive or a zoom, the concept of specific energy has tactical significance. For example, it would seem more important for an interceptor to have a specific energy capability greater than that of its bombing adversary than to have simply an altitude or speed advantage. Even in the case of other than tactical aircraft (research vehicles, for example), the concept of specific energy is useful in that it permits a rapid estimation of the maximum speed in a dive or the maximum altitude in a zoom. A first estimate can be made simply by finding the maximum specific energy capability of the aircraft in level flight. The other combinations of speed and altitude corresponding to this energy level then represent capabilities of the aircraft not attainable in level flight. On the basis of these arguments, it appears that specific energy is a useful concept. It remains only to show that it is a usable concept.

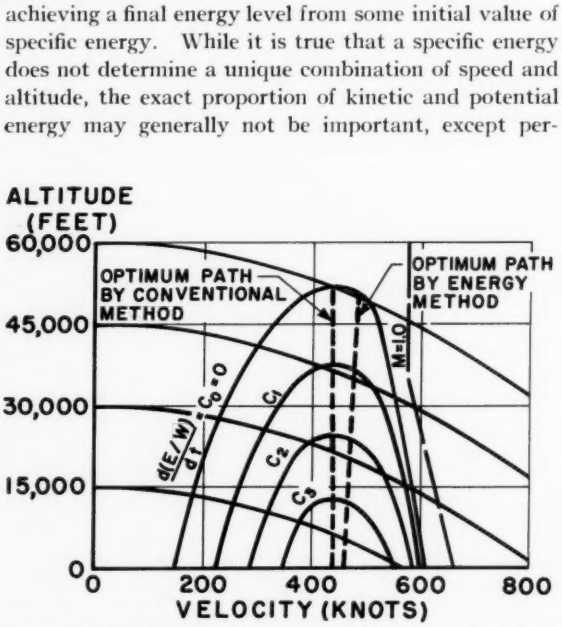

FIG. 3. Comparison of minimum time to climb paths for typical subsonic fighter.

The usability of the specific energy concept can perhaps best be shown by its application to a specific problem. For this purpose, the problem chosen is that of finding the path of minimum time to change from one combination of speed and altitude to another. Using specific energy as the independent variable, the time can be written as

$$t = \int_{(E/W)_1}^{(E/W)_2} \frac{1}{d(E/W)/dt}\, d\left(\frac{E}{W}\right) \tag{8}$$

But

$$d(E/W)/dt = (T - D)V/W = f(V, h)$$

or since

$$E/W = h + (V^2/2g)$$

$$\left[\frac{d(E/W)}{dt}\right]^{-1} = f_1\left[\frac{E}{W}, h\right] \text{ or } f_2\left[\frac{E}{W}, V\right]$$

Eq. (8) then becomes

$$t = \int_{(E/W)_1}^{(E/W)_2} f_1\left(\frac{E}{W}, h\right) d\left(\frac{E}{W}\right) \quad \text{or}$$

$$t = \int_{(E/W)_1}^{(E/W)_2} f_2\left(\frac{E}{W}, V\right) d\left(\frac{E}{W}\right) \tag{9}$$

The problem can now be stated mathematically as one of minimizing the above integral. The simple condition, easily verified by the calculus of variations,* that this integral be a minimum is

* Due to E. W. Graham, Consultant, Douglas Aircraft Company, Inc.

$$\frac{\partial}{\partial h}\left[\frac{dt}{d(E/W)}\right]_{E/W=\text{const.}} = 0 \quad \text{or}$$

$$\frac{\partial}{\partial V}\left[\frac{dt}{d(E/W)}\right]_{E/W=\text{const.}} = 0 \quad (10)$$

or since, in general, for $f(x, y) \neq 0$

$$(\partial/\partial y)\ [f(x, y)] = 0$$

then

$$(\partial/\partial y)\ [f^{-1}(x, y)] = 0$$

and we may write

$$\frac{\partial}{\partial h}\left[\frac{d(E/W)}{dt}\right]_{E/W=\text{const.}} = 0 \quad \text{or}$$

$$\frac{\partial}{\partial V}\left[\frac{d(E/W)}{dt}\right]_{E/W=\text{const.}} = 0$$

or, finally,

$$\frac{\partial}{\partial h}\left[\frac{(T-D)V}{W}\right]_{E/W=\text{const.}} = 0 \quad \text{or}$$

$$\frac{\partial}{\partial V}\left[\frac{(T-D)V}{W}\right]_{E/W=\text{const.}} = 0 \quad (11)$$

The path of minimum time is therefore the one that satisfies this condition at every point. This path cannot be obtained analytically in general, but a simple graphical method analogous to the common method used with the "fundamental" performance equation can be used. The usual method can be mathematically described as one in which the path satisfies the condition

$$(\partial/\partial V)\ [(T-D)V/W]_{h=\text{const.}} = 0 \quad (12)$$

Graphically interpreted, Eq. (12) defines the procedure of selecting at a given altitude the speed for maximum climb from a plot of excess power per pound of weight versus speed. The interpretation of Eq. (11) is completely analogous, except that in this case the excess power per pound of weight is plotted at a constant value of specific energy. Here, either speed or altitude can be used as the independent variable for purposes of plotting as indicated by Eq. (11). The distinction between using Eqs. (11) and (12) for determining a climb technique is demonstrated graphically in Fig. 3. This figure shows contours of constant excess power per pound of weight superimposed on contours of constant specific energy. The two different paths shown in the figure result depending upon whether Eq. (11) or (12) is used as the governing condition. The use of Eq. (12) corresponds to the choosing of a speed where the excess power contours are tangent to a line of constant altitude. On the other hand, the use of Eq. (11) corresponds to the choosing of a speed where the contours are tangent to a line of constant specific energy.

The advantages of the energy method in a minimum time problem are much more pronounced in the case of a supersonic fighter, such as described in Fig. 2. Here the conventional method defined by Eq. (12) is virtually useless because of the large speed change involved if a speed near the maximum is desired at the end of the climb. The energy method, on the other hand, is well adapted to this case. The path defined by Eq. (11), which consists of selecting at each level of specific energy the speed and altitude for maximum excess power per pound of aircraft, is shown in Fig. 4. The flexibility of the energy method is here demonstrated in that it may describe a climb with acceleration or even an acceleration in a *dive* as part of the optimum *climb* path. The solution to this problem, essentially intractable by conventional methods, is thus easily obtained by the application of the specific energy concept.

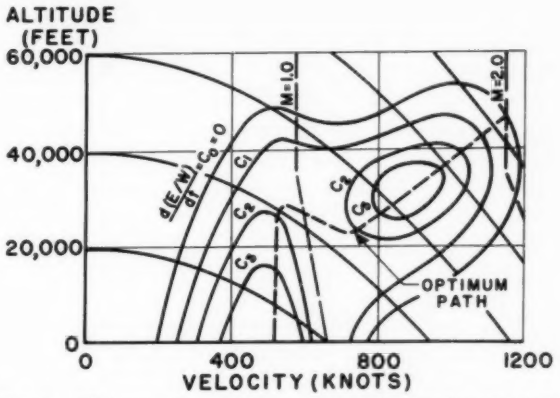

FIG. 4. Minimum time path by energy method for hypothetical supersonic fighter.

The effect of the difference in path on the time to the final speed and altitude can be visualized qualitatively in Fig. 5. The time represented by the integral (8) is shown in this figure as the area under the curves of the reciprocal of the excess power per pound of weight between the limits of integration $(E/W)_1$ and $(E/W)_2$. These curves are plotted at a constant altitude so that the variation in specific energy implies also a variation in velocity along the curves. The ap-

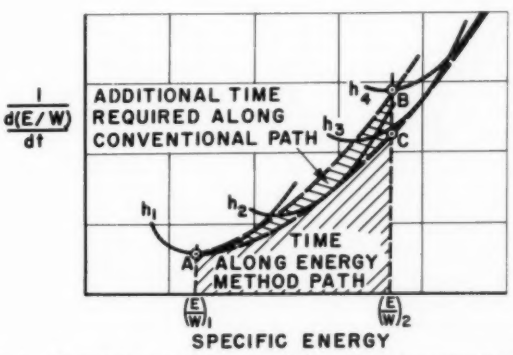

FIG. 5. Comparison of time to climb integrals as represented by areas.

plication of Eq. (11), which states that the minimum value of the integrand be selected at each abscissa (E/W), defines the envelope of the series of curves. The area under the envelope between $(E/W)_1$ and $(E/W)_2$ then represents the minimum value of the integral and, hence, the minimum time. The curve corresponding to the application of condition (12) is also shown and is seen to give a somewhat greater area. This comparison is not strictly valid because, in general, the final condition of speed and altitude desired will not lie on the envelope—for example, point B in Fig. 5. The specific energy method gives the time from A to the point on the envelope that has the same specific energy as B—that is, point C. It essentially assumes that the zoom—that is, the conversion of the excess kinetic energy into potential energy necessary in going from point C to point B—can be accomplished in zero time. This, of course, is impossible, so that, in general, it will be necessary to depart from the envelope before reaching point C. The energy method generally results in the technique of acquiring a relatively high kinetic energy at low altitudes, where the excess power is the greatest for conversion, if necessary, into potential energy at the higher altitudes. The modification of the integral due to departure from the envelope will depend upon the maneuvering capabilities of the aircraft and the amount of energy gained in the zoom. Some judgment will be required in this modification, although calculations indicate that its effect on the time in a long climb is small so that the greater portion of the theoretical advantage can be attained. Thus, the time from A to B via C (approximately), which is the minimum time path defined by the energy method, will be less than that from A to B along the conventional climb path.

The problem of minimizing the fuel to achieve a speed and altitude can be treated by the energy method in the same fashion as the minimum time problem. This problem is significant in the case of aircraft, such as research vehicles, for which the flight durations at the desired test conditions are to be maximized. The fuel integral can be written as

$$W_f = \int_{(E/W)_1}^{(E/W)_2} \frac{1}{d(E/W)/dW_f}\, d\left(\frac{E}{W}\right) \qquad (13)$$

But

$$\frac{d(E/W)}{dW_f} = \frac{d(E/W)/dt}{dW_f/dt} = \frac{(T-D)V}{WT\,\text{S.F.C.}}$$

The only new variable introduced is the specific fuel consumption, S.F.C., which is a function of speed, altitude, and throttle setting. However, in a climb or accelerating condition, the throttle is generally wide open or at least at a fixed setting, so that the S.F.C. is a function only of speed and altitude. This permits us to write

$$\left[\frac{d(E/W)}{dW_f}\right]^{-1} = f_3\,[h,\ V] = f_4\left[\left(\frac{E}{W}\right),\ V\right] = f_5\left[\left(\frac{E}{W}\right),\ h\right] \qquad (14)$$

The integral can now be written as

$$W_f = \int_{(E/W)_1}^{(E/W)_2} f_4\left(\frac{E}{W},\ V\right) d\left(\frac{E}{W}\right) \quad \text{or}$$

$$W_f = \int_{(E/W)_1}^{(E/W)_2} f_5\left(\frac{E}{W},\ h\right) d\left(\frac{E}{W}\right) \qquad (15)$$

The application of the calculus of variations yields the following condition for the path of minimum fuel expenditure:

$$\frac{\partial}{\partial h}\left[\frac{(T-D)\,V}{WT\,\text{S.F.C.}}\right]_{E/W=\text{const.}} = 0 \quad \text{or}$$

$$\frac{\partial}{\partial V}\left[\frac{(T-D)V}{WT\,\text{S.F.C.}}\right]_{E/W=\text{const.}} = 0 \qquad (16)$$

The use of this result in an actual problem is completely analogous to that in the minimum time problem.

Since the primary purpose of the application of the specific energy concept to two typical problems was the demonstration of its usability, several details in the process were neglected. Among these are the variation of gross weight in the climb and the difference in the drag from the level flight value in the maneuvers required to follow the optimum path. However, these details should offer no greater difficulty than that encountered in the usual analysis of climb performance. Therefore, on the basis of this demonstration of its adaptability to problems for which the conventional methods yield no simple solutions, it is felt that the concept of specific energy deserves wider use in modern aircraft performance work.

The Energy Balance Approach to the Range Equation

Range in the classic textbook approach is treated as a special problem completely independently of the other equations of performance. Here, however, the derivation of the range equation is made using the same energy balance relationship that was used to obtain the rate of change of specific energy equation. This relationship as the starting point in the derivation is rewritten here for convenience,

$$W d(E/W) = \eta_0 H_c dW_f - DV\,dt \qquad (2)$$

since $V\,dt = dR$, Eq. (2) may be written as

$$dR = \frac{\eta_0 H_c}{D}\, dW_f - \frac{W}{D}\, d\left(\frac{E}{W}\right)$$

Making use of the relations for normal airplane cruising flight,

$$dW = -dW_f$$
$$L = W$$

so that $D = \dfrac{W}{(L/D)}$, we may write

$$dR = -\eta_0 H_c \left(\frac{L}{D}\right) \frac{dW}{W} - \left(\frac{L}{D}\right) d\left(\frac{E}{W}\right) \qquad (17)$$

Now making the assumption that η_0 and (L/D) are constant during the cruising portion of the flight, Eq. (17) may be integrated to give

$$R = \eta_0 H_c \left(\frac{L}{D}\right) \ln \frac{W_0}{W_1} - \left(\frac{L}{D}\right)\left[\left(\frac{E}{W}\right)_1 - \left(\frac{E}{W}\right)_0\right] \qquad (18)$$

Recalling that $\eta_0 H_c$ represents the useful work of propulsion done per pound of fuel, it may be expressed with the use of Eq. (4) as

$$\eta_0 H_c = \frac{TV}{(dW_f/dt)} = \frac{TV}{T\,\text{S.F.C.}} = \frac{V}{\text{S.F.C.}}$$

Substituting this relation into the first term of Eq. (18) and discarding the second term, the more familiar expression for range is obtained

$$R = (V/\text{S.F.C.})\,(L/D) \ln (W_0/W_1) \qquad (19)$$

This equation is recognized as the usual expression for the range of a jet-powered aircraft. The features distinguishing Eq. (18) from this more familiar form of the range equation are its second term, as well as the parameters appearing in the first term.

It may be seen from Eq. (18) that the need for the additional term arises only if there is a change in energy level during the cruising portion of the flight. Since the constant (L/D) operation, assumed in order to perform the integration, essentially implies a constant airplane attitude, the dynamic pressure will decrease with the gross weight. This type of operation will therefore generally result in a change in energy level and, strictly, will require the consideration of the additional term if the cruise is considered apart from the other portions of the flight.

The magnitude of this term may be readily ascertained for the case of a turbojet-powered aircraft. For operation under the conditions of constant throttle setting, constant Mach Number, and altitudes above 35,000 ft., the following relationship between a change in altitude and a change in gross weight may be written (see Appendix):

$$dW/W = -(g/R_0T_0)dh \qquad (20)$$

Since a constant Mach Number at altitudes above 35,000 ft. implies a constant speed in a standard atmosphere, the energy level changes only by virtue of an altitude change, so that Eq. (17) may be written as

$$dR = -\eta_0 H_c \left(\frac{L}{D}\right) \frac{dW}{W} - \left(\frac{L}{D}\right) dh \qquad (21)$$

Using Eq. (20),

$$dR = -\eta_0 H_c \left(\frac{L}{D}\right) \frac{dW}{W} + \frac{g}{R_0T_0} \left(\frac{L}{D}\right) \frac{dW}{W}$$

Combining

$$dR = -\left[\eta_0 H_c - \frac{g}{R_0T_0}\right] \left(\frac{L}{D}\right) \frac{dW}{W}$$

and integrating, using the same assumptions as before,

$$R = \left[\eta_0 H_c - \frac{g}{R_0T_0}\right] \left(\frac{L}{D}\right) \ln \frac{W_0}{W_1} \qquad (22)$$

or

$$R = \left[\frac{V}{\text{S.F.C.}} - \frac{g}{R_0T_0}\right] \left(\frac{L}{D}\right) \ln \left(\frac{W_0}{W_1}\right) \qquad (23)$$

In this form of the range equation, the second term appears as a correction on the $V/\text{S.F.C.}$ factor. For a turbojet having a S.F.C. of approximately 1.0 and cruising at a speed of 500 m.p.h. at altitudes above 35,000 ft., the correction on the range is approximately 0.8 per cent. Although this analysis shows it to be small, a correction for the climb during cruise is applicable. The use of Eq. (18) or the more specialized form, Eq. (22), should facilitate the making of this correction.

Where the additional term can be neglected, Eq. (18) may be written as

$$R = \eta_0 H_c\,(L/D) \ln (W_0/W_1) \qquad (24)$$

The unique feature of the range equation in this form is the isolation of the fuel characteristics from the characteristics of the power plant.

The heat content of the fuel, H_c, is a property of the fuel only, whereas the specific fuel consumption used in the more familiar forms of the range equation is dependent upon the characteristics of the power plant, as well as those of the fuel. For hydrocarbon fuels such as gasoline, this heat content has a value of approximately 18,800 B.t.u.'s per lb. However, by converting the B.t.u.'s to foot-pounds of energy using the mechanical equivalent of heat, it can be seen that the dimension is that of a length, so that H_c can be expressed in the units in which range is usually given. This value for gasoline is about 2,760 statute-miles. The dimension and the order of magnitude of aircraft range are therefore given by the heat content of the fuel. This fact makes clear the direction in which large improvements in range can be made. The advantage of nuclear fuels lies in their enormously high heat content. On the other hand, the poor range performance of rocket aircraft is largely the result of the low energy content of its fuel. "Fuel," as used here, is considered to be made up of the oxidizer a rocket aircraft necessarily carries, as well as its actual fuel. The heat content of the fuel and oxidizer combination is as low as one-fifth of that of fuels such as gasoline used in air-breathing engines.

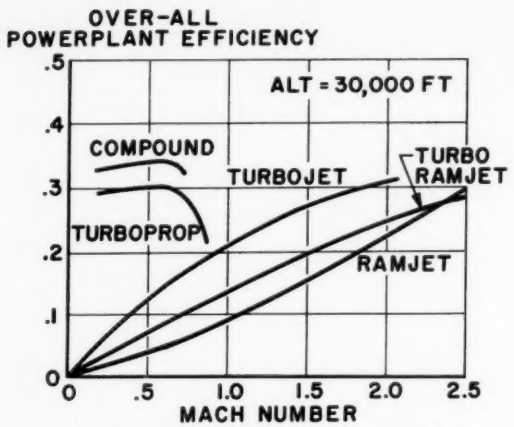

FIG. 6. Overall power-plant efficiency comparison.

The other parameter of Eq. (24) not found in the more familiar forms of the range equation is the overall power-plant efficiency, η_0. Considered in the light of this parameter, the power plant is simply a device for converting the chemical energy contained in the fuel into useful work of propulsion on the aircraft. The efficiency with which it accomplishes this conversion is the overall power-plant efficiency. A typical value for this efficiency for, say, a reciprocating-engine-propeller combination operating near its peak, is 30 per cent. As shown before, the product of this efficiency and the heat content of the fuel gives the useful work done per pound of fuel.

The form of the range equation given in Eq. (24) is not particularly convenient for purposes of range calculations of specific airplanes, since the power-plant characteristics are usually given in terms of specific fuel consumption. The advantage of the alternate form lies rather in its clear isolation of the four basic elements that determine aircraft range. For this reason, as well as for its general applicability to all power-plant types, this form is well adapted to range problems of a general nature.

Relative Range Capabilities of Aircraft at Subsonic and Supersonic Speeds

Eq. (24) is particularly appropriate for the investigation of the relative range capabilities of aircraft at subsonic and supersonic speeds. This problem has been considered elsewhere in detail, so that the discussion here will be limited simply to an interpretation of the results in terms of the four basic elements of aircraft range.

(1) H_c, the heat content of the fuel, is a function of the fuel only. Assuming that the same fuel is used at subsonic and supersonic speeds, this factor will introduce no difference in the range capabilities in the two speed régimes.

(2) η_0, the overall power-plant efficiency, is a function primarily of speed and power-plant type. A plot of this factor in Fig. 6, calculated from data given in reference 3, indicates that essentially the same efficiency can be achieved at supersonic speeds as at subsonic speeds, assuming the proper choice of power plant. This factor need not, therefore, introduce any difference in the range capabilities in the two speed régimes. An interesting point here is that, since $V/\text{S.F.C.} = \eta_0 H_c$, it is to be expected that the specific fuel consumption will increase with speed for any one fuel unless engines become basically more efficient.

(3) L/D, the aerodynamic lift to drag ratio, is low at supersonic speeds because of the fundamentally different character of the airflow. In fact, its maximum value now appears to be approximately only one-fourth of that attainable at subsonic speeds. The reduction in lift to drag ratio will therefore introduce a corresponding reduction in the range capabilities of supersonic aircraft.

(4) W_0/W_1, the initial to final gross weight, is a function of the fuel weight to gross weight ratio of the airplane. In turn, this ratio depends upon the fractions of the gross weight required for power plant and structure. It appears, at present, that these fractions, in general, are not far different at supersonic than at subsonic speeds for airplanes of a similar function. This observation is made in the case of the structure weight on the basis that the weight increasing effects of aerodynamic heating, higher fuselage fineness ratios, and higher wing span to root thickness ratios are offset by the reducing effects of the higher wing loadings. Similarly, in the case of the power plant, the effect of the lower (L/D) on the power-plant requirement is approximately offset by the lower weight to thrust ratios available in the jet engines suitable for propulsion at supersonic speeds. A reasonable tentative conclusion would thus say that the weight ratios at supersonic speeds, in general, will be similar to those at subsonic speeds. No large difference is expected in the range capabilities in the two speed régimes as a result of the weight ratio.

The overall conclusion from the foregoing examination of the parameters of the range equation is that the range capabilities in the two speed régimes differ primarily only as the result of a difference in the lift to drag ratios. Since this lift to drag ratio at supersonic speeds at the present time reaches a value only one-fourth of that attainable at subsonic speeds, the range capabilities are lower by essentially the same factor.

The form of the range equation, Eq. (24), has permitted a clear interpretation of the results of the problem discussed above. The use of this equation has thus been shown to be appropriate for range studies of a general nature.

Concluding Remarks

The energy approach to the general aircraft performance problem has yielded several important re-

sults. In climb performance, it has pointed to the use of specific energy rather than altitude as the significant independent variable. This concept has been shown to be particularly useful in solving minimum time and minimum fuel problems of high-speed aircraft. In range performance, it has provided a clear isolation of the elements that determine aircraft range. In the case of both climb and range, it has led to equations incorporating corrections that have been found necessary in modern performance work. Lastly, it has yielded a basic energy balance relationship that has general application in aircraft performance analysis.

References

[1] Lush, K. J., *A Review of the Problem of Choosing a Climb Technique With Proposals for a New Climb Technique for High Performance Aircraft*, A.R.C. R. and M. No. 2557, 1951.

[2] Kelly, L., *Optimum Climb Technique for a Jet Propelled Aircraft*, The College of Aeronautics, Cranfield, Report No. 57, April, 1952.

[3] Staff, Cleveland Laboratory, *Performance and Ranges of Application of Various Types of Aircraft-Propulsion System*, NACA TN No. 1349, August, 1947.

Appendix

Analytical Expression Relating Change in Flight Altitude to Change in Gross Weight

A turbojet-powered aircraft operating under the common conditions of constant attitude and altitudes above 35,000 ft. maintains as well, approximately, the following conditions: (1) constant throttle setting and (2) constant Mach Number. The altitude in this type of operation then depends only on the gross weight in a manner that can be analytically expressed as shown below.

In level unaccelerated flight,

$$L = W = (\gamma/2)pM^2SC_L \tag{A1}$$

When C_L and M are constant, a differentiation yields

$$dW = (\gamma/2)M^2SC_L\,dp$$

or

$$dW/W = dp/p \tag{A2}$$

Now, combining the atmospheric pressure law,

$$dp = -\rho g\,dh \tag{A3}$$

with the perfect gas law,

$$p = \rho R_0T_0 \tag{A4}$$

the following relationship is obtained:

$$dp/p = -(g/R_0T_0)dh \tag{A5}$$

Equating (2) and (5),

$$dW/W = -(g/R_0T_0)dh \tag{A6}$$

Above 35,000 ft., the temperature is constant so that

$$dW/W = -dh/20{,}940 \tag{A7}$$

This expression then gives the analytical relationship between a change in gross weight and a change in flight altitude for the special conditions given above. In integrated form, this relationship may be written as

$$h_2 - h_1 = 20{,}940 \ln (W_1/W_2)$$

The Bursting Speed of a Rotating Plastic Disc†

H. J. WEISS‡ AND W. PRAGER**
Brown University

ABSTRACT

The paper presents an analysis of the stresses and strains in a fully plastic, rotating, annular disc that has initially uniform thickness and is made of a strain-hardening material. This analysis is based on Tresca's yield condition and the associated flow rule and assumes that the elastic strains may be neglected in comparison with the finite plastic strains that are considered. The bursting speed of the disc is expressed in the form of a definite integral that involves the strain-hardening function of the material. In general, this integral must be evaluated numerically, but analytical evaluation is possible for certain strain-hardening functions. In particular, it is shown that, for linear strain-hardening, instability can occur only at the onset of plastic flow, whereas for logarithmic strain-hardening considerable plastic deformation of a stable character may occur before the process of deformation becomes unstable at the bursting speed.

NOTATIONS

a_0, b_0	= initial inner and outer radii of disc
ϵ_r, ϵ_θ, ϵ_z	= instantaneous (true) rates of strain in the radial, circumferential, and axial directions
h_0	= initial uniform thickness of disc
h	= thickness of disc during plastic flow
k, l, m	= constants in logarithmic stress-strain relation, Eq. (16)
r_0	= initial radial distance of a particle
r	= radial distance of a particle initially at r_0
s_r, s_θ, s_z	= nominal stresses in the radial, circumferential, and axial directions
s^*	= critical nominal stress (initial yield stress)
u	= radial displacement of a particle
v	= radial velocity of a particle
α	= b_0/a_0
ϵ_r, ϵ_θ, ϵ_z	= nominal strains in the radial, circumferential, and axial directions
ϵ^*	= critical nominal strain
η	= u/a_0
ξ	= r_0/a_0
ρ	= density of disc material
σ_r, σ_θ, σ_z	= true stress in the radial, circumferential, and axial directions
σ	= twice the critical value of the true shearing stress
ω	= angular speed of the rotating disc

(I) INTRODUCTION

THE ANALYSIS OF STRESSES AND STRAINS in elastic or partially plastic rotating discs has been discussed repeatedly.[1–6] In these problems the strains are of the order of magnitude of elastic strains and may therefore be treated as infinitesimal. As a consequence of this, the equations of equilibrium may be satisfied for the undeformed rather than the deformed disc. Considerable simplification of the mathematical work results from this approximation. It would be unrealistic, however, to treat the strains as infinitesimal when the bursting speed of a strain-hardening plastic disc is to be determined. In fact, as the angular speed of such a disc is gradually increased, considerable plastic deformation of a stable character may occur before the process of deformation finally becomes unstable at the bursting speed.

Since the prediction of the bursting speed of a strain-hardening plastic disc requires the consideration of finite plastic strains, the analyst who has to forego the simplifications resulting from infinitesimal strains will look for other possibilities of reducing the mathematical work. Thus, Zaid[7] uses a deformation theory of plasticity rather than a flow theory, in spite of his realization of the questionable value of this type of theory.[8] The alternative analysis offered in the present paper has recourse to other simplifying assumptions. First, it is assumed that the elastic strains are negligible in comparison with the plastic strains. Secondly, it is assumed that the material of the disc obeys Tresca's yield condition[9] and the associated flow rule.[10]

(II) TRESCA'S YIELD CONDITION AND FLOW RULE

In a rotationally symmetric stress field, the principal stresses are the hoop stress σ_θ, the radial stress σ_r, and the axial stress σ_z. The principal shearing stresses therefore are $(1/2)|\sigma_\theta - \sigma_z|$, $(1/2)|\sigma_r - \sigma_z|$, and $(1/2)|\sigma_\theta - \sigma_r|$. According to Tresca's yield condition, none of these principal shearing stresses can exceed a critical value that depends on the stage of strain-hardening of the material. Moreover, for plastic flow to occur, at least one of the principal shearing stresses must have the critical value.

If only one of the principal shearing stresses has the critical value, the flow rule associated with Tresca's yield condition stipulates that the instantaneous strain rate corresponds to pure shear in the plane of maximum shearing stress. The sense of this shear deformation must be "appropriate"—i.e., it must correspond to the sense of the maximum shearing stress.

If two principal shearing stresses attain the critical value, the flow rule admits any strain rate that can be considered as resulting from the superposition of appropriate states of pure shear in the two planes of

Received September 11, 1953.

† The results presented in this paper were obtained in the course of research sponsored by the Office of Naval Research under Contract N7onr-35801.

‡ Assistant Professor of Applied Mathematics.

** Professor of Applied Mechanics.

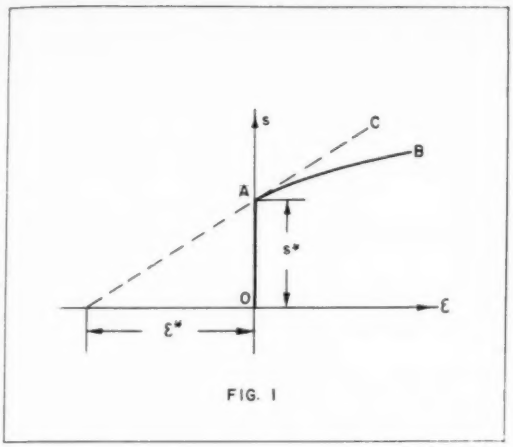

FIG. 1

critical shearing stress. It should be noted that in both cases the volume is preserved during plastic flow.

To express this yield condition and flow rule analytically, denote by $\sigma/2$ the critical value of the shearing stress for the considered state of strain-hardening, and by e_θ, e_r, and e_z denote the instantaneous rates of extension in the circumferential, radial, and axial directions. For the state of generalized plane stress occurring in a thin rotating disc, the axial stress σ_z is zero. Moreover, for an annular disc of initially uniform thickness, it may be tentatively assumed that the hoop stress σ_θ and the radial stress σ_r are tensile and that σ_θ everywhere exceeds σ_r. Under these circumstances, Tresca's yield condition and the associated flow rule lead to the following relations:

$$\sigma_\theta = \sigma > \sigma_r > 0, \qquad \sigma_z = 0 \tag{1}$$

$$e_r = 0, \qquad e_\theta = -e_z \geq 0 \tag{2}$$

Since σ_θ and e_r are thus known explicitly, the number of unknown functions is reduced and the analysis is thereby simplified.

To complete the description of the assumed mechanical behavior of the disc material, it is necessary to formulate a law of strain-hardening. For simple tension, let the stress-strain diagram have the general shape of the line 0AB in Fig. 1. The material remains rigid until the tensile stress s reaches the value s^*; during the ensuing plastic flow, the stress increases with the strain ϵ according to

$$s = f(\epsilon) \tag{3}$$

The rate of strain-hardening $ds/d\epsilon$ has the initial value s^*/ϵ^* (see Fig. 1) and decreases monotonically with increasing strain.

In Eq. (3), s and ϵ should be interpreted as the conventional stress and strain computed with reference to the original dimensions of the test specimen. On the other hand, the quantities σ_θ, σ_r, σ_z, σ, e_θ, e_r, and e_z introduced above should be interpreted as the true stresses and strain rates; they are defined with respect to the dimensions in the considered state of deformation.

It remains to discuss the application of the strain-hardening law, Eq. (3), to the states of stress and plastic flow occurring in a rotating disc. The state of plastic flow described by Eqs. (2) is independent of the value of the intermediate principal stress σ_r. Moreover, this type of plastic flow is possible under Tresca's flow rule when the state of stress is simple tension in the circumferential direction. It is therefore reasonable to assume that Eq. (3) can be applied to the problem on hand, provided that s is interpreted as the conventional hoop stress s_θ and ϵ as the conventional hoop strain ϵ_θ.

(III) Fully Plastic Disc

Consider a rotating annular disc of the uniform initial thickness h_0, the initial interior radius a_0, and the initial exterior radius b_0. From the elastic stress analysis it is known that, as the angular speed ω of the disc is gradually increased, the yield limit is first reached at the interior surface. At somewhat higher speeds there will be an inner plastic region surrounded by an elastic region. Any flow that may occur in the plastic region would have to satisfy Eqs. (2). If $v = v(r)$ is the distribution of the radial velocity at a generic instant during this plastic flow, the radial strain rate is $e_r = \partial v/\partial r$. Since this must vanish according to Eq. (2), the radial velocity must be independent of r. Moreover, since all elastic strains are neglected, the radial displacement u at the elastic-plastic interface is zero. This means that v and, hence, the circumferential strain rate $e_\theta = v/r$ must vanish throughout the plastic region. This region thus remains rigid until the elastic-plastic interface reaches the exterior surface of the disc. The angular speed ω_1 at which this occurs is given by [see reference 6, page 103, Eq. (9.58)]

$$\omega_1^2 = (3s^*/\rho)\,[(b_0 - a_0)/(b_0^3 - a_0^3)] \tag{4}$$

where ρ is the density of the disc material. The fully plastic stress distribution at the onset of plastic flow is readily analyzed [see reference 6, page 104, Eq. (9.59) and Fig. 9.5]. It is found that, at this instant, the radial stress nowhere reaches the yield stress regardless of the values of $b_0 > a_0 > 0$. Thus, Eqs. (1) and (2) apply, initially at least, during the ensuing plastic flow.

Let r_0 denote the initial radius of a particle that is found at the radius r when the speed is ω. If the radial displacement is denoted by u, then

$$r = r_0 + u \tag{5}$$

Here, r and u may be considered as functions of the independent variables r_0 and ω^2. (It is convenient to use ω^2 rather than ω, since the sense of the plastic flow is independent of the sense of rotation or the sign of the angular speed.)

As has been shown above, the first Eq. (2) requires that all particles have the same radial velocity at any given instant. This implies that the radial displacement depends only on ω^2 but not on r_0. Thus, the material bounded in the undeformed state by the coaxial cylinders of radii r_0 and $r_0 + dr_0$ undergoes the radial displacement u and is then bounded by cylinders of radii $r = r_0 + u$ and $r + dr = r + dr_0$ in the deformed state. Simultaneously, the original thickness h_0 decreases to h. Because of the incompressibility of the material, $h_0 r_0 dr_0 = hrdr$ or, since $dr = dr_0$,

$$h = h_0(r_0/r) = h_0[r_0/(r_0 + u)] \tag{6}$$

The true radial stress σ_r is transmitted across a section that is proportional to hr. Since $hr = h_0 r_0$, by Eq. (6), the conventional and true radial stresses have the same value: $\sigma_r = s_r$. The true circumferential stress σ_θ is transmitted across a section that is proportional to hdr; the corresponding value in the undeformed state is $h_0 dr_0 = h_0 dr$. The conventional circumferential stress is therefore given by

$$s_\theta = \sigma_\theta(h/h_0) \tag{7}$$

This stress is related to the conventional circumferential strain

$$\epsilon_\theta = u/r_0 \tag{8}$$

by an equation of the form of Eq. (3).

The equation of equilibrium in the deformed state is

$$\partial(rh\sigma_r)/\partial r = h\sigma_\theta - h\rho\omega^2 r^2 \tag{9}$$

With reference to the undeformed state, this equation may be written as follows:

$$\begin{aligned} \partial(r_0 s_r)/\partial r_0 &= s_\theta - \rho\omega^2 r_0(r_0 + u) \\ &= f(u/r_0) - \rho\omega^2 r_0(r_0 + u) \end{aligned} \tag{10}$$

Since s_r vanishes at the interior and exterior surfaces of the disc—i.e., for $r_0 = a_0$ and $r_0 = b_0$—the integral of the right-hand side of Eq. (10) between the limits a_0 and b_0 must vanish. With $\alpha = b_0/a_0$, $\eta = u/a_0$, and $\xi = r_0/a_0$, this condition yields

$$\rho a_0^2\omega^2/6 = \int_1^\alpha f(\eta/\xi)\, d\xi/[2(\alpha^3 - 1) + 3\eta(\alpha^2 - 1)] \tag{11}$$

For a known strain-hardening function f and given initial dimensions, the right-hand side of Eq. (11) must be evaluated, analytically or numerically, for a set of values of $\eta = u/a_0$. Each such evaluation furnishes one point of the plot ω^2 vs. u. For $\eta = 0$, in particular, $f(0) = s^*$ and the integral in Eq. (11) equals $(\alpha - 1)s^*$. Eq. (11) therefore yields the correct value, Eq. (4), for the angular speed at which plastic flow begins.

As long as an increase in ω^2 is required to produce an increase in u, the considered plastic flow is stable. The bursting speed ω_2 corresponds to the maximum of the curve ω^2 vs. u.

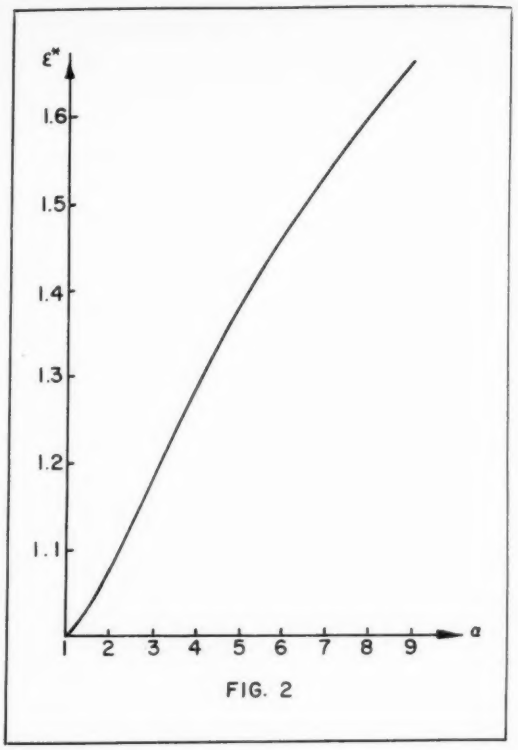

FIG. 2

The preceding analysis is based on the assumption that the radial stress σ_r is smaller than the circumferential stress σ_θ. A formula for the maximum radial stress occurring at a given speed ω can be obtained by carrying out the differentiation on the left-hand side of Eq. (10) and equating $\partial s_r/\partial r_0$ to zero. Thus,

$$\text{max. } s_r = s_\theta - \rho\omega^2 r_0(r_0 + u) \tag{12}$$

where r_0 is now the initial value of the radius at which the maximum of s_r occurs. Eq. (12) shows that even this maximum of s_r is smaller than the corresponding value of s_θ. Now, $\sigma_r = s_r$ and $\sigma_\theta > s_\theta$ by Eq. (7). The maximum of σ_r is therefore smaller than the corresponding value of σ_θ.

(IV) Linear Strain-Hardening

As a rule, the integral in Eq. (11) must be evaluated numerically, but strain-hardening laws can be devised that make analytical evaluation possible. The simplest law of this kind is represented by the line 0AC of Fig. 1. With

$$f(\epsilon) = s^*[1 + (\epsilon/\epsilon^*)] \tag{13}$$

Eq. (11) yields

$$\frac{\rho a_0^2\omega^2}{6s^*} = \frac{\alpha - 1 + (\eta/\epsilon^*)\log\alpha}{2(\alpha^3 - 1) + 3\eta(\alpha^2 - 1)} \tag{14}$$

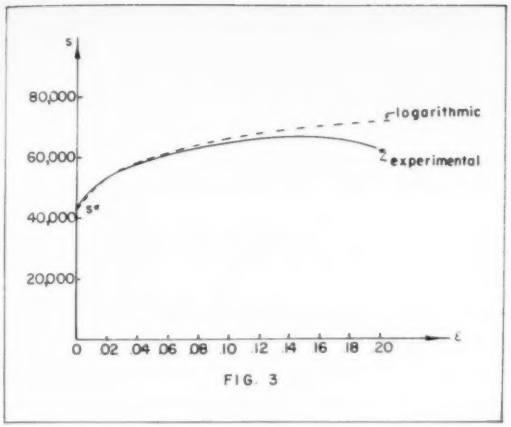

FIG. 3

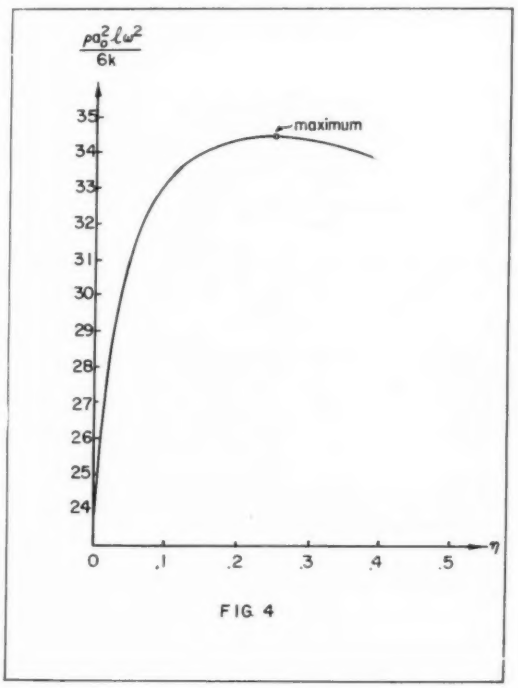

FIG. 4

Differentiation of Eq. (14) with respect to η shows that $d(\omega^2)/d\eta = 0$ when

$$\epsilon^* = 2(\alpha^2 + \alpha + 1) \log \alpha / 3(\alpha^2 - 1) \qquad (15)$$

Eq. (15) establishes the critical rate of linear strain-hardening. For a given value of $\alpha = b_0/a_0$, the strain-hardening parameter ϵ^* (see Fig. 1) must not exceed

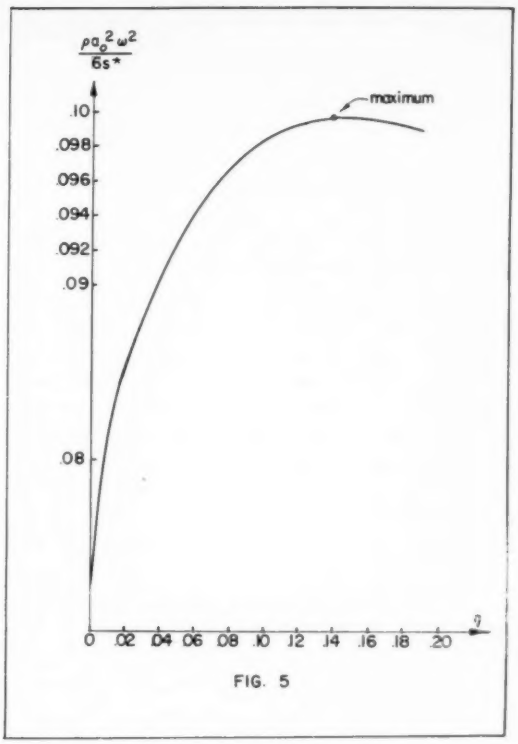

FIG. 5

the value of Eq. (15) if plastic deformation is to be stable. In Fig. 2, ϵ^* as given by Eq. (15) is plotted versus α. As $\alpha \to 1$—i.e., as the width of the annulus tends toward zero—the critical value of ϵ^* tends toward 1. This result is familiar from Laszlo's paper.[11]

The sign of $d(\omega^2)/d\eta$ as found from Eq. (14) does not change with increasing η. This means that, for linear strain-hardening, instability can occur only at the onset of plastic flow. A disc that starts to flow in a stable manner will continue to do so as the angular speed is increased.

(V) Logarithmic Strain-Hardening

Another strain-hardening law for which the integral in Eq. (11) can be evaluated analytically is given by

$$f(\epsilon) = k \log (l + m\epsilon) \qquad (16)$$

where k, l, and m are constants. These may be chosen so as to fit an experimental stress-strain curve. With the function (16), Eq. (11) yields

$$\frac{\rho a_0^2 l \omega^2}{6k} = \frac{(\alpha l + m\eta) \log (\alpha l + m\eta) - (l + m\eta) \log (l + m\eta) - \alpha l \log \alpha}{2(\alpha^3 - 1) + 3\eta(\alpha^2 - 1)} \qquad (17)$$

Fig. 3 shows the actual stress-strain curve† for Al 24S-T4 in simple tension (full line) and the curve obtained from Eq. (16), with k = 9,780 lbs. per sq.in., l = 77, and m = 8,060. Fig. 4 shows the left-hand

† The authors are indebted to Prof. E. D'Appolonia, Carnegie Institute of Technology, Pittsburgh, for the use of this curve.

side of Eq. (17) vs. $\eta = u/a_0$ for $\alpha = b_0/a_0 = 2$. The bursting speed ω_2 is obtained from the maximum point of this curve. As can be seen, the disc bursts for $\eta = \eta_2 = 0.25$. Since $\eta = u/a_0$ and $\epsilon = u/r_0$, $\epsilon = \eta a_0/r_0$; since the maximum nominal hoop strain occurs at $r_0 = a_0$, the disc would burst at a hoop strain of 25 per cent. From Fig. 3, it can be seen, however, that this hoop strain is beyond the range of validity of the experimental stress-strain curve. A more realistic picture is obtained by integrating the right-hand side of Eq. (11) numerically, using the experimental stress-strain curve in Fig. 3 (full line) as $s = f(\epsilon)$. Fig. 5 shows a plot of $\rho a_0^2\omega^2/6s^*$ (where s^* is as indicated in Fig. 3) vs. η, for $\alpha = 2$. Again, the bursting speed, ω_2, is obtained from the maximum point of this curve, which occurs at $\eta = \eta_2 = 0.14$, and thus at a maximum nominal hoop strain of 14 per cent. This maximum strain occurs before necking takes place in the test specimen and thus is in the range of validity of the experimental stress-strain curve. The results just obtained illustrate the fact that, for logarithmic strain-hardening as well as actual strain-hardening of a similar type, there is a considerable range of stable plastic deformation before bursting occurs.

References

[1] Timoshenko, S., and Goodier, J. N., *Theory of Elasticity*, pp. 69–73 and 352–354; McGraw-Hill Book Company, Inc., New York, 1951.

[2] Nadai, A., and Donnell, L. H., *Stress Distribution in Rotating Disks of Ductile Material After the Yield Point Has Been Reached*, Transactions, ASME, APM-51-61, 1929.

[3] Nadai, A., *Theory of Flow and Fracture of Solids*, pp. 482–489; McGraw-Hill Book Company, Inc., New York, 1950.

[4] Lee Wu, M. H., *General Plastic Behavior and Approximate Solutions of Rotating Disk in Strain-Hardening Range*, NACA Report No. 1021, May, 1951.

[5] Zaid, M., *Partially Plastic Discs*, Journal of the Aeronautical Sciences, Vol. 19, No. 10, pp. 697–704, October, 1952.

[6] Hoffman, O., and Sachs, G., *Introduction to the Theory of Plasticity for Engineers*, pp. 96–104; McGraw-Hill Book Company, Inc., New York, 1953.

[7] Zaid, M., *Fully Plastic Rotating Disc with Large Strains*, Journal of the Aeronautical Sciences, Vol. 20, No. 6, pp. 369–377, June, 1953.

[8] Prager, W., *Theory of Plastic Flow Versus Theory of Plastic Deformation*, Journal of Applied Physics, Vol. 19, No. 6, pp. 540–543, June, 1948.

[9] Tresca, H., *Mémoire sur l'Ecoulement des Corps Solides*, Mémoires Presentés par Divers Savants, Vol. 18, pp. 733–799, 1868.

[10] Prager, W., *On the Use of Singular Yield Conditions and the Associated Flow Rules*, Journal of Applied Mechanics, Vol. 20, No. 3, pp. 317–320, September, 1953.

[11] Laszlo, F., *Geschleuderte Umdrehungskoerper im Gebiet bleibender Deformation*, Zeitschrift fuer angewandte Mathematik und Mechanik, Vol. 5, No. 4, pp. 281–293, August, 1929.

Notice to Contributors

Manuscripts submitted for publication *must* be double- or triple-spaced originals. There should be wide margins on both sides of the sheets and triple spacing around formulas to allow for the marking of directions to the printer.

Original drawings (jet black India ink on white paper or tracing cloth) should accompany the manuscript. (*Blueprints are not acceptable.*) Photographs *must* be on glossy paper. The smallest lettering on 8- by 10-in. figures should be no less than ¼ in. high.

Only the simplest formulas should be typewritten, all others should be carefully written in pen and ink. The differences between capital and lower-case letters and Greek symbols should be clearly distinguished.

See Inside Back Cover of this issue for further details.

Readers' Forum

BRIEF REPORTS of investigations in the aeronautical sciences and discussions of papers published in the JOURNAL are presented in this special department. The publication will be completed as soon as possible after receipt of the material. The Editorial Committee does not hold itself responsible for the opinions expressed by the correspondents. Contributions should not exceed 800 words in length.

The Calculation of Wall Shearing Stress from Heat-Transfer Measurements in Compressible Flows

Nick S. Diaconis
Lewis Flight Propulsion Laboratory, NACA, Cleveland, Ohio
December 9, 1953

IT HAS BEEN SHOWN by Ludwieg[1] that the wall shearing stress of a laminar or turbulent boundary layer in an incompressible flow can be determined from a heat-transfer measurement at the surface. The instrument used in that investigation was essentially a small, locally insulated, heating element embedded in the test surface. The size of the instrument was restricted by the condition that the thermal boundary layer generated by the heating element be contained locally within the laminar sublayer. In the present analysis Ludwieg's theory for such an instrument is extended to compressible flow over an insulated flat plate With the same limitations on the design and operation of the instrument as mentioned above, it can also be assumed for compressible laminar and turbulent boundary layers that only the flow in the immediate vicinity of the wall or the laminar sublayer will be affected in the region of the heated element. This assumption then permits the use of the laminar boundary-layer equations as the governing equations for this analysis for both laminar and turbulent boundary layers.

If the specific heat and Prandtl Number are taken to be constant and if a linear viscosity-temperature relation is assumed, the compressible equations become in dimensionless notation and in a transformed coordinate system similar to reference 2.

Momentum:

$$\psi_n\psi_{nx} - \psi_{nn}\psi_x = \psi_{nnn} \tag{1}$$

Energy

$$\psi_n T_x - \psi_x T_n = (1/Pr)T_{nn} + (\gamma - 1)M_\infty{}^2(\psi_{nn})^2 \tag{2}$$

where

$\psi = \psi^*/\sqrt{\nu_\infty{}^* U_\infty{}^* L^* C}$ = stream function
$T = T^*/T_\infty{}^*$ = absolute static temperature ratio
$n = \int_0^\psi \frac{d\psi}{u}$ = transformed normal coordinate
$x = x^*/L^*$ = longitudinal coordinate
$C = (\mu^*/\mu_\infty{}^*)(\rho^*/\rho_\infty{}^*)$ = viscosity-temperature proportionality factor
L^* = a characteristic length
$*$ = dimensional quantity
$(\ )_\infty$ = conditions in the free stream

(Independent variables used as subscripts denote partial differentiation.)

If Eqs. (1) and (2) are restricted to the laminar sublayer, certain simplifications can be made. From the low-speed results of Laufer,[3] it appears that the shear in the laminar sublayer is practically constant. It is believed, however (see reference 4), that such a condition could also be assumed for the compressible case. As a consequence it can be shown that $\psi_{nn} = K$ = constant and $\psi_{nnn} = \psi_{nx} = \psi_x = 0$, so that the momentum equation reduces to

$$\psi_{nnn} = 0 \tag{3}$$

The solution of Eq. (3) with the boundary condition $\psi_n(x, 0) = 0$, is

$$\psi = (Kn^2/2) + \text{constant} \tag{4}$$

The energy equation simplifies to the following

$$\psi_n T_x - (1/Pr)T_{nn} = (\gamma - 1)M_\infty{}^2(\psi_{nn})^2 \tag{5}$$

Substituting Eq. (4) into Eq. (5) and introducing the new variables ζ and η yields

$$\eta T_\zeta - T_{\eta\eta} = (\gamma - 1)M_\infty{}^2 K \tag{6}$$

where

$$\zeta = \sqrt{K\,Pr}\,x, \qquad \eta = \sqrt{K\,Pr}\,n \tag{7}$$

Introducing the similarity variable α (see reference 1), where

$$\alpha = \eta/(9\zeta)^{1/3} \tag{8}$$

results in the transformation of Eq. (6) into the ordinary differential equation

$$(d^2T/d\alpha^2) + 3\alpha^2(dT/d\alpha) = (\gamma - 1)M_\infty{}^2 K \tag{9}$$

Since Eq (9) is linear, the temperature T can be expressed as

$$T = T_1 + T_2 \tag{10}$$

where T_1 is the temperature distribution when the plate is at the adiabatic wall temperature and T_2 is the perturbation caused by slightly heating a small segment of the wall (i.e., at the heat-transfer instrument) from T_{ad} to T_w. Both T_1 and T_2 satisfy Eq. (9), which can then be solved for the following boundary conditions:

$$\left.\begin{array}{lll} \alpha = 0 \text{ (i.e., } \eta = 0) & T_1 = T_{ad} & \\ & dT_1/d\alpha = 0 & \\ & T_2 = T_w - T_{ad} & \\ \alpha = \infty \text{(i.e., } \eta > 0 \text{ and } \zeta \to 0) & T_2 = 0 & \end{array}\right\} \tag{11}$$

where

T_{ad} = adiabatic wall temperature
T_w = wall temperature with heating element operating

The solutions for T_1 and T_2 are

$$T_1 = T_{ad} + (\gamma - 1)M_\infty{}^2 K_1 \int_0^\alpha \left[e^{-\omega^3} \int_0^\omega e^{\lambda^3}\, d\lambda \right] d\omega \tag{12}$$

$$T_2 = T_w - T_{ad} + (\gamma - 1)M_\infty{}^2 (K - K_1) \times \int_0^\alpha \left[e^{-\omega^3} \int_0^\omega e^{\lambda^3}\, d\lambda \right] d\omega + (T_{ad} - T_w) \frac{\int_0^\alpha e^{-\omega^3}\, d\omega}{\int_0^\infty e^{-\omega^3}\, d\omega} \tag{13}$$

The addition of Eqs. (12) and (13) then gives the complete solution of Eq. (9). Note that the constant K_1 does not appear in this solution and need not be evaluated. The constant K, however, is related to the wall shearing stress τ_w^* through Eq. (4) and can be expressed as follows, where the subscript w represents wall values

$$K = (\psi_{nn})_w = \left(\frac{\sqrt{\tau_w^*/\rho_w^*}}{U_\infty^*}\right)^2 \sqrt{\frac{U_\infty^* L^*}{\nu_w^*}} \tag{14}$$

The Nusselt Number is then defined as follows

$$Nu = \frac{h^* l^*}{k^*} = \frac{\int_0^{l^*} \left(\frac{\partial T^*}{\partial y^*}\right)_{y^*=0} dx^*}{T_{ad}^* - T_w^*} = \frac{\sqrt{\frac{U_\infty^* L^*}{\nu_w^*}} \int_0^{\bar{l}} \left(\frac{\partial T}{\partial \eta}\right)_{\eta=0} d\zeta}{T_{ad} - T_w} \tag{15}$$

where

$\bar{l} = \sqrt{K\ Pr}\ (l^*/L^*)$

l^* = length of heating element in measuring instrument

Substituting the expression for the temperature distribution in Eq. (15) gives for the Nusselt Number in compressible flow in the physical plane

$$Nu = 0.807(\tau_w^* \rho_w^* Pr)^{1/3} (l^*/\mu_w^*)^{2/3} \tag{16}$$

Eq. (16) shows that the compressible Nusselt Number is obtained from the incompressible form by replacing ρ_∞^* and μ_∞^* by ρ_w^* and μ_w^*, respectively. Although the compressible temperature distribution in the sublayer has an additional term (a function of stream Mach Number) that does not appear in the expression of reference 1, this term does not contribute to the heat transfer. Finally, Eq. (16) shows that, even in the compressible case with the use of an instrument of Ludwieg's type, it is possible to determine local skin friction values (τ_w^*) for an insulated flat plate from measurements of the heat transfer at a heated element in the wall.

Liepmann and Skinner[5] have obtained essentially the same result by means of a physical argument.

References

[1] Ludwieg, H., *Instrument for Measuring the Wall Shearing Stress of Turbulent Boundary Layers*, NACA TM No. 1284, May, 1950.

[2] Low, George M., *The Compressible Laminar Boundary Layer With Heat Transfer and Small Pressure Gradient*, NACA TN No. 3028, October, 1953.

[3] Laufer, John, *Investigation of Turbulent Flow in a Two-Dimensional Channel*, Progress Rep., Contract NAw (3661), GALCIT.

[4] Donaldson, Coleman duP., *On the Form of the Turbulent Skin Friction Law and Its Extension to Compressible Flow*, NACA TN No. 2692, May, 1952.

[5] Liepmann, H. W., and Skinner, G. T., *On Shearing Stress Measurements by a Heated Element*, Contract NAw-6154, GALCIT.

On a Perturbation Theory Based on the Method of Characteristics

C. C. Lin

Professor of Mathematics, Massachusetts Institute of Technology, Cambridge, Mass.

December 1, 1953

IT IS KNOWN THAT a perturbation theory in the physical plane for supersonic flow and wave propagation is not free from difficulties. A method for improvement has been proposed by Lighthill and Whitham[1] for dealing with outgoing waves. On the other hand, the characteristic parameters are the natural independent variables to use for hyperbolic differential equations, and it may be expected that, in a perturbation theory developed in terms of the characteristic form of the differential equations, such difficulties will not occur.

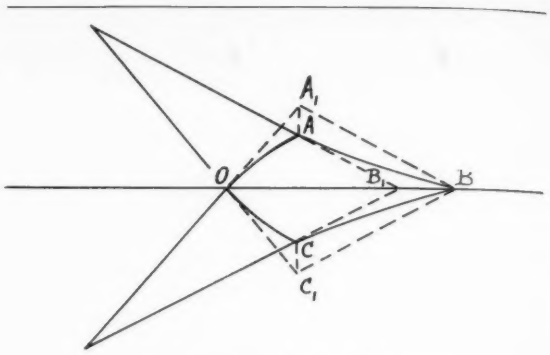

FIG. 1. Interaction of two simple waves.

The method of characteristics is well known, but it does not seem to be extensively used in connection with the perturbation theory.[2] In fact, in this case, an additional convenience can be easily introduced. Since the characteristics are nearly straight in the physical plane, the mapping between the characteristic parameters and the physical coordinates can be made an approximately affine transformation, which is easy to visualize. The complication that sometimes arises with the hodograph method is avoided.

On the other hand, when the hodograph method is useful the characteristics are fixed in the hodograph plane. Thus, the present method would also embody the advantages of the hodograph method.

Briefly, the method works as follows. If $u(x, y)$ and $v(x, y)$ are the solutions sought, we introduce the characteristic parameters α and β and seek the solution in the form

$$\left.\begin{aligned} u &= u^{(0)}(\alpha, \beta) + \epsilon u^{(1)}(\alpha, \beta) + \dots \\ v &= v^{(0)}(\alpha, \beta) + \epsilon v^{(1)}(\alpha, \beta) + \dots \\ x &= x^{(0)}(\alpha, \beta) + \epsilon x^{(1)}(\alpha, \beta) + \dots \\ y &= y^{(0)}(\alpha, \beta) + \epsilon y^{(1)}(\alpha, \beta) + \dots \end{aligned}\right\} \tag{1}$$

Thus, the solution is given by a parametric representation. The initial approximations to x and y are expected to be linear functions of α and β.

Several examples have been worked out by the present writer and Miss Phyllis Fox,[3] using the method just explained. Convergence proof is given in certain cases. The reflection of a Prandtl-Meyer expansion from the plane boundary will now be described to show how the method works. It is clear that the divergence of the characteristics is important here, and hence the perturbation theory in the physical plane does not work satisfactorily.

The problem is equivalent to that of the interaction of two expansion waves of equal strength, and we shall therefore consider the general case of interaction of two simple waves. The interaction region is bounded by four characteristics forming a rectangle in the (α, β) plane.

Along the two characteristics OA and OC, the solution is known; thus, we have a characteristic initial value problem. The choice of the scales of α and β is still at our disposal. It is important, for convenience of application, that this choice be properly made to simplify the mapping between the (x, y) plane and the (α, β) plane. This can be done simply by taking $x = \alpha$ along OA and $x = \beta$ along OC. The given physical conditions along OA and OC should be presented as functions of x. It has been found convenient to describe the state of the gas by using the Mach angle A and the angle θ for the direction of flow. Thus,

if $\theta = \epsilon f(x)$ along OA and $\theta = \epsilon g(x)$ along OC, the characteristic value problem is formulated as follows:

$$\left.\begin{aligned} \theta &= \epsilon f(\alpha), \quad x = \alpha \qquad \text{along OA} \\ \theta &= \epsilon g(\beta), \quad x = \beta \qquad \text{along OC} \end{aligned}\right\} \tag{2}$$

The equations for θ and A can be integrated in closed form, and we have

$$\left.\begin{aligned} \theta &= \epsilon[f(\alpha) + g(\beta)] \\ \psi(A) - \psi(A_0) &= \epsilon[f(\alpha) - g(\beta)] \end{aligned}\right\} \tag{3}$$

where

$$\left.\begin{aligned} \psi(A) &= A - (\pi/2) + (1/\mu)\tan^{-1}(\mu \cot A) \\ \mu^2 &= (\gamma - 1)/(\gamma + 1) \end{aligned}\right\} \tag{4}$$

The equations for x and y then give

$$\left.\begin{aligned} x &= (\alpha + \beta) + \epsilon(n/2\lambda)\,[\beta f(\alpha) - \alpha g(\beta)] \\ y &= \lambda(\alpha - \beta) + \epsilon/(n/2)\,[\beta f(\alpha) + \alpha g(\beta)] + \\ &\quad \epsilon\,(m/2)\left[\int_0^{\alpha} f(\alpha)\,d\alpha + \int_0^{\beta} g(\beta)\,d\beta\right] \end{aligned}\right\} \tag{5}$$

where

$$\left.\begin{aligned} m &= \sec^2 A_0\,\{1 + [1/\psi'(A_0)]\} \\ n &= \sec^2 A_0\,\{1 - [1/\psi'(A_0)]\} \end{aligned}\right\} \quad (\lambda = \tan A_0) \tag{6}$$

The reflection of a simple wave from a solid boundary can be obtained by taking $g(\beta) = -f(\beta)$. The boundary $y = 0$ becomes $\alpha = \beta$, where θ also vanishes. We have then

$$\left.\begin{aligned} \psi(A) - \psi(A_0) &= 2\epsilon f(\alpha) \\ x &= 2\alpha + \epsilon(n/\lambda)\alpha f(\alpha) \end{aligned}\right\} \tag{7}$$

for the pressure distribution along the solid boundary.

A detailed account of the method and the discussion of the results will be published later.

References

[1] Whitham, G. B., Comm. on Pure and Appl. Math., Vol. 5, pp. 301–349 (1952), and the references quoted.

[2] Courant, R., and Friedrichs, K. O., *Supersonic Flow and Wave Propagation*, Interscience, 1948, esp. p. 361.

[3] Fox, Phyllis, Sc.D. Thesis, M.I.T., November 13, 1953.

Experimental Velocity Profiles for Adiabatic Supersonic Flow of Air in a Tube

Joseph Kaye,* George A. Brown,† and John J. Dieckmann‡
Massachusetts Institute of Technology

December 1, 1953

During the past several years, a program has been under way to measure recovery factors and heat-transfer coefficients for supersonic flow of air in a round tube. It has been assumed in the interpretations of the data obtained that, for smooth entrance into a tube, the flow of air at supersonic speeds is attended by the gradual growth of a boundary layer in the direction of flow and by the filling of the tube cross section with this boundary layer. In the last few months, measurements of the velocity profiles of adiabatic supersonic flow of air in a round tube, $^1/_2$ in. in diameter, by means of small impact pressure probes, have demonstrated that it is possible to permit a *laminar boundary layer* to develop and grow over a long length of tube flow. These data, establishing the existence of a laminar boundary layer over a long length of tube flow, permit a more secure foundation to be established for the comparison of theoretical work with experimental results and also permit a better comparison of tube flow with supersonic flow over a flat plate.

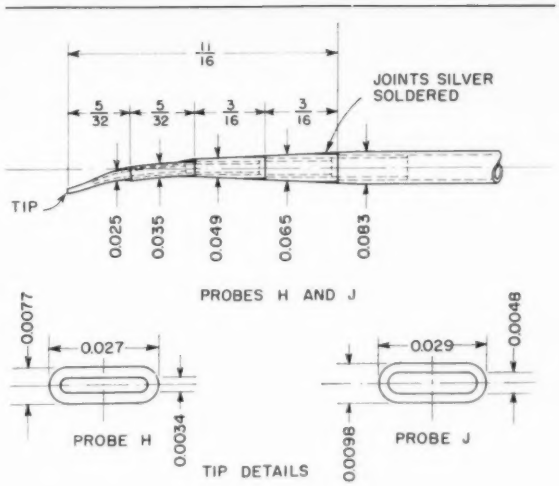

FIG. 1 DIMENSIONS OF PROBES H AND J

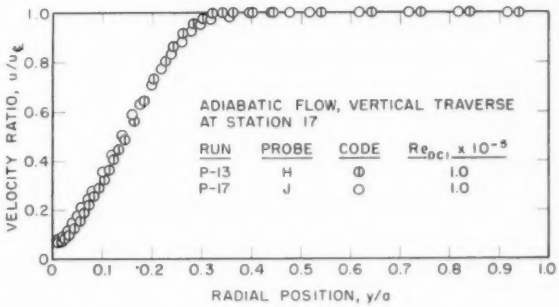
VELOCITY RATIO, u/u_e
RADIAL POSITION, y/a
ADIABATIC FLOW, VERTICAL TRAVERSE AT STATION 17
RUN PROBE CODE Re_oc, x 10^-5
P-13 H Φ 1.0
P-17 J O 1.0

FIG. 2 – COMPARISON OF PROBES H AND J

These measurements of velocity profiles were performed as part of a research program sponsored by the Office of Naval Research on measurement of heat-transfer coefficients for supersonic flow of air. The details of the apparatus used and the results obtained are to be found in previous reports.[1–3]

Several small impact pressure probes were constructed with the severe limitation that the probes should result in a minimum interference with the supersonic flow in the tube. The $^1/_2$-in. diameter tube is approximately 25 in. long, and the probe was to be inserted about 2.75 in. from the downstream end. The details of two such successful impact pressure probes are shown in Fig. 1. The probes were mounted on a traversing rig, which was situated in the downstream stagnation tank of the apparatus. This traversing rig enabled the position of the tip of the probe to be varied, in small increments, from the center of the tube to within about 0.004 in. from the wall of the tube. An electronic device was used to indicate when the probe tip was in actual physical contact with the tube wall; this device operated very successfully. Furthermore, the design of the rig permitted a rotation of the probe by 90° to allow measurements of the asymmetry of the velocity profiles for two planes at right angles to each other. The actual vibration of the probe tip in the experiments, especially near the tube wall, was found to be less than 0.003 in. in amplitude.

* Associate Professor Mechanical Engineering, M.I.T.
† Shell Fellow, Department of Mechanical Engineering, M.I.T.
‡ United States Air Force (present address).

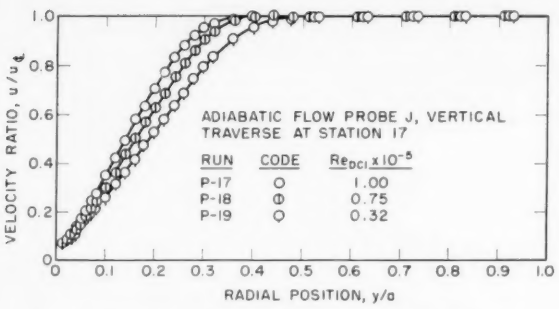
VELOCITY RATIO, u/u_ℓ
RADIAL POSITION, y/a
ADIABATIC FLOW PROBE J, VERTICAL TRAVERSE AT STATION 17
RUN CODE Re_DCI x10^-5
P-17 O 1.00
P-18 Φ 0.75
P-19 O 0.32

FIG. 3 - EFFECT OF INLET DIAMETER REYNOLDS NUMBER ON VELOCITY PROFILES

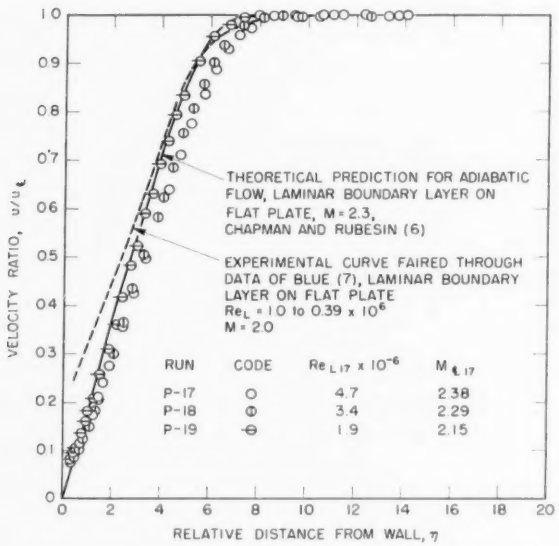
VELOCITY RATIO, u/u_ℓ
RELATIVE DISTANCE FROM WALL, η
THEORETICAL PREDICTION FOR ADIABATIC FLOW, LAMINAR BOUNDARY LAYER ON FLAT PLATE, M = 2.3, CHAPMAN AND RUBESIN (6)
EXPERIMENTAL CURVE FAIRED THROUGH DATA OF BLUE (7), LAMINAR BOUNDARY LAYER ON FLAT PLATE
Re_L = 1.0 to 0.39 x 10^6
M = 2.0
RUN CODE Re_L17 x 10^-6 M_ℓ17
P-17 O 4.7 2.38
P-18 Φ 3.4 2.29
P-19 Θ 1.9 2.15

FIG. 4 COMPARISON OF VELOCITY PROFILES FOR TUBE FLOW AND FOR FLOW OVER A FLAT PLATE.

The preliminary measurements of velocity profiles presented here were obtained with a stainless-steel nozzle designed to produce a supersonic flow at a Mach Number of 2.8 at the entrance plane of the tube, 25 in. long. For adiabatic flow the inlet diameter Reynolds Number could be varied from 0.3 to 1.0×10^6 to produce a laminar boundary layer over the entire length of this tube. For an inlet diameter Reynolds Number of about 2×10^6, a shock was established beyond the entrance of the tube; the resulting flow downstream of this shock produced a subsonic turbulent boundary layer extending over the rest of the tube length. Velocity profiles are shown here for both the laminar and the turbulent boundary layers.

Fig. 2 compares the profiles obtained with probes *H* and *J*. The velocity ratio is the ratio of computed local velocity to computed centerline velocity; the radial position is the ratio of the distance of the center of the probe tip from the tube wall to the radius of the tube. The agreement of the results obtained with the two probes is excellent.

Fig. 3 shows the effect of changing the diameter Reynolds Number at tube inlet on the velocity profiles near the exit of the tube. Increasing this Reynolds Number from 0.3 to 1.0×10^6 increases the slope of the velocity profile in the laminar boundary layer, but the nearly linear characteristic slope is evident in each of the three profiles.

Fig. 4 compares the velocity profiles obtained at station 17 (2.75 in. from tube exit) in the tube with those predicted by Chapman and Rubesin[6] for adiabatic laminar flow over a flat plate and with the measured profiles of Blue[7] for flow of a laminar boundary layer over a flat plate. The abscissa is the customary one used in analyses of flat-plate flows—namely,

$$\eta \equiv (y/L)\sqrt{Re_L} \tag{1}$$

where L is the distance from the leading edge, and the length Reynolds Number, Re_L, is given by

$$Re_L \equiv u_\infty L/\nu_\infty \tag{2}$$

where u_∞ and ν_∞ denote the free-stream velocity and kinematic viscosity, respectively. For the case of tube flow, however, where the centerline velocity and fluid properties vary with the distance downstream from tube entrance, a convenient though arbitrary definition of η is used here—namely,

$$\eta \equiv (y/L)\sqrt{Re_{L17}} \tag{3}$$

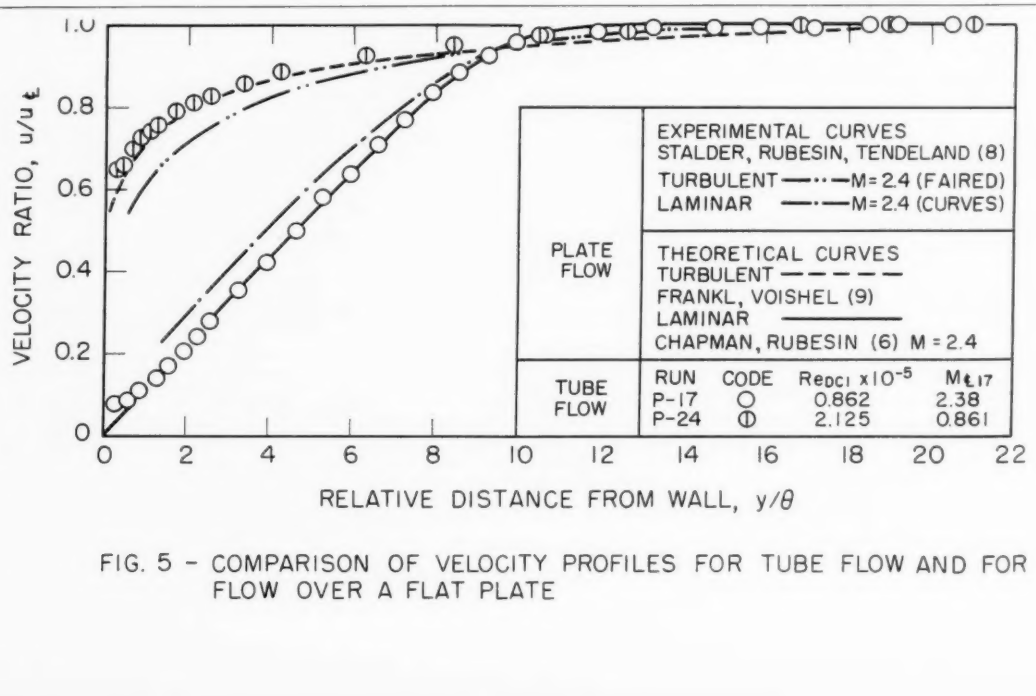

FIG. 5 - COMPARISON OF VELOCITY PROFILES FOR TUBE FLOW AND FOR FLOW OVER A FLAT PLATE

where L is the distance from entrance plane of the tube and the Reynolds Number is arbitrarily chosen for convenience to be

$$Re_{L17} = u_{e1}L_{17}/\nu_{e1} \tag{4}$$

in which the fluid properties are to be evaluated at tube entrance (to correspond to flat-plate flow), or at station 1, and by assuming that an isentropic core exists for the flow at tube entrance.

In Fig. 4, the tube-flow profiles show excellent agreement with both experimental and theoretical profiles for flat-plate flow. Since the definition of η used in this comparison is arbitrary, this excellent agreement may be, in part, fortuitous. The effect of this arbitrary definition will be examined later in greater detail in comparing the velocity profiles with the results based on a theoretical analysis of tube flow. In Fig. 4 the values of $M_{t_{17}}$ are the Mach Numbers computed for the centerline velocities at station 17.

Fig. 5 shows another means of comparison of velocity profiles for tube flow and flat-plate flow for both laminar and turbulent boundary layers. The abscissa is the ratio of distance from the wall to the momentum thickness of the boundary layer, defined by

$$\theta \equiv \int_0^\delta \frac{\rho u}{\rho_1 u_1}\left(1 - \frac{u}{u_1}\right)dy \tag{5}$$

where subscript 1 refers to the free-stream conditions for plate flow and to the centerline conditions for tube flow. Although Eq. (5) is not strictly correct for tube flow, it is used here only as a first approximation. For the laminar boundary layers, excellent agreement is obtained between the velocity profiles for tube flow and plate flow, although the remarkable agreement between the tube-flow profile and the theoretical curve for a flat-plate flow may be coincidental.

Fig. 5 shows also that, for subsonic flow in the tube, where a turbulent profile should be obtained after a shock, the measured velocity profiles agree well with those for turbulent boundary layer on a flat plate. Again the agreement of the experimental tube-flow profile with the theoretical flat-plate profile is better than with the experimental flat-plate profile; this result may be fortuitous.

The assistance of Edward A. Sziklas and W. S. Wu in aiding in the experiments is gratefully acknowledged.

References

[1] Kaye, J., Keenan, J. H., and McAdams, W. H., *Report of Progress on Measurements of Friction Coefficients, Recovery Factors, and Heat-Transfer Coefficients for Supersonic Flow of Air in a Pipe*, Heat Transfer and Fluid Mechanics Institute, pp. 147–164, June, 1949.

[2] Kaye, J., Keenan, J. H., and Shoulberg, R. H., *Measurement of Recovery Factors and Friction Coefficients for Supersonic Flow of Air in a Tube*, General Discussion on Heat Transmission, London Conference, Special Publication, ASME, Sect. II, pp. 1–5, September, 1951.

[3] Kaye, J., Keenan, J. H., Klingensmith, K. K., Ketchum, G. M., and Toong, T. Y., *Measurement of Recovery Factors and Friction Coefficients for Supersonic Flow of Air in a Tube*, J. Applied Mechanics, Trans. ASME, Vol. 74, pp. A-77–A-96, 1952.

[4] Kaye, J., Toong, T. Y., and Shoulberg, R. H., *Measurement of Recovery Factors and Friction Coefficients for Supersonic Flow of Air in a Tube*, J. Applied Mechanics, Trans. ASME, Vol. 74, pp. A-185–A-194, 1952.

[5] Kaye, J., and Toong, T. Y., *Measurements of Friction Coefficients for Supersonic Flow of Air in the Entrance Region of a Tube With and Without Heat Transfer*, First Iowa Thermodynamics Symposium, State University of Iowa, April 27–28, 1953.

[6] Chapman, D. R., and Rubesin, M. W., *Temperature and Velocity Profiles in the Compressible Laminar Boundary Layer with Arbitrary Distribution of Surface Temperature*, Journal of the Aeronautical Sciences, pp. 547–565, September, 1949.

[7] Blue, R. E., *Interferometer Corrections and Measurements of Laminar Boundary Layers in Supersonic Streams*, NACA TN No. 2110, June, 1950.

[8] Stalder, J. R., Rubesin, M. W., and Tendeland, T., *A Determination of the Laminar-Transitional-, and Turbulent-Boundary Layer Temperature Recovery Factors in Supersonic Flow*, NACA TN No. 2077, June, 1950.

[9] Frankl, F., and Voishel, V., *Turbulent Friction in the Boundary Layer of a Flat Plate in a Two-Dimensional Compressible Flow at High Speeds*, NACA TM No. 1053, 1943.

The Numerical Solution of Certain Nonlinear Supersonic Flow Problems on the IBM Card Programmed Calculator

R. E. Bower and J. H. Higman
Research Engineers, Grumman Aircraft Engineering Corporation, Bethpage, L.I., N.Y.
December 8, 1953

THE COMPLEXITY OF NONLINEAR SUPERSONIC FLOW PROBLEMS precludes an exact analytical solution except in certain rare instances. Generally, the powerful numerical procedures, such as the method of characteristics, are resorted to, but their application is restricted because of the extensive amount of time which must be expended by better than average computing personnel. The recent increase in the availability of automatic computing equipment, however, is eliminating this obstacle, and procedures previously considered prohibitive in practice now take on new elegance. Clippinger and Gerber[1] have already treated the automatic computation of bodies of revolution at zero angle of attack on the ENIAC. This note is concerned with similar work performed on the IBM Card Programmed Calculator (C.P.C.).[2] The C.P.C. is an electronic digital computor which, in contrast to the ENIAC, is available to most computing groups.

The study is restricted to steady-state problems that are functions of not more than two independent variables. Future work is contemplated, however, to consider the effects of a third variable. The numerical procedures are in the main developed from the theory of characteristics for hyperbolic partial differential equations. In the case of conical flow, however, Busemann's radius of curvature solution in the hodograph plane[3] is used, and, of course, for two-dimensional oblique shock waves, the conventional methods for solving a cubic are employed.

The characteristic relations are revised to avoid trigonometric functions. This not only results in a saving in machine time but also allows more versatility in the use of the C.P.C. installation at Grumman in that problems can be card-programmed for use with the more general purpose type of calculator setup which is capable of performing the basic arithmetical operations of multiplication, division, addition, subtraction, and square root. The form of the equations used is

$$\frac{dr}{dx} = \frac{uv + a\sqrt{V^2 - a^2}}{u^2 - a^2} = \frac{1}{\mu} \tag{1a}$$

$$\frac{du}{dr} + \lambda\frac{dv}{dr} - \frac{a^2}{uv + a\sqrt{V^2 - a^2}} \times \left[\epsilon\frac{v}{r} - \frac{a\sqrt{V^2 - a^2}}{\gamma VR}\frac{dS}{dn}\right] = 0 \tag{1b}$$

and

$$\frac{dr}{dx} = \frac{v^2 - a^2}{uv + a\sqrt{V^2 - a^2}} = \lambda \tag{2a}$$

$$\mu\frac{du}{dx} + \frac{dv}{dx} - \frac{a^2}{uv + a\sqrt{V^2 - a^2}} \times \left[\epsilon\frac{v}{r} + \frac{a\sqrt{V^2 - a^2}}{\gamma VR}\frac{dS}{dn}\right] = 0 \tag{2b}$$

where u and v are the velocity components of V along the cylindrical or rectangular axes x and r, a is the local sound velocity, dS/dn is the gradient of entropy normal to a stream line, γ is the ratio of specific heats, R is the universal gas constant, and ϵ is zero for two-dimensional flow and unity for axially symmetric phenomena. The arrangement of Eqs. (1) and (2) avoids indeterminate forms when $u = a$.

The solution of a particular problem by the method of characteristics involves the repetitious application of certain basic

TABLE 1

C.P.C. Running Times of Some Representative Calculation Decks

Function of Deck	Running Time (Min.) First* approximation	Each iteration
Calculation of an interior point in a rotational, axially symmetric flow field	1.2	0.6
Calculation of the axially symmetric flow conditions at a fixed point on a physical boundary (at a wall)	1.4	0.5
Calculation of flow conditions at a point on the axis of symmetry	1.0	0.2
Calculation of a point on a shock boundary in uniform, axially symmetric, rotational flow	2.1	0.9
Calculation of a point on a shock boundary in a nonuniform, axially symmetric, rotational flow field	3.9	2.7
Calculation of the flow crossing an oblique shock wave	1.7†	...

* Includes punching of results.
† Total calculation time.

computations based on Eqs. (1) and (2) and appropriate boundary conditions. The programming on an automatic machine consists then in setting up these elementary calculation decks with a provision for their combination. The decks in this study were card-programmed for use with the C.P.C. storage capacity set at 48 positions. With such a limitation it is not possible to store sizable portions of the flow field so the effective storage of the calculator must be increased by the development of a systematic method of punching and storing the space coordinates and velocities identified with each mesh point. As these quantities are calculated for each point, they are punched with proper coding for future use and, when necessary, held in storage for immediate use in the solution of a subsequent mesh point.

A total of 30 basic computation decks were programmed on the C.P.C. They allow the completely automatic solution of such nonlinear supersonic problems as (1) the flow transition through oblique shock waves, (2) conical flow phenomena for circular cones, (3) the rotational flow over two-dimensional bodies, (4) external irrotational or rotational flow about pointed or open-nose bodies of revolution, (5) the irrotational flow through diffusers or nozzles, and (6) jet exhaust flow. The programming of an extremely lengthy computation such as an axially symmetric shock boundary in a nonuniform flow field was attempted as perhaps a practical upper limit for a single calculation performed on the C.P.C. Although the solution was successful, the complexity and tediousness of the programming indicated the impracticability of treating a more involved problem with a single deck. The development of the nonuniform shock boundary computation, however, extended the list of soluble flow problems to include ducted two-dimensional or axially symmetric bodies.

Because of the obvious enormity of the problem, a detailed error study is not considered. The characteristic relations are solved by a second-order iterative type of solution, and eight digits are carried in the fixed decimal system to minimize round-off errors. The error considerations of reference 1 allow increased accuracy for a given amount of time in some cases by an extrapolation to zero mesh size. With the assumption that the error varies as $h^2 = 1/n^2$, where n is the number of integration steps taken on the body or along an initial characteristic, Richardson's h^2 extrapolation coefficients may be used on two solutions performed at different grid sizes.

The saving in time realized by the C.P.C. is dependent upon the complexity of the problem and the type of hand method employed in the comparison. Perhaps quoting some actual machine running times for the calculations as is done in Table 1 is the best measure. The number of iterations necessary for convergence depends upon the Mach Number and grid size, but usually two or three are sufficient. The time to solve any particular problem is easily obtained from the number of mesh points to be considered, since the solution is automatic and continuous.

REFERENCES

[1] Clippinger, R. F., and Gerber, N., *Supersonic Flow over Bodies of Revolution (with Special Reference to High-Speed Computing)*, Ballistic Research Laboratories Report No. 719, May, 1950.

[2] Higman, J. H., and Bower, R. E., *The Numerical Solution of Certain Nonlinear Supersonic Flow Problems on the I.B.M. Card-Programmed Calculator*, Grumman Aircraft Engineering Corporation Research Department, Report R.E.-67, October 15, 1953.

[3] Busemann, A., *Druck Auf Kegelformige Spitzen Bei Bewegung Mit Überschallgeschwindigkeit*, Zeitschrift Für Angewandte Mathematik Und Mechanik, Vol. 9, No. 6, 1929.

Effect of Local Modifications in Redundant Structures

E. Kosko
Assistant Chief Stress Engineer, A. V. Roe Canada Limited
December 9, 1953

THERE APPEARS TO BE A NEED for some means of evaluating the effect of a local modification in a redundant structure on the stress distribution and on the deflections. Reference 1 suggests that an extension of Best's "Stress Area Method"[2] is suitable for that purpose. A more recent contribution[3] points out that a similar condition exists in electrical engineering, where the so-called Compensation Theorem provides a solution. This writer, however, being unfamiliar with electrical networks, has found the description of the method somewhat difficult to follow. It is therefore proposed to present an alternative formula with a derivation based on matrix algebra.[4]

Let us assume that a linear relation exists in the form

$$A_0 U = P \tag{1}$$

between n load components $\{P_1, P_2, \ldots, P_n\}$ forming a column vector P and the corresponding deflections $\{U_1, U_2, \ldots, U_n\}$ of an elastic system, where A_0 is a square matrix of order n, generally symmetrical, called the *elastic* or *stiffness matrix*. For any system encountered in engineering, this matrix is certainly nonsingular, and we may assume that a unique solution of Eq. (1) has been obtained in the form

$$U = A_0^{-1} P \tag{2}$$

The elements of the inverse matrix A_0^{-1} are the influence coefficients of the structure, and A_0^{-1} is called the *influence* or *flexibility matrix*.

Assume now, as in reference 3, that the modification in the structure affects a square submatrix of A_0^{-1} which is of the order $m < n$. Without loss of generality, this submatrix may be placed in the top left-hand corner of the stiffness matrix; such a position can always be obtained by suitable interchange of rows and columns. The modified stiffness matrix may then be written

$$A = A_0 + a \tag{3}$$

where

$$a = \begin{bmatrix} b & O \\ O & O \end{bmatrix} \tag{4}$$

b being a square matrix of order m, while the symbols O represent zero submatrices. In order to invert the modified matrix A, it is advantageous to present it in the form of a product rather than a sum—viz.,

$$A = QA_0 \tag{5}$$

where

$$Q = I_n + aA_0^{-1} \tag{6}$$

Then it is possible to write

$$A^{-1} = A_0^{-1}Q^{-1} \tag{7}$$

The "quotient" matrix Q is of a special type and is generally easier to invert than A. Let the leading m by m submatrix of A_0^{-1} be denoted by K, so that A_0^{-1} is partitioned as follows:

$$A_0^{-1} = \begin{bmatrix} K & L \\ M & N \end{bmatrix} \tag{8}$$

where L, M, and N are (m by r), (r by m), and (r by r) submatrices, respectively, with $r = n - m$. Then

$$Q = I_n + \begin{bmatrix} b & O \\ O & O \end{bmatrix}\begin{bmatrix} K & L \\ M & N \end{bmatrix} = I_n + \begin{bmatrix} bK & bL \\ O & O \end{bmatrix} = \begin{bmatrix} I_m + bK & bL \\ O & I_r \end{bmatrix} \tag{9}$$

where I_m and I_r are unit matrices of order m and r, respectively. Using the notation

$$q = I_m + bK \tag{10}$$

the inverse of Q is obtained

$$Q^{-1} = \begin{bmatrix} q^{-1} & -q^{-1}bL \\ O & I_r \end{bmatrix} \tag{11}$$

provided q is nonsingular. It is thus seen that, instead of inverting a matrix of order n, it is necessary only to invert a matrix q of lower order m, using the results of a previous inversion of the original matrix of order n. Substituting Eqs. (8) and (11) into Eq. (7), we obtain the desired result

$$A^{-1} = \begin{bmatrix} Kq^{-1}, & (I_m - Kq^{-1}b)L \\ Mq^{-1}, & N - Mq^{-1}bL \end{bmatrix} \tag{12}$$

A simplification results if we consider the difference between the inverse of the original matrix and that of the modified one. It is easy to verify that this correction term may be put in the form of a matrix product

$$\Delta = A_0^{-1} - A^{-1} = \begin{bmatrix} K \\ M \end{bmatrix} q^{-1}b[KL] \tag{13}$$

Had a "quotient" matrix been introduced as in Eq. (5), but on the right-hand side of A_0, as follows:

$$A = A_0R \tag{5'}$$

with

$$R = I_n + A_0^{-1}a \tag{6'}$$

the result would have been obtained in a slightly different form—namely,

$$\Delta = A_0^{-1} - A^{-1} = \begin{bmatrix} K \\ M \end{bmatrix} br^{-1}[KL] \tag{13'}$$

where

$$r = I_m + Kb \tag{10'}$$

It is to be noted that, in case of both K and b being symmetrical r is the transpose of q.

When only a single term of A_0 is modified, assuming this to be the leading term of the principal diagonal, we have

$$q = 1 + bk$$

(a scalar), where k is the leading term of A_0^{-1}, and

$$q^{-1}b = b/(1 + bk)$$

The correction matrix becomes now

$$\Delta = \frac{b}{1 + bk}\begin{bmatrix} k \\ M \end{bmatrix}[k, L] \tag{14}$$

where $[k, L]$ is the first row and $\{k, M\}$ the first column of A_0^{-1}. This correction is seen to be a matrix of rank 1, each row of which is proportional to the first row and each column proportional to the first column of A_0^{-1}. In the more general case of Eq. (13), the correction matrix is also singular, but its rank may be as high as m.

The formulas derived above may also be used when only an approximate answer is required. Noting that the elements of the product matrix bK will generally be small compared to unity, the inverse of q may be expanded into a matrix power series

$$q^{-1} = I_m - bK + (bK)^2 - (bK)^3 + \ldots$$

which in many cases should converge rapidly. The series may be broken off at a convenient number of terms, and their sum may be used instead of the exact value of q^{-1}.

As with the Compensation Theorem, the above formulas are applicable to matrices of any kind. It has been thought expedient, however, to limit the discussion to structural matrices, which today are the subject of wide interest.

References

[1] Michielsen, H. F., and Dijk, A., *Structural Modifications in Redundant Structures*, Journal of the Aeronautical Sciences, Vol. 20, No. 4, p. 286, April, 1953.

[2] Best, G. C., *The Stress Area Method of Designing Beams*, Journal of the Aeronautical Sciences, Vol. 12, No. 3, p. 208, July, 1945.

[3] MacNeal, R. H., *Application of the Compensation Theorem to the Modification of Redundant Structures*, Journal of the Aeronautical Sciences, Vol. 20, No. 10, p. 726, October, 1953.

[4] Wade, Thomas L., *The Algebra of Vectors and Matrices*; Addison-Wesley Press, Cambridge, Mass., 1951.

On the Calculation of Laminar Boundary-Layer Stability

Martin Bloom

Assistant Professor of Aeronautical Engineering, Polytechnic Institute of Brooklyn, Brooklyn, N.Y.

December 14, 1953

THE WRITER HAS PREVIOUSLY[1, 2] COMMENTED upon certain aspects of the calculation of laminar boundary-layer stability with respect to small two-dimensional disturbances according to the Lin-Lees theory, citing an improvement in the procedure suggested by Lees.[3] Results similar to those shown in reference 1 have been independently obtained by Van Driest[4] with an analogous but slightly different procedure. In the course of preparing for publication the work upon which references 1 and 2 were based, it was found to be advisable to revise Lees's procedure still further. A brief statement of the revisions and some results, more completely given in reference 5, follow. (The notation of Lees[3] is used here. Maximum, minimum, and critical values are denoted by the subscripts *max.*, *min.*, and *crit.*, respectively.)

Eqs. (19)[3] and (20)[3] are rearranged as follows:

$$v^{-1} = \Phi_i^{-1}[1 - (2\Phi_r - 1)\lambda + (\Phi_r^2 + \Phi_i^2)\lambda^2 \times (1 + \lambda)^{-1}] \equiv G(z, \lambda) \tag{1}$$

$$u = \Phi_r\,[1 - (\Phi_r^2 + \Phi_i^2 - \Phi_r)\Phi_r^{-1}\lambda]\,[1 - 2\,(\Phi_r - 1)\lambda + (\Phi_i^2 + \Phi_r^2 - 2\Phi_r + 1)\lambda^2]^{-1} \tag{2}$$

where $v = v(c, M_0, T_1)$, provided that α is not much greater than 1 [cf. Eq. (24)[3]]; also $\lambda = \lambda(c, M_0, T_1)$. Plots of G versus z for various values of λ show that $G > 0$ may be double-valued in z when $-0.1 < \lambda < 7$, that $G < 0$ may be double-valued when $\lambda > -0.1$, and that $|G|$ has a minimum for these ranges of λ (see Fig. 1). With v and λ calculated for given values of c, M_0, and T_1, the value or values of z which satisfy Eq. (1) can be found from the aforementioned plots of G. If no such value of z can be found

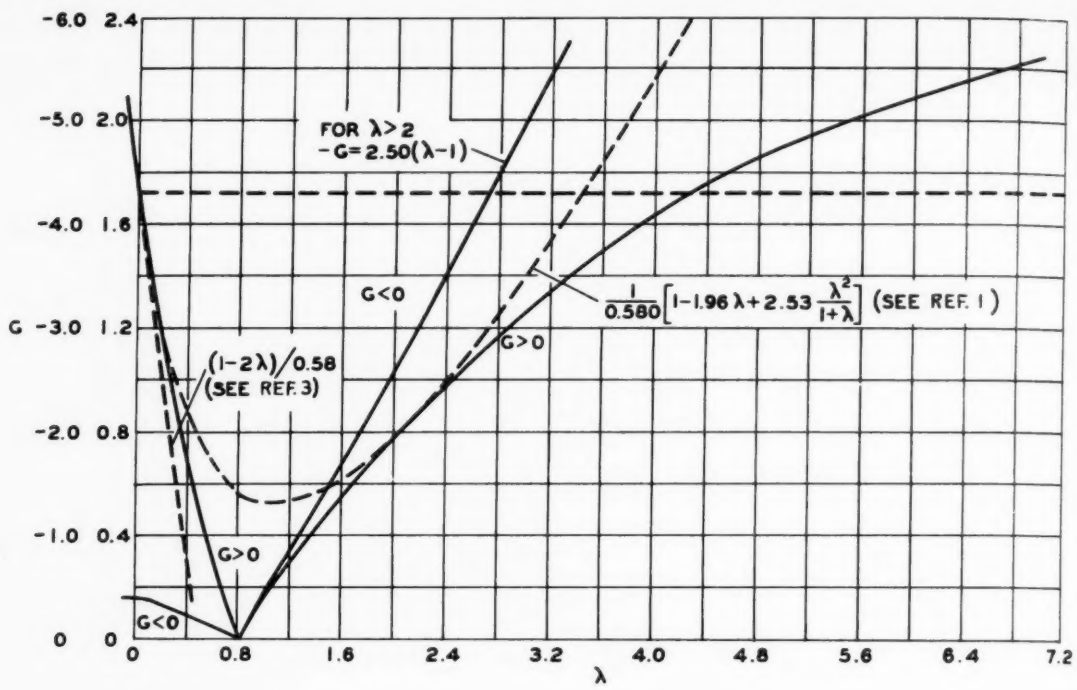

FIG. 1 VALUES OF G REQUIRED TO CORRESPOND TO GIVEN VALUES OF λ IF ε IS TO HAVE A SINGLE VALUE; MINIMA OF |G|

in a given case, no neutral disturbance that satisfies the necessary physical conditions exists in that case. Corresponding values of u follow from Eq. (2) and values of α follow in principle from Eq. (27);[3] the reliable calculation of α can be difficult if α is much larger than 1. Appropriate values of the Reynolds Number R are derived from Eq. (26).[3]

Of particular interest is the fact that, for given values of M_0 and T_1, the $c_{max.}$ for a neutral subsonic disturbance generally occurs together with $|G|_{min.}$ rather than with $\Phi_{i,\ max.}$ (= 0.58) as assumed by Lees. However, for very small values of λ and for $v > 0$, $|G|_{min.}$ and $\Phi_{i,\ max.}$ occur together, and Lees's assumption is valid. This is important because of Lees's further assumption that the minimum critical R (i.e., $R_{crit.}$) occurs together with $c_{max.}$. It is shown in reference 5 that $c_{max.}$ does not occur precisely with $R_{crit.}$ and that $c_{max.}$ occurs simultaneously with $\alpha_{max.}$ only when λ is near zero. (Lees's curves, Fig. 4,[3] show that the values of R corresponding to $\alpha_{max.}$ are close to $R_{crit.}$, but only small values of λ were encountered in the calculations he cited.) Therefore, no positive correlation between $c_{max.}$ and $R_{crit.}$ could be established by the writer in reference 5 for general values of λ which may be fairly large. On the other hand, the absence of an approximate correlation between $c_{max.}$ and $R_{crit.}$ could not be demonstrated either. However, the solid curves in Fig. 1 can be used to calculate the value of $c_{max.}$ for given values of M_0 and T_1. Also shown in Fig. 1 is the curve suggested by Lees[3] for calculating $c_{max.}$ with small values of λ, and the curve previously suggested by the writer[1] for all values of λ but based upon the erroneous assumption that $c_{max.}$ and $\Phi_{i,\ max.}$ occur simultaneously for all values of λ.

It is also shown in reference 5 that the correlation between $R_{crit.}$ and $c_{max.}$ is not a factor in the calculation of surface temperatures that result in infinitely large values of $R_{crit.}$. This is because the necessary and sufficient condition for $R_{crit.}$ to be infinite is that $c_{max.}$ should approach $1 - M_0^{-1}$. The results of these calculations, which utilize the solid curves of Fig. 1, are shown in Fig. 2.

Only a tentative interpretation of the results in Fig. 2 can be offered for reasons explained in reference 5. In brief, it is considered probable that flows in regions I, IV, and V are unstable at sufficiently high Reynolds Numbers, while flows in region II are probably stable. The flows in region III require further investigation, although they have previously been considered to be stable.[4] Thus, the curves bounding regions IV and V are interpreted as being possibly narrow bands of greatly increased stability.

It has been authoritatively suggested to the writer that the curves bounding regions IV and V may indicate stability with respect to an additional mode of disturbance—that is, that an unstable mode might also exist for the indicated combinations of T_1 and M_0. This possibility cannot be proved or disproved with the present form of the theory, since large values of c and α would probably occur simultaneously for any additional unstable mode in these narrow regions and therefore could not be treated with the present form of the theory. In this connection it can also be pointed out that Lees's extension of the Heisenberg criterion[3] appears to be valid for large values of c, provided that α is very small, but may not be valid when both c and α are large simultaneously.

In the work described above no attempt was made to consider the problem of improving the viscous solutions as discussed by Lin[7] and by Cheng[8] or to consider the effect of the three-dimensional character of the disturbances.

References

[1] Bloom, M., *The Effect of Surface Cooling on Laminar Boundary-Layer Stability*, Readers' Forum, Journal of the Aeronautical Sciences, Vol. 18, No. 9, p. 635, September, 1951.

(*Continued on page 210*)

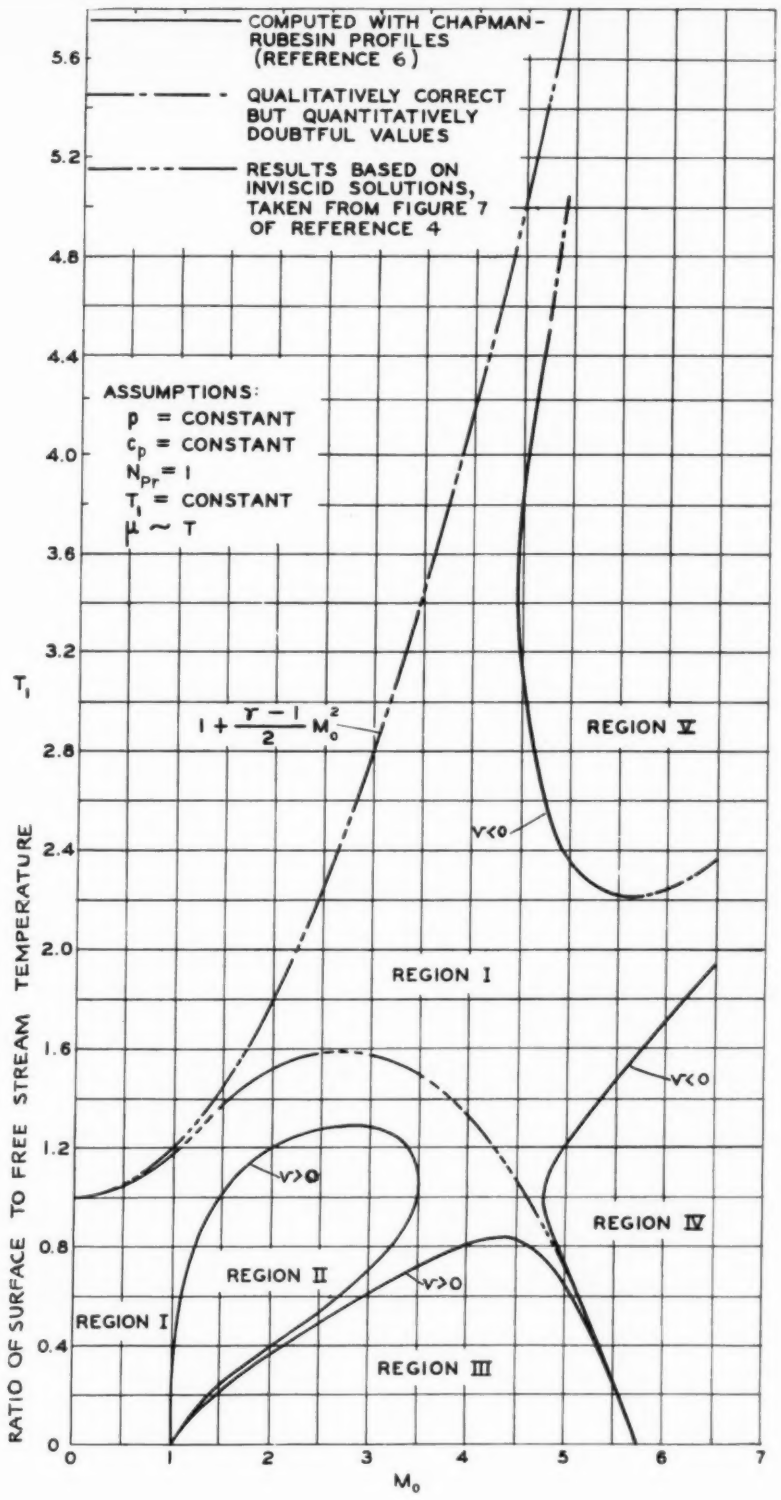

FIG. 2 SURFACE TEMPERATURES WHICH RESULT IN AN INFINITE MINIMUM CRITICAL REYNOLDS NUMBER AT VARIOUS FREE STREAM MACH NUMBERS

(*Continued from page 208*)

[2] Bloom, M., *Further Comments on "The Effect of Surface Cooling on Laminar Boundary-Layer Stability,"* Readers' Forum, Journal of the Aeronautical Sciences, Vol. 19, No. 5, p. 359, May, 1952.

[3] Lees, L., *The Stability of the Laminar Boundary Layer in a Compressible Fluid*, NACA Report No. 876, 1947.

[4] Van Driest, E. R., *Calculation of the Stability of the Laminar Boundary Layer in a Compressible Fluid on a Flat Plate with Heat Transfer*, Journal of the Aeronautical Sciences, Vol. 19, No. 12, pp. 801–812, 829, December, 1952.

[5] Bloom, M., *Calculation of Stability of Constant-Pressure Boundary Layers on Isothermal Surfaces with an Integral-Method Mean-Flow Solution*, Polytechnic Institute of Brooklyn, PIBAL No. 179 (revised September 25, 1953). (To appear as a NACA TN, Contract No. NAw-5809.)

[6] Chapman, D. R., and Rubesin, M. W., *Temperature and Velocity Profiles in the Compressible Laminar Boundary Layer with Arbitrary Distribution of Surface Temperature*, Journal of the Aeronautical Sciences, Vol. 16, No. 9, p. 547, September, 1949.

[7] Lin, C. C., *On the Stability of the Boundary Layer with Respect to Disturbances of Large Wave Velocity*, Readers' Forum, Journal of the Aeronautical Sciences, Vol. 19, No. 2, p. 138, February, 1952.

[8] Cheng, S.-I., *On the Stability of Laminar Boundary Layer Flow*, Quarterly of Applied Mathematics, Vol. XI, No. 3, p. 346, October, 1953.

The Interaction of Two Similarly Facing Shock Waves

G. V. Bull,* L. R. Fowell, and D. H. Henshaw†

Research Assistants, Institute of Aerophysics, University of Toronto, Toronto, Ontario, Canada

December 10, 1953

Summary

When one shock wave overtakes another traveling in the same direction, in a medium for which $\gamma \leq 5/3$, the configuration resulting from the interaction consists of a reflected rarefaction wave, a transmitted shock wave, and a contact surface separating the states behind these waves.

For $\gamma > 5/3$ one may obtain the above result or a reflected shock wave with the contact surface and transmitted shock.

The analytical relationships enabling the determination of the final wave strengths as a function of the initial conditions are given, and graphs are presented showing the strengths of the transmitted shock wave and reflected rarefaction wave for the case of $\gamma = 1.40$.

Notation

(R, S, m, r, s)	=	subscripts denoting the state of the physical system concerned
S	=	the undisturbed region ahead of the first shock wave
R	=	the region behind the second (overtaking) shock wave
m	=	the region separating the first and second shock waves before interaction
r	=	the region between the reflected wave and the contact surface after interaction
s	=	the region between the transmitted wave and the contact surface after interaction
S, R $\rightarrow\rightarrow$	=	a shock or rarefaction wave, respectively, such that the fluid enters the wave from the right
S, R $\leftarrow\leftarrow$	=	waves such that the fluid enters from the left
C	=	contact surface
p	=	pressure
ρ	=	density
γ	=	specific heat ratio
u	=	a velocity measured relative to axes fixed in the physical system
$1/P$	=	pressure ratio across the system $= p_R/p_S$
P_{Rm}	=	p_R/p_m
P_{mS}	=	p_m/p_S
P_s	=	p_s/p_S
P_r	=	p_r/p_R
α	=	$(\gamma + 1)/(\gamma - 1)$
β	=	$(\gamma - 1)/2\gamma$

* Now Chief Aerodynamicist, Canadian Armament Research and Development Establishment, Quebec, Canada.

† Now Research Officer, National Aeronautical Establishment, Ottawa, Ontario, Canada.

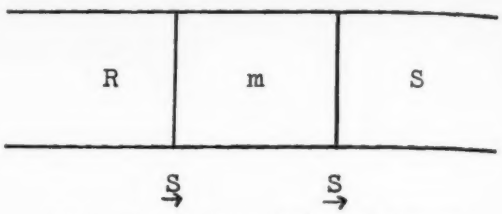

FIG. 1. The initial states in the physical system.

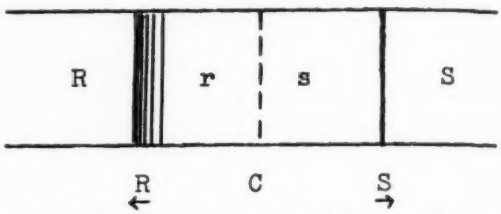

FIG. 2. Physical states after interaction yielding reflected rarefaction.

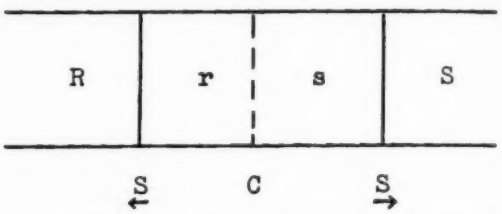

FIG. 3. Physical states after interaction yielding reflected shock.

(I) Resultant Wave Configuration

INITIALLY, ONE CONSIDERS two shock waves traveling in the same direction (Fig. 1). Relative to the right-hand shock the flow in (m) is subsonic, while relative to the left-hand shock it is supersonic; hence, the shocks must collide.

A qualitative analysis in the (p, u) plane shows that this interaction may yield a reflected rarefaction wave (Fig. 2), a reflected shock wave (Fig. 3), or a reflected Mach line; while a "transmitted" shock wave continues in the direction of the original waves in every case.

In the quantitative discussion a one-dimensional flow was considered in an ideal gas (γ being constant throughout any one system considered). The pressure and density relationships across rarefaction and shock waves yielded the fact that a contact surface lies between the reflected and transmitted waves in every nontrivial case.

A criterion was developed which, by means of the initial shock strengths and γ for a given system, determines whether the reflected wave is a rarefaction or shock wave for that system.

The velocity increment across the initial system was written

$$u_R - u_S = \sqrt{\left(\frac{p_S}{\rho_S}\right)\left(\frac{\alpha - 1}{1 + \alpha P_{mS}}\right)} \times \left\{(P_{mS} - 1) + (1 - PP_{mS})\sqrt{\frac{P_{mS} + \alpha}{P(\alpha + PP_{mS})}}\right\} \quad (1.1)$$

while that across the transmitted shock in the case of a reflected Mach line is

$$u_s - u_S = \sqrt{\frac{p_S}{\rho_S}}\sqrt{\frac{(\alpha - 1)}{P(P + \alpha)}}(1 - P) \quad (1.2)$$

Letting Δ designate the ratio $(u_R - u_S)/(u_s - u_S)$ one sees that $\Delta > 1$ implies a reflected shock, $\Delta = 1$ implies a reflected Mach line, while $\Delta < 1$ corresponds to a reflected rarefaction wave.

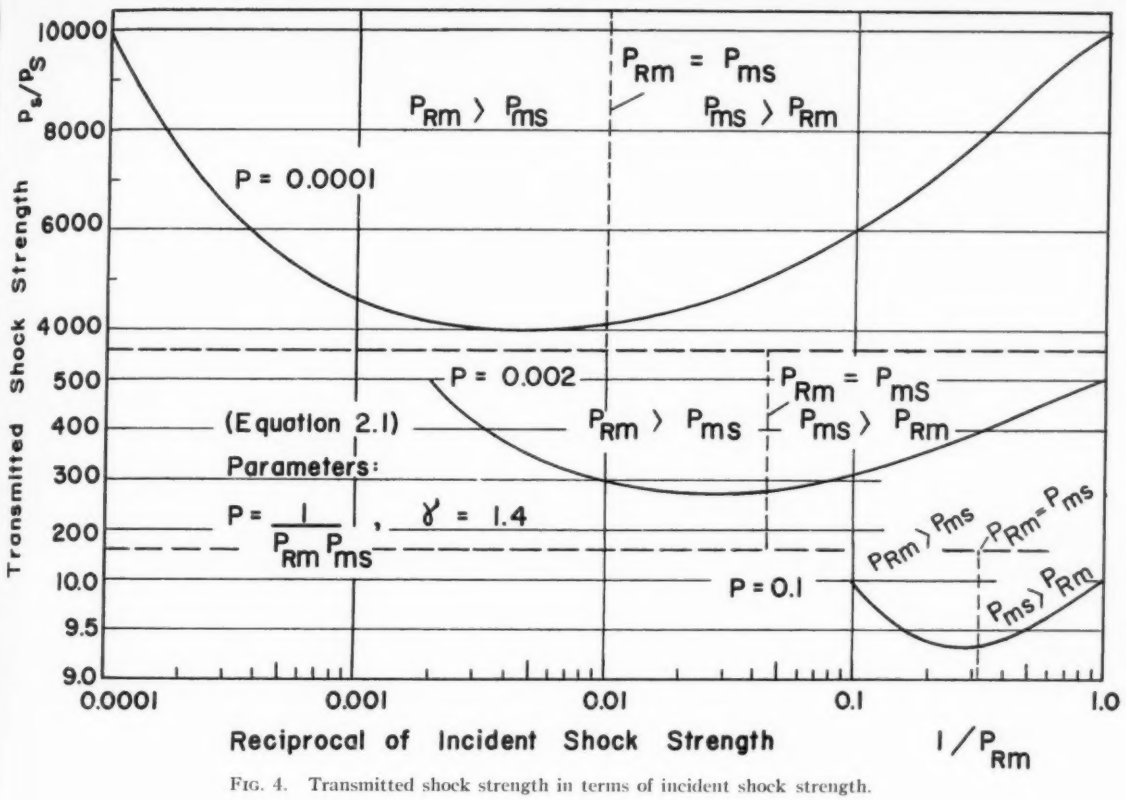

FIG. 4. Transmitted shock strength in terms of incident shock strength.

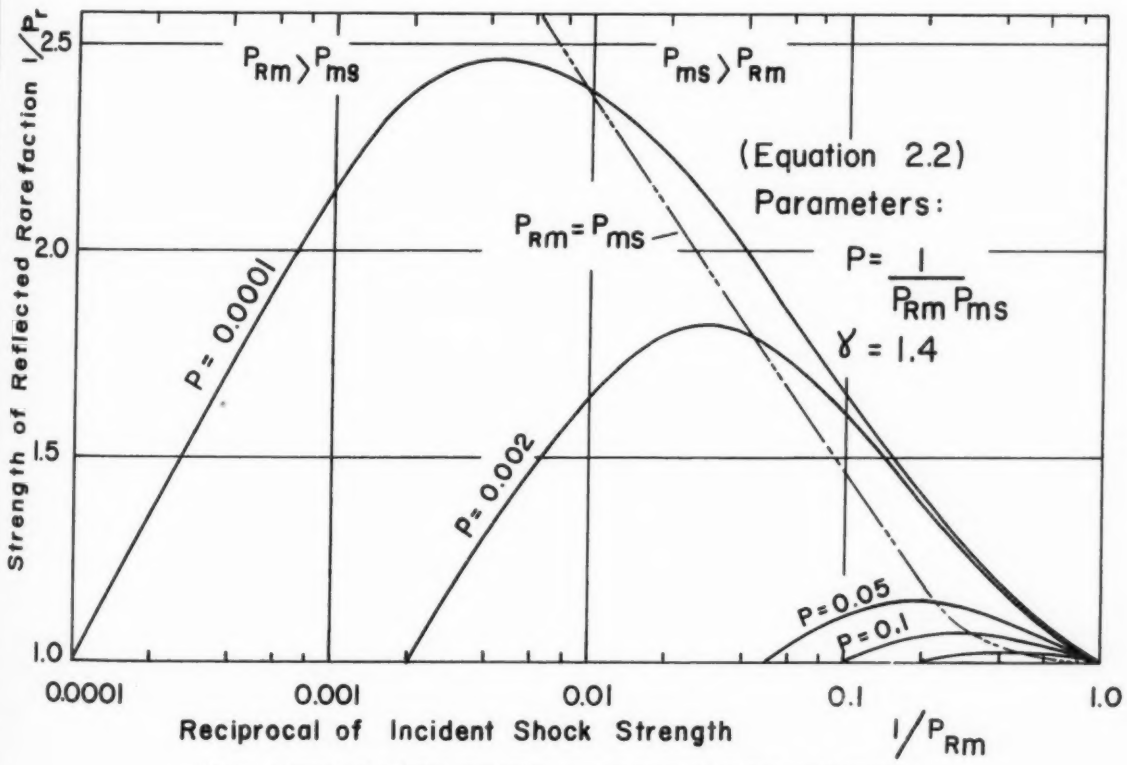

FIG. 5. Strength of reflected rarefaction wave in terms of incident shock strength.

The condition $\Delta = 1$ was written

$$[(P_{mS} - 1)^2 (kP_{mS} - 1)^2 (kP_{mS}^2 - 1)^2\alpha] \times \left[\alpha^3 - 2\alpha^2 + \alpha\left(1 - \frac{4}{kP_{mS}} - \frac{4}{kP_{mS}^2}\right) - \frac{4}{k^2P_{mS}^3}\right] = 0 \quad (1.3)$$

where $k = P_{Rm}/P_{mS}$. Considered as a function of γ, this relation yields a critical $\gamma = \gamma_C$ as a solution of the cubic in α. For $\gamma > \gamma_C$ a reflected shock occurs, while $\gamma < \gamma_C$ implies a reflected rarefaction wave. Consideration concerning the smallest possible physically admissible critical γ showed that a reflected shock wave could not be obtained for $\gamma \leq 6/5$ under the assumptions of this analysis.

(II) Wave Strengths

The transmitted shock strength (P_s) was obtained in terms of the initial shock strengths in the following form:

$$(P_s - 1)\sqrt{\frac{\beta P}{(1 + \alpha P_s)}\left(\frac{1 + \alpha P_{Rm}}{\alpha + P_{Rm}}\right)\left(\frac{1 + \alpha P_{mS}}{\alpha + P_{mS}}\right)} - \beta\sqrt{\gamma}\left\{\sqrt{\left(\frac{1 - P_{Rm}}{P_{Rm}}\right)\left(1 - \frac{1 + \alpha P_{Rm}}{\alpha + P_{Rm}}\right)} + \sqrt{P}\sqrt{(1 - P)_{mS}\left(1 - \frac{1 + \alpha P_{mS}}{\alpha + P_{mS}}\right)\left(\frac{1 + \alpha P_{Rm}}{\alpha + P_{Rm}}\right)}\right\} + (PP_s)^\beta - 1 = 0 \quad (2.1)$$

Fig. 4 shows a plot of this relationship for $\gamma = 1.4$ with P as parameter. The strength of the reflected rarefaction wave ($1/P_r$) was found to satisfy

$$\left\{\sqrt{\frac{\beta\,(1 + \alpha P_{Rm})}{(\alpha + P_{Rm})\,(PP_{Rm}\alpha + 1)\,(P_{Rm})}}\right\} \times \left\{\begin{array}{l}(P_r - P)\sqrt{\dfrac{(PP_{Rm} + \alpha)P_{Rm}}{(P + \alpha P_r)}} \\ -(P_{Rm} - 1)\sqrt{\dfrac{PP_{Rm}\,\alpha + 1}{(1 + \alpha P_{Rm})}} - (1 - PP_{Rm})\end{array}\right\} + P_r^\beta - 1 = 0 \quad (2.2)$$

and is shown in Fig 5.

The relationship giving the strength of the reflected shock for cases with $\gamma > 6/5$ was also found, and the reflected shock strength was plotted for a hypothetical case with $\gamma = 2$.

(III) Applications

In wave interaction experiments the Eqs. (2.1) and (2.2) and the graphs of Figs. 4 and 5 enable one to specify the strengths of the waves resulting from the overtaking of a given shock wave by another of known strength.

It will be noted that, for a given total pressure ratio ($1/P$), the strength of the transmitted wave is greater the more completely this pressure rise can be made to occur over only one of the initial waves. For initial waves of comparable strength the transmitted wave strength is roughly one-half of the product of the initial pressure ratios, if the total pressure ratio is in the range 500 to 10,000, and approaches this product in magnitude as ($1/P$) approaches one.

An attempt to produce very strong shocks in a shock tube by this method, using two fairly strong initial shocks, has recently been brought to the authors' attention. In this connection it is noted that for comparable initial waves a stronger transmitted wave should result when the first wave exceeds the overtaking wave in strength, because of asymmetry in this sense with respect to the line $P_{Rm} = P_{mS}$.

Experimental results have recently been obtained at the Institute of Aerophysics confirming this analysis and will be discussed in a forthcoming report.

Reference

[1] Bull, G. V., Fowell, L. R., and Henshaw, D. H., *The Interaction of Two Similarly Facing Shock Waves*, Institute of Aerophysics, University of Toronto, UTIA Report No. 25, January, 1953.

Remarks on Nonlinear Lift and Vortex Separation

Hsien K. Cheng
Aerodynamic Section, Bell Aircraft Corporation, Buffalo, N.Y.
December 1, 1953

In a recent note, Adams[1] has given an interpretation of the results of a theoretical investigation on vortex separation from the leading edges of slender delta wings,[2] in which a simplified physical picture has been considered in that the free vortices separated from both edges are replaced by a pair of concentrated vortices in the cross-flow plane. Adams' conclusion shows that, with the occurrence of the "free vortex pair," the result of the Jones low aspect ratio theory remains valid to the first order of approximation and that the nonlinear lift due to the vortex separation appears of the order of $(\text{A.R.})^{1/2}(\alpha)^{3/2}$. Nevertheless, his solution does not lead to a consistent determination of the nonlinear lift. Meanwhile, Edwards[3] points out that the inconsistency in Adams's results arises actually from an error in the compatibility condition of the free vortices with their surrounding stream; by applying the correct condition, the system of the vortex pair (together with their "feedlines") becomes dynamically free, and the inconsistency as to the question of including the forces on the vortex feedlines is removed.

By using essentially the same model in describing the vortex separation phenomenon near the edge, the writer has obtained the lift of a rectangular plate at supersonic speed, which includes the contribution of the vortex separation from the *side edge*;[4] in a similar manner, one can also determine, to the first order of approximation, the impulse of motion of a flat plate, taking into account the phenomena of vortex separation;[4] the latter problem can again be interpreted through the cross-flow concept as one involving the "side-edge separation" from a low aspect ratio airfoil.[5] Since results of investigation of this type are not generally known for the side-edge problem, it may be of interest to give a close examination of their characteristic features and to compare them with those that occurred in the other case previously mentioned.

(1) The Vortex Pair Behind a Moving Plate

It will serve the present purpose to consider only an example of reference 4, in that a plate of width $2a$ submerged in an infinite expanse of fluid is set into transverse motion instantaneously with a uniform velocity αU, as illustrated in Fig. 1. The classical solution to the problem which admits infinite flow velocity and stream curvature at each of the edges is well known. By introducing into the flow field a vortex pair, the infinite velocities at the edges can be eliminated, and the solution is determined finally by applying the compatibility condition of the free vortex pair with its surrounding stream. Dynamical consideration of the free vortices leads to the condition that the mean velocity of the group of vortices which has been shed before the instant t be equal to the mean velocity of the surrounding stream at the same instant. An essential point contributed by Edwards is that, in calculating the velocity of the free vortices, the path of the vortex center of the free vortex group under consideration should not be confused with the locus of the c.g. of the total vortices in all time.[3] Let ν denote the site of one of the "vortex pair" and Γ the total circulation around the free vortex

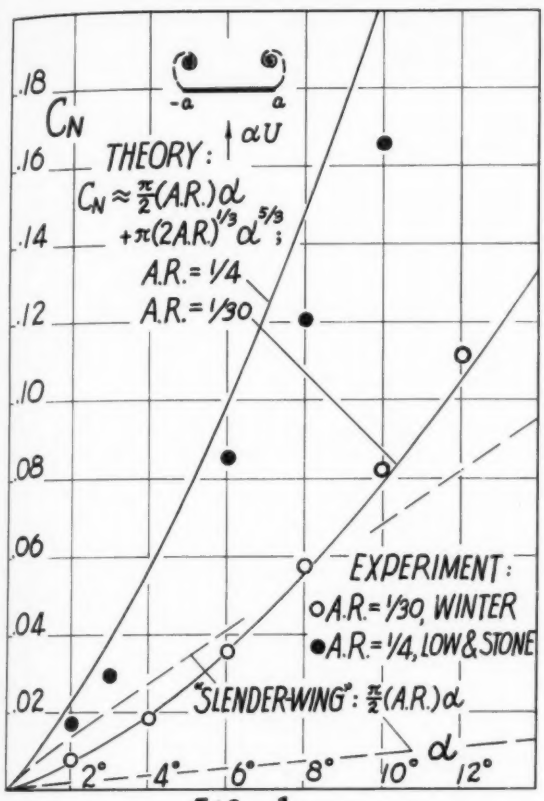

FIG. 1.

region; the motion of the vortex center of the free vortex group at the instant t may then be determined by

$$\frac{d\nu^*}{dt} = \frac{1}{\Gamma}\left[\frac{d}{dt}(\Gamma\nu) - a\frac{d\Gamma}{dt}\right] \tag{1}$$

The compatibility condition now reads as

$$\frac{1}{\Gamma}\left[\frac{d}{dt}(\Gamma\nu) - a\frac{d\Gamma}{dt}\right] = \overline{W_m'} \tag{2}$$

where the function on the right-hand side is the conjugate of the complex "vortex-velocity" at the vortex center $\zeta = \nu$. Both the circulation and the vortex-velocity appeared in Eq. (2) and are functions of ν and a. The differential equation, Eq. (2), together with the initial condition $\nu = a$ at $t = 0$, is sufficient in principle to determine the location of the vortex pair as function of time and leads finally to the solution desired.

Accordingly, the equivalent solution for the delta wing problem of references 1, 2, and 3 appears to differ from the general case only at the last step—namely Eq. (2)—in that the first-order differential equation becomes immediately integrable because of conical symmetry in t (in particular, the width $2a$ being in that case a linear function of time, resulting in an expanding plate in a uniform stream).

For the present case, the width $2a$ remains constant throughout, and the integral solution of Eq. (2) is again seen possible by a separation of the variables. Moreover, if only the solution corresponding to small values of $|\nu - a|$ is of primary interest, which implies a sufficiently small value of α, an explicit solution of the differential equation can be obtained by solving for $\epsilon = \nu - a$, which is the location of the free vortex center with respect to the edge. As a result of the boundary conditions given and the assumptions mentioned previously, Eq. (2) can be written, to its first order, as

$$\frac{1}{\Gamma}\frac{d}{dt}(\Gamma\epsilon) \approx -i\alpha U\sqrt{\frac{a}{2}}\frac{1}{\sqrt{\epsilon}} + i\frac{\Gamma}{4\pi}\left[\frac{1}{2\epsilon} + \frac{1}{\epsilon - \bar{\epsilon}}\left(1 - \frac{\sqrt{\epsilon}}{\sqrt{\bar{\epsilon}}}\right)\right] \tag{3}$$

where

$$\Gamma \approx aU\sqrt{a/2}\left[\sqrt{\epsilon}\sqrt{\bar{\epsilon}}/(\sqrt{\epsilon} + \sqrt{\bar{\epsilon}})\right]$$

which yields the first order solution for ϵ as

$$\epsilon/a \approx \pm i\,(\pm\alpha Ut/4a)^{2/3} \tag{4}$$

where the negative signs correspond to the upward motion of the plate. It is seen from the above that the vortex pair trails *directly behind* the edges according to a time law of $t^{2/3}$. The corresponding value of the circulation around each of the free vortex pair, which measures its total strength, is

$$\Gamma \approx 2\pi Ua(\alpha Ut/4a)^{1/3}\alpha \tag{5}$$

The solution is thereby completely determined. By virtue of the symmetry in the flow pattern, the total momentum received by the fluid medium may be evaluated simply as

$$I(t) = 2\pi\rho \lim_{|\zeta|\to\infty} i\zeta^2 W'(\zeta) \approx \pi\rho a^2\alpha\ U + \pi\rho\alpha Ua^2\left(\frac{2\alpha t}{a}\right)^{2/3} \tag{6}$$

(2) An Interpretation of the Above Solution

Obviously, the above solution pictures the cross-flow field of a slender airfoil in the event of vortex separation from its side edges. By multiplying the right-hand side by U and putting x/U for t, Eq. (6) provides a formula for the lift of a slender airfoil possessing sharp side edges, which is correct up to the order considered—namely,

$$\text{lift}\,\Big|_{\text{L.E.}}^{x} \approx \pi\rho a^2\alpha U^2 + \pi\rho U^2a^2\alpha\left(\frac{2\alpha x}{a}\right)^{2/3} \tag{7}$$

where x is the Cartesian coordinate running downstream along the chord and its origin is chosen at the section where the vortex separation first occurs.

Unfortunately, the present result interpreted from the previous solution implies the assumption of slenderness of the airfoil throughout the whole length of x, which will certainly limit its application to a great extent. However, in approaching the extreme of "infinitely small aspect ratio," Eq. (7) must hold valid within the range of sufficiently small angle of attack α. Indeed, upon comparison with a set of early data obtained by Winter,[6] the agreement appears to be almost perfect, in that an extremely narrow rectangular flat plate of aspect ratio $^1/_{30}$ was used (see Fig. 1). For rectangular plan form of higher aspect ratio, say between 1/2 and 1/10, the discrepancy becomes appreciable (the data for aspect ratio of 1/4 appeared in the figure are taken from reference 5), yet Eq. (7) still accounts for the total nonlinear effect to a substantial degree; the corresponding lift distribution has also been qualitatively confirmed by Winter's measurement. Furthermore, within the degree of accuracy afforded by the present theory, the equation of the free vortex core in space deduced directly from Eq. (4) seems to agree also with a side-view photograph in reference 6.

The discrepancy between theory and tests that occur in the higher aspect ratio range is perhaps due mainly to the separation phenomena at both the vicinities of the leading edge and the trailing edge of the rectangular plate, which are in fact the real stalling phenomena that cause a decrease in lift. Since for a narrow rectangular plate the nonlinear effect contributed by the latter phenomenon is not large in comparison with the effect due to side-edge separations, an empirical formula may be adopted after Eq. (7) for the higher aspect ratio range as

$$C_L \approx (\pi/2)\,(\text{A.R.})\alpha + k\alpha^{5/3} \tag{8}$$

where the coefficient of the linear terms may be modified according to reference 5 for aspect ratio higher than 1/2. It is interesting to note that the nonlinear lift coefficient deduced

from Eq. (7), as presented in the figure, happens to differ from either formulas of Adams and Edwards by a factor of $(2)^{1/3}$.

(3) Comparison with the Delta Wing Solution

In view of the fact that the ordinary solution of the flow around a leading edge possesses a singularity of a higher order of infinity than around a side edge, it is to be anticipated that a stronger separation phenomenon may occur in the event of the leading-edge separation. Indeed, this is revealed by comparing the solutions of the separation models themselves, for, according to the solution above, the total strength of the free vortex is of the order $\alpha^{4/3}$ with a typical dimension of the region in the order of $\alpha^{2/3}$, whereas close examination of the solution of references 1, 2, and 3 shows that the strength is of the order α and the size of the vortex region of order $\alpha^{3/2}$. To be sure, for the narrow delta wing problem,

$$P \approx \pi U a \alpha \tag{9}$$

$$\frac{\epsilon}{a} \approx -\frac{1}{2}\left(\frac{\alpha}{4a}\right)^{2/3} + i\left(\frac{\alpha}{4a}\right) \tag{10}$$

Inasmuch as the nonlinear lifts belong to the same order of magnitude in both cases—that is, the order of $(\text{A.R.})^{1/3}\alpha^{5/3}$—whereas the strengths of the vortex region differ, it seems possible that the error implied in Eq. (7) could be less than that which occurred in the corresponding formula for the delta wing.

Finally, it should be noted that the power law $t^{2/3}$ or $x^{2/3}$ for the vortex core has likewise occurred in the case of the rolling up of the trailing vortex sheet behind a lifting surface.[7] Further remarks and interpretations of the results of the similar nature can be found in reference 4.

References

[1] Adams, M. C., *Leading-Edge Separation from Delta Wing at Supersonic Speeds*, Readers' Forum, Journal of the Aeronautical Sciences, Vol. 20, No. 6, p. 430, June, 1953.

[2] Legendre, R., *Ecoulement au Voisinage De La Pointe Avant D'une Aile A Forte Fleche Aux Incidences Moyennes*, La Recherche Aeronautique, Bulletin Bimestriel, De L'Office National D'Études Et De Recherches Aéronautiques, Novembre-Décembre, 1952, and Janvier-Fevrier, 1953.

[3] Edwards, R. H., *On Leading-Edge Separation from Delta Wing*, Readers' Forum, Journal of the Aeronautical Sciences, Vol. 21, No. 2, p. 134, February, 1954.

[4] Cheng, H. K., *Aerodynamics of a Rectangular Plate with Vortex Separation in Supersonic Flow*, Bell Aircraft Aerodynamic Section, Theoretical Research Note No. 1; *An Approximate Solution to a Problem of Vortex Separation with Application to the Prediction of Nonlinear Lift*, Bell Aircraft Corporation Aerodynamics Section, Theoretical Research Note No. 2.

[5] Flax, A. L., and Lawrence, H. R., *The Aerodynamics of Low Aspect Ratio Wings and Wing-Body Combinations*, paper presented at the Third Anglo-American Aeronautical Conference, 1951.

[6] Winter, H., *Strömungsvorgange an Platten und Profilierten Körpern bei Spannweiten*, V.D.I., 1936. (English translation available as NACA TM No. 798.)

[7] Kaden, H., *Aufwicklung einer Unstabilen Umstetigkeitsfläche*, Ing. Archiv., II Band, pp. 140–168, 1931.

Remarks on "Subsonic Compressibility Corrections for Propellers and Helicopter Rotors"[1]

M. Z. v. Krzywoblocki
Professor of Gasdynamics and Theoretical Aerodynamics, University of Illinois, Urbana, Ill.

December 3, 1953

In reference 1 the authors came to the conclusion that the assumptions of previous authors[2, 3] concerning the axial interference velocity factor due to induced axial flow are incorrect. They object to the assumption made in reference 2 that $\rho_2 = \rho_1$ (no change in density through the propeller disc), on the basis that for a perfect gas any pressure discontinuity in an adiabatic flow must be accompanied by a corresponding density discontinuity. They further object to the assumption made in reference 3 that $\rho_2 = \rho_0$, where ρ_3 refers to slipstream conditions at an infinite distance downstream, on the basis that one cannot assume the existence of a thin actuator disc. As a possible solution, they propose to use the exact incompressible flow relations as the first step of an iterative process; but, they neither go beyond that first approximation nor discuss the iteration process nor mention anything about it. Hence, the following facts must be stated:

(i) The first-order approximation proposed by the author refers fundamentally to the subsonic incompressible flow and to that region of compressible flow where one can neglect higher order terms.

(ii) The above implies that the authors did not find a solution of problem in question in the region where the compressibility phenomena play a full part and where the first-order term is not strong enough; they object to previous suggestions but do not offer any improvement.

(iii) Concerning the iteration process, there may be an equal probability of obtaining equivalent results by assuming that ρ_1 is a first approximation to ρ_2 (reference 2) or that ρ_0 is a first approximation to ρ_3 (reference 3) and performing the iteration process for ρ_2 or ρ_3. There is absolutely no obvious reason why the iteration process for δ_1 in terms of δ_2 proposed by the authors should be superior to the iteration processes for ρ_2 or ρ_3.

Now a few words about the iteration process. Any iteration process may give acceptable results, but very often the domain of the validity of that process is small. Thus, it seems possible that the iteration process on ρ_2 in terms of ρ_1, limited to the thin actuator disc, may give acceptable results. Similarly, the process for ρ_3 in terms of ρ_0, limited to some narrow domain, may be acceptable. In the past the author of the present remarks applied a few iteration processes with a negative result—i.e., they diverged. It looks as if, in the problem in question, there were some inherent properties repudiating even the law of an iterative process and may be subject only to some experimental procedure. This is a situation similar to a system having more unknowns than available equations, and here may be an explanation of the failure of iterative processes. But, of course, it does not mean that some way will not be found to solve the problem analytically.

References

[1] Laitone, E. V., and Talbot, L., *Subsonic Compressibility Corrections for Propellers and Helicopter Rotors*, Journal of the Aeronautical Sciences, Vol. 20, No. 11, pp. 683–690, November, 1953.

[2] von Krzywoblocki, M. Z., *Elementary Propeller Theories in Compressible Inviscid Fluids*, Appl. Scient. Res. Ser. A, Vol. 2, No. 3, pp. 205–224, 1950.

[3] Vogeley, A. W., *Axial Momentum Theory for Propellers in Compressible Flow*, NACA TN No. 2164, July, 1951.

On the Curved Shock Wave Due to an Infinite Wedge

Kinzo Hida
Naniwa University, Sakai Near Osaka, Japan

December 14, 1953

So far it has been known that there are two possible configurations of the shock wave due to an infinite wedge placed in a supersonic uniform flow, provided that its vertex angle $(2\theta_0)$ is smaller than a certain critical value. Both are straight shock

waves and are called "strong-shock" and "weak-shock," respectively.

In this paper we shall show, with the aid of analysis in the hodograph plane, that two more shock configurations are possible. They are both curved shocks; one is an attached shock that is weak at the vertex and becomes strong at infinity, while the other is a detached shock changing from normal-shock to strong one at infinity.

When the Mach Number M_1 of the uniform flow at infinity upstream is prescribed, not only the magnitude and the direction of the velocity but also the initial curvatures of stream lines immediately behind the shock are given by a shock polar as well as the shock spines (see Fig. 1).[1]

Let a straight line be drawn through the origin 0, making an angle θ_0 with $0P$ and let A, B denote the points of intersection of such a straight line with the shock polar. Then these two points correspond to the weak-shock and strong-shock, respectively. In these cases the flow behind the shock wave becomes uniform again, and the flow field shrinks into a point in the hodograph plane. But we can show two other possibilities of shock configuration by considering the solutions that correspond to the region $B0N$ (II) or the region BMA (I).

For brevity's sake, we take the Laplace equation $\Delta\psi = 0$ as the fundamental equation for the stream function Ψ in each region. (This simplification is justified if use is made of a suitable affine transformation or the W.K.B. method suggested by Prof. I. Imai.[2])

Boundary conditions are as follows:

(i) $\Psi = 0$ $\begin{cases} \text{on } AB \text{ (for the region I),} \\ \text{on } B0 \text{ and } 0N \text{ (for the region II).} \end{cases}$

(ii) Initial direction of every stream line should coincide with that of the spine at each point on the shock polar.

To find appropriate solutions we shall discuss the two cases separately.

(i) Region I (Weak-Strong Shock)

In this region we shall find the solution as shown in Fig. 2. Considering a corner flow and a generalized doublet flow in the close vicinity of A and B, respectively, and superposing them, we get

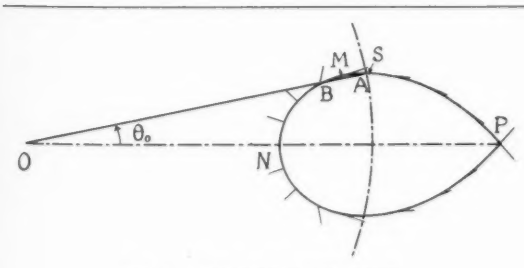

Fig. 1. Shock polar and spines.

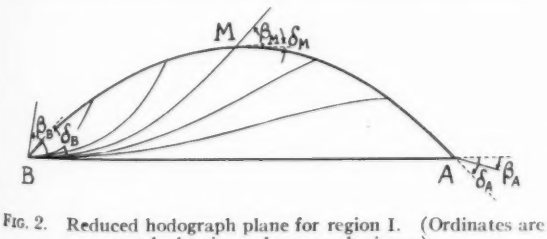

Fig. 2. Reduced hodograph plane for region I. (Ordinates are stretched twice as large as abscissae.)

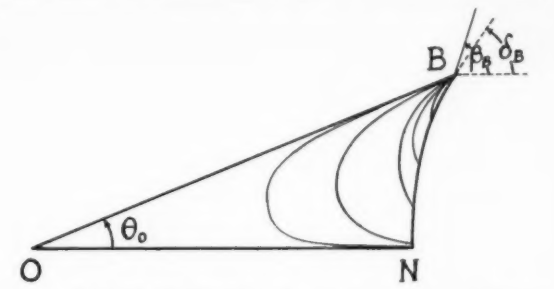

Fig. 3. Reduced hodograph plane for region II. (Ordinates are stretched twice as large as abscissae.)

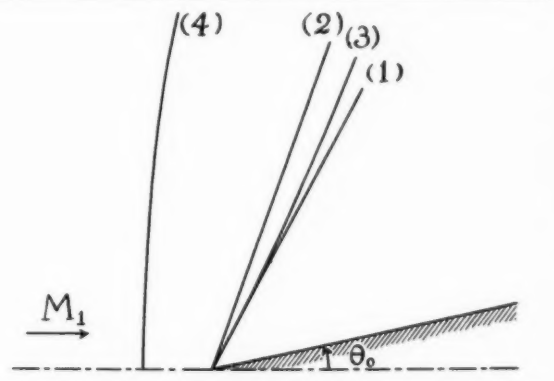

Fig. 4. Possible shock configurations due to an infinite wedge. (1) Weak shock; (2) strong shock; (3) weak-strong shock; (4) normal-strong shock.

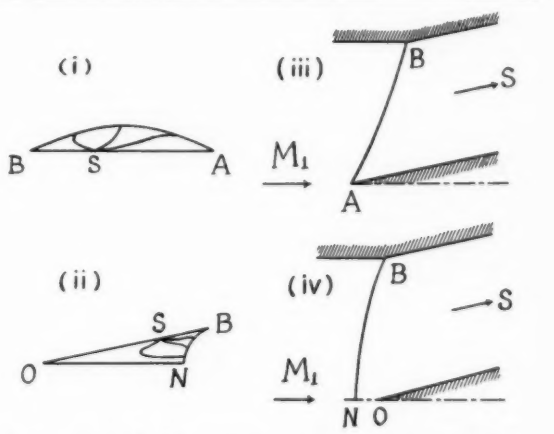

Fig. 5. Probable flow patterns tending to our cases as limit.

$$\Psi = C_1 r^{-m} \sin m\theta + C_2 \rho^n \sin n(\pi - \vartheta)$$

where (r, θ) and (ρ, ϑ) are the polar coordinates with the initial line BA and the origin at A and B, respectively. If indices m, n be determined so as to satisfy the second boundary condition (ii) at A and B, we have

$$m = \beta_B/\delta_B - 1, \qquad n = 1 - \beta_A/\delta_A$$

Moreover, we can determine the ratio of arbitrary constants, $C_1 \div$

C_2, in such a way that the boundary condition (ii) is satisfied at one more point, say M (i.e., point of maximum deflection). We then have

$$\frac{C_1}{C_2} = -\frac{nr_M{}^{m+1}\sin\{n(\vartheta_M - \pi) + \beta_M - \vartheta_M\}}{m\rho_M{}^{1-n}\sin\{\beta_M - (m+1)\theta_M\}}$$

(ii) Region II (Normal-Strong Shock)

To obtain the solution having the singularity at B as shown in Fig. 3, we take

$$\Psi = Im[C/(z^m + b^m)^n]$$

with

$$m = \pi/\theta_0, \qquad n = (\beta_B - \delta_B)/(\pi + \delta_B - \theta_0)$$

Here, $z = qe^{i\theta}$ is the complex variable in the hodograph plane and b denotes the magnitude of $0B$. This function takes the value $\Psi = 0$ on $N0$ and $0B$ and satisfies the condition of the spine at B. (The second condition (ii) at N is automatically satisfied.)

Fig. 4 shows an example of four possible shock configurations for the case when $M_1 = 1.50$ and $\theta_0 = 11° 45'$.

At first sight these flow patterns seem to be rather curious because of having a certain characteristic length (e.g., the radius of curvature of the shock wave at its nose), notwithstanding that an infinite wedge has no such quantities. This may, however, be interpreted at least qualitatively as follows:

Taking the solution with the sink S at a certain point on BA or $B0$ as shown in Fig. 5 (i), (ii), the corresponding flow patterns may be expected to be those given in Fig. 5 (iii), (iv). These flow patterns will be reduced to either of the above-mentioned cases by making S approach B.

The detailed discussions with some numerical calculations will be reported elsewhere in the near future.

In conclusion, the author wishes to express his cordial thanks to Prof. S. Tomotika, of the University of Kyoto, and to Dr. K. Tamada for their continual guidance and encouragement throughout this work.

References

[1] Busemann, A., *A Review of Analytical Methods for the Treatment of Flows with Detached Shocks*, NACA TN No. 1858, 1949.

[2] Imai, I., *Application of the W.K.B. Method to the Flow of a Compressible Fluid, I*, Jour. Math. Phys., Vol. 28, pp. 173–182, 1949.

Changes of Address

Since the Post Office Department does not as a rule forward magazines to forwarding addresses, it is important that the Institute be notified of changes in address 30 days in advance of publishing date to ensure receipt of every issue of the Journal and Review.

Notices should be printed legibly and sent directly to:

Institute of the Aeronautical Sciences, Inc.
2 East 64th Street, New York 21, New York